

**FUZZY SIMILARITY MEASURE AND ITS
APPLICATION TO HIGH RESOLUTION COLOUR
REMOTE SENSING IMAGE PROCESSING**

Yu Li, B. Sc.

XiDian University, Xi'an, CHINA, 1984

**A Thesis Submitted to the School of Graduate Studies at Ryerson University
in Partial Fulfillment of the Requirements for the Degree of
Master of Applied Science
in the Program of Civil Engraining**

Toronto, Ontario, Canada

©Yu Li, 2004

RECEIVED
RYERSON UNIVERSITY
2004

UMI Number: EC53467

INFORMATION TO USERS

The quality of this reproduction is dependent upon the quality of the copy submitted. Broken or indistinct print, colored or poor quality illustrations and photographs, print bleed-through, substandard margins, and improper alignment can adversely affect reproduction.

In the unlikely event that the author did not send a complete manuscript and there are missing pages, these will be noted. Also, if unauthorized copyright material had to be removed, a note will indicate the deletion.



UMI Microform EC53467
Copyright 2009 by ProQuest LLC
All rights reserved. This microform edition is protected against
unauthorized copying under Title 17, United States Code.

ProQuest LLC
789 East Eisenhower Parkway
P.O. Box 1346
Ann Arbor, MI 48106-1346

DECLARATION

I hereby declare that I am the sole author of this thesis.

I authorize Ryerson University to lend this thesis to other institutions or individuals for the purpose of scholarly research.

I further authorize Ryerson University to reproduce this thesis by photocopying or by other means, in total or in part, at the request of other institutions or individuals for the purpose of scholarly research.

Yu Li

Department of Civil Engineering

Ryerson University

September 16, 2004

ABSTRACT

Fuzzy Similarity Measure and Its Application to High-resolution Colour Remote Sensing Image Processing

Yu Li, MASc

Civil Engineering, Ryerson University, Toronto, 2004

The focus of the study in this thesis is placed on developing basic algorithms and tools for high-resolution colour remote sensing image processing tasks such as colour morphology, multivariate clustering, and multivariate filtering.

First, the fuzzy similarity measure (FSM) among vectors in a vector space is introduced. This measure is based on two assumptions for the relationship among vectors: short-range ordering and fuzzification. Second, based on the FSM, the colour morphology, multivariate fuzzy clustering, and multivariate filtering are defined. The performances of all proposed methods will be evaluated numerically and subjectively. Third, this study also places more emphases on solving some applied problems related to recognizing colour edges, detecting and extracting complex road network and building rooftops, and reducing noise in high-resolution remote sensing images such as QuickBird, Ikonos, and aerial images. The results obtained in the study demonstrate the effectiveness and efficacy of the FSM and the proposed methods.

BORROWER’S PAGE

Ryerson University requires the signatures of all persons using or photocopying this thesis. Please sign below, and give address and date.

Name	Address	Date	Signature

ACKNOWLEDGEMENTS

I express my sincere gratitude and appreciation to many people who have made this thesis possible.

I would firstly like to express my heartfelt thanks to my supervisors, Prof. Dr. Jonathan Li and Prof. Dr. Kunquan Lan. I believe that no one has ever had so much supportive, generous, and encouraging supervisors. They are the impelling force behind this study and have freely given their precious time and ensured that I have always felt that my work has been their own priority. The success of this study is solely due to the generosity of their ideas and amazing intellect. I greatly appreciate their efforts to provide me their financial supports through their NSERC Discovery grants during the course of the study are also appreciated.

I would like to thank the members of examining committee, Prof. Dr. Michael A. Chapman, Prof. Dr. Mohamed Lachemi, and Prof. Dr. Songnian Li for reviewing my thesis and providing the helpful comments.

Special thanks to the School of Graduate Studies for providing me the Ryerson Graduate Scholarships and the opportunities to study at Ryerson University and do this research during the period of 2002 to 2004.

I also wish to thank my best friend Xiangqian Gao, his wife Shuying Wang, and their daughter Kaikai for their tremendous help. The days of living with them always recall my beautiful and happy recollections. Many thanks also to my classmates at the Department of Civil Engineering of Ryerson University, Hongmei Zhao, Haibin Dong, and Lijun Gu.

Most of all, my deepest thanks go to my parents, my sisters, brother and their families for their unconditional love and support.

To my beloved Xiao Qu, thanks for her trust and patience concern, encouragement and prayers. Her soulful love made my life enjoyable.

At last, I want to devote this thesis to my beloved son Jianjian. Thank him for giving me hope and mettle to live in this new country. It would not have been possible to complete this study without his accompaniments.

TO MY BELOVED SON

Jianjian

TABLE OF CONTENTS

TITLE	i
DECLARATION	ii
BORROWER'S PAGE	iii
ABSTRAC	iv
ACKNOWLEDGEMENTS	v
DEDICATION	vii
TABLE OF CONTENT	viii
LIST OF FIGURES.	xii
LIST OF TABLES	xvi
LIST OF ABBREVIATIONS.	vxii
LIST OF SYMBOLS	xviii
1 INTRODUCTION.. . . .	1
1.1 Motivations.. . . .	1
1.2 Goals and Key Issues	2
1.3 Methodologies.	4
1.4 Organization of the Thesis.	5
2 PRELIMINARIES	7
2.1 Colour Space.	7
2.1.1 RGB Colour Space.	8
2.1.2 Uniform Colour Space.	9

2.2	Similarity Measures among Vectors.12
2.3	Mathematical Morphology.	16
2.3.1	Binary Morphology.	16
2.3.2	Grayscale Morphology.18
2.3.3	Fuzzy Morphology.19
2.3.4	Colour Morphology.22
2.4	Fuzzy Set Theory.23
2.5	Vector-based Filters.	25
3	FUZZY SIMILARITY MEASURE30
3.1	Definition of FSM30
3.2	Numerical Properties of FSM.34
3.3	Colour Similarity in RGB Colour Space: An Example.38
3.4	Chapter Summary.43
4	COLOUR MORPHOLOGY BASED ON FSM.	44
4.1	Introduction.44
4.2	Infimum and Supremum Operators Based on FSM47
4.3	Colour Morphological Operations.51
4.3.1	Definition.51
4.3.2	Illustration.52
4.3.3	Properties.54
4.4	Colour Edge Detection58
4.4.1	Definition of Colour Edge.59
4.4.2	Similarity Measure between Two Colour Images.61

4.4.3 Fuzzy Similarity Edge Extractor.61
4.4.4 Experimental Results and Discussions64
4.5 Chapter Summary.69
5 FUZZY CLUSTERING BASED ON FSM.	71
5.1 Fuzzy C-Partition Algorithm Based on FSM.72
5.2 Colour Histogram.76
5.3 Segmentation Based on Fuzzy C-Partition Algorithm.78
5.3.1 Pre-clustering Procedure.79
5.3.2 Post-processing Procedure.80
5.3.3 Experiment and Results81
5.4 Object Extraction Application.87
5.4.1 Road Centerline Extraction.87
5.4.1.1 Extraction of Road Networks.88
5.4.1.2 Delineation of Road Centrelines.89
5.4.1.3 Experiments and Results of Road Extraction.90
5.4.2 Building Extraction.93
5.5 Chapter Summary.97
6 MULTIVARIATE FILTERING BASED ON FSM99
6.1 Fuzzy Similarity Filter100
6.2 Simulation Results.105
6.2.1 Impact of Parameters on Performances of FSF.108
6.2.2 Comparison of Performances.113
6.3 Chapter Summary.116

7 CONCLUSIONS AND RECOMMENDATIONS.	117
7.1 Summary.	117
7.2 Conclusions.	118
7.2.1 Fuzzy Similarity Measure.	118
7.2.2 Colour Morphology.	119
7.2.3 Fuzzy Clustering.	119
7.2.4 Multivariate Filtering.	120
7.3 Recommendations for Future Research.	120
REFERENCES	122
INDEX.	132

LIST OF FIGURES

Fig. 2.1 Visible electromagnetic spectrum.	7
Fig. 2.2 RGB colour space.	8
Fig. 3.1 Convexity of FSM in 2-D case.	34
Fig. 3.2 Impact of k_1 on FSM, when $k_2 = 1$	35
Fig. 3.3 Impact of k_2 on FSM, when $k_1 = 1$	36
Fig. 3.4 Impact of k_1 and k_2 to FSM, when $d = 1$, $\theta = \pi/4$	37
Fig. 3.5 Colour in Group 1.	39
Fig. 3.6 Colour in Group 2.	39
Fig. 3.7 Colour for Group 3.	40
Fig. 4.1 Definitions of max-min vector pair, similar vector classes, and the most similar vectors.	49
Fig. 4.2 Illustration of proposed morphological operations.	53
Fig. 4.3 Colour Ikonos image.	54
Fig. 4.4 Dilation with parameters in Table 4.1.	55
Fig. 4.5 Erosion with parameters in Table 4.1.	56
Fig. 4.6 Closing with parameters in Table 4.1.	57
Fig. 4.7 Opening with parameters in Table 4.1.	58
Fig. 4.8 Block diagram of colour edge extractor.	59
Fig. 4.9 Definition of colour edge.	60
Fig. 4.10 Illustration of FSEE.	63

Fig. 4.11 Original images: (a) QuickBird, (b) Ikonos, and (c) aerial images.	64
Fig. 4.12 Result of morphological operations.	65
Fig. 4.13 Profile curves of similarity measure between selected image pair for (a) QuickBird, (b) Ikonos, and (c) aerial images.	65
Fig. 4.14 Grayscale images of similarity measure between selected image pair for (a) QuickBird, (b) Ikonos, and (c) aerial images.	66
Fig. 4.15 Binary edge images.	67
Fig. 4.16 Results of directly binary morphological dilation of edge images.	68
Fig. 4.17 Extracted object edges.	69
Fig. 4.18 Overlaying edges (in red) on original images.	70
Fig. 5.1 Discretization of RGB colour space and codes of bins.	78
Fig. 5.2 Test images: (a) QuickBird, (b) Ikonos, and (c) aerial images.	81
Fig. 5.3 Colour Histograms of (a) QuickBird, (b) Ikonos, and (c) aerial images.	82
Fig. 5.4 Profile curves of fuzzy c-partition matrix of QuickBird image.	84
Fig. 5.5 Pseudo colour images of fuzzy c-partition matrix of QuickBird image.	84
Fig. 5.6 Profile curves of fuzzy c-partition matrix of Ikonos image.	84
Fig. 5.7 Pseudo colour image of fuzzy c-partition matrix of Ikonos image.	85
Fig. 5.8 Profile curves of fuzzy c-partition matrix of aerial image.	85
Fig. 5.9 Pseudo colour image of fuzzy c-partition matrix of aerial image.	85
Fig. 5.10 Segmented images: (a) QuickBird, (b) Ikonos, and (c) aerial images.	86
Fig. 5.11 Road extraction strategy.	88
Fig. 5.12 Neighborhood arrangement.	90
Fig. 5.13 Original images: (a) aerial, (b) Ikonos, and (c) QuickBird images.	91

Fig. 5.14 Segmented images (a) aerial, (b) Ikonos, and (c) QuickBird images.	91
Fig. 5.15 Binary images of road regions: (a) aerial, (b) Ikonos, (c) QuickBird from segmented images.	91
Fig.5.16 Filtered road networks (a) aerial, (b) Ikonos, and (c) QuickBird images.	92
Fig. 5.17 Road centerlines: (a) aerial, (b) Ikonos, and (c) QuickBird images.	92
Fig. 5.18 Road centerlines (in red) overlaid on original images: (a) aerial, (b) Ikonos, and (c) QuickBird.	93
Fig. 5.19 Building extraction strategy.	94
Fig. 5.20 Test images: (a) QuickBird, (b) Ikonos, and (c) aerial images	95
Fig. 5.21 Segmented images: (a) QuickBird, (b) Ikonos, and (c) aerial images	95
Fig. 5.22 Detected buildings: (a) QuickBird, (b) Ikonos, and (c) aerial images.	96
Fig. 5.23 Building roof regions after filtered: (a) QuickBird, (b) Ikonos, and (c) aerial images.	96
Fig. 5.24 Delineating building roofs: (a) QuickBird, (b) Ikonos, and (c) aerial images.	97
Fig. 5.25 Building edges (in red) overlaid on original images: (a) QuickBird, (b) Ikonos, and (c) aerial images.	97
Fig. 6.1 Test image.	103
Fig. 6.2 Noise images.	108
Fig. 6.3 NMSE of FSF, k_1 from 0 to 100, $k_2 = 0.2$, and $\alpha = 0.9$	109
Fig. 6.4 NCD of FSF, k_1 from 0 to 100, $k_2 = 0.02$, and $\alpha = 0.9$	110
Fig. 6.5 NMSE and NCD of FSF, k_2 from 0 to 1, $k_1 = 0.02$, and $\alpha = 0.9$	111
Fig. 6.6 NMSE and NCD of FSF, α from 0 to 1, $k_1 = 0.02$, and $k_2 = 0.2$	112
Fig. 6.7 Images after filtering by FSF.	112

Fig. 6.8 NMSE and NCD of FSF with different window sizes.	113
Fig. 6.9 NMSEs of VMF, VDF, DDF, and FSF.	114
Fig. 6.10 NCDs of VMF, VDF, DDF, and FSF.	114
Fig. 6.11 Filtered images of Model 1 noise image by (a) VMF, (b) VDF, (c) DDF, and (d) FSF.	115
Fig. 6.12 Filtered images of Model 2 noise image by (a) VMF, (b) VDF, (c) DDF, and (d) FSF.	115
Fig. 6.13 Filtered images of Model 3 noise image by (a) VMF, (b) VDF, (c) DDF, and (d) FSF.	115
Fig. 6.14 Filtered images of Model 4 noise image by (a) VMF, (b) VDF, (c) DDF, and (d) FSF.	116

LIST OF TABLES

Table 3.1 Similarity measure values and colours in Groups 1, 2, and 3.41
Table 3.2 Similarity measure values and colours in Group 3.42
Table 4.1 Parameters used in colour morphological operators.54
Table 4.2 Morphological operation pairs and thresholds.66
Table 5.1 Results of pro-clustering and optimal centre vectors.83
Table 6.1 Noise models and distributions.	108

LIST OF ABBREVIATIONS

CIE	Commission Internationale de l'Eclairage
C-ordering	Conditional ordering
CYM	Cyan, Magenta, Yellow
DDF	Distance-Direction Filter
FSEE	Fuzzy Similarity Edge Extractor
FSF	Fuzzy Similarity Filter
FSM	Fuzzy Similarity Measure
GIS	Geographical Information Systems
HSI	Hue, Saturation, Intensity
M-ordering	Marginal ordering
NCD	Normalized Colour Difference
NMSE	Normalized Mean Square Error
P-ordering	Partial ordering
RGB	Red, Green, Blue
R-ordering	Reduced or Aggregated Ordering
VDF	Vector Directional Filter
VMF	Vector Median Filter

LIST OF SYMBOLS

a	scale value; threshold
\mathbf{a}	constant vector
A	aggregation angle function
BI	binary image
BIN	set of bins
b	blue component of RGB colour vector
\mathbf{b}	constant vector
b_p	blue component of colour vector of pixel p
c	number of clusters in fuzzy c -partition
CI	colour image
$CL1$	Class 1 subset of a vector set
$CL2$	Class 2 subset of a vector set
$Conj$	conjunctive
d	distance measure
D	aggregation distance function
d_1	city-block distance
d_2	Euclidean distance
d_∞	cheeseboard distance
d_A	domain of grayscale image
DA	aggregation distance and angle products function

d_B	domain of structuring element
d_p	distance between two vectors induced by p -norm
d_{wp}	weighted distance
E	Euclidean space
F	fuzzy set on universe
$FSEE$	set indicating edge pixels
$FSEE_i$	i th element of $FSEE$
FSF	output of FSF filter
FR	fuzzy relation
$F(U)$	set of all fuzzy sets
g	green component of RGB colour vector
GI	grayscale image
g_p	green component of RGB colour vector of pixel p
H	colour histogram
h_i	element of a colour histogram
i	colour histogram index
Imp	implicator
inf	Infimum
i_p	bin index in which the pixel p is
J	objection function for fuzzy c -partition; family index
k_1	parameter in FSM
k_2	parameter in FSM
L	complete lattice

L^*	L component of colour in $L^*u^*v^*$ colour space
m	fuzzification parameter in objection function
M	complete lattice
M	similarity measure between two colour images
max	maximum operator
MI	multivariate image
min	minimum operator
n	number of pixels in a colour space
n_i	number of pixels in i th bins
N	number of bins in a colour space; number of nonzero neighbors
N_B	number by which B coordinate of RGB clue is discretized
N_G	number by which G coordinate of RGB clue is discretized
N_{ge}	negator
N_{ge_I}	negator induced by implicator
N_R	number by which R coordinate of RGB clue is discretized
OV	object vector
p	intensity value of pixel p
P	fuzzy c -partition matrix
P_b	best fuzzy c -partition matrix
P_c	crip c -partition matrix
P_p	percent partition matrix
p_i	8-neighbourhood intensity values of pixel p
p_{ij}	element in a fuzzy c -partition matrix

r	correlation function; r component of RGB colour vector
R	real number space
R^m	m -dimensional real number space
r_p	red component of colour vector of pixel p
S	number of 0-1 transitions in the ordered sequence
SE	structuring element
sup	supremum
SV	sum vector induced by a fuzzy relation
t	constant in unit interval
T_a	translation operator
u	element of a universe U
u	vector in vector space V
u^*	u component of colour in $L^*u^*v^*$ colour space
U	universe
v	vector in vector space V
v^*	v component of colour in $L^*u^*v^*$ colour space
V	vector space or vector set
V_0	initial centre vector set
$V_{(1)}$	minimum vector in vector order
VC	centre vector set
VC_i	centre vector
V_i	vector in vector set
$V_{(i)}$	i th order statistic in vector order

$V_{(n)}$	maximum vector in vector order
$V_{([n/2])}$	media vector in vector order
$v_{i1}, v_{i2}, \dots, v_{im}$	elements of a vector
w	pixel point of multi-dimensional image
W	window variable
w_i	weighted factor
W_p	vector subset corresponding to window centered at pixel p
x	pixel point of multi-dimensional image
X	X component of colour in CIE XYZ colour space
X	subset of vector set V
X_α	α -cut
X_{Cl}	vector set representing colour image
X_{CL1}	most similar vector in Class 1
X_{CL2}	most similar vector in Class 2
X_i	elements of vector subset X
x_{ij}	j th component of vector X_i
X_{\max}	maximum vector in a vector set
X_{\maxs}	maximum similar vector
X_{\min}	minimum vector in a vector set
X_n	X component of reference colour in CIE XYZ colour space
X_p	feature vector of pixel p
y	pixel point of multi-dimensional image
Y	Y component of colour in CIE XYZ colour space

Y_n	Y component of reference colour in CIE XYZ colour space
z	pixel point of multi-dimensional image
Z	Z component of colour in CIE XYZ colour space
Z^m	m -dimensional integer space
Z_n	Z component of reference colour in CIE XYZ colour space
α	angle measure
δ	dilation operator
ε	erosion operator
θ	angle between vectors
μ	characteristic function of set U
μ_F	fuzzy membership function of fuzzy set or fuzzy similarity measure
μ_i	aggregated similarity of a vector
o	opening operator
σ	standard deviation; standard deviation
χ_U	characteristic function of universe
χ	closing operator
ψ	mapping between lattices
Φ	empty set
$\ \, \ $	norm
$\ \, \ _2$	Euclidean norm
$\ \, \ _p$	p -norm of V_i
$< \, >$	inner product
\cdot	dot product

-	reflection (symmetry) operator; minus; negtive
\vee	infimum operator
\wedge	supremum operator
\cup	union operator on fuzzy sets
\cap	intersection operator on fuzzy sets
'	complement operator on fuzzy sets
$ $ $ $	absolute value; cardinal of a set
Δ	error
\forall	universal quantifier
\in	is member of set
\times	Cartesian; multiplied by
Σ	summation of
$f : X \rightarrow Y$	function; mapping
\leq	partial relation; less then or equal to
\geq	larger than
\subseteq	contained in or equal to
\subset	contained in but unequal to
\leftrightarrow	if and only if
∞	infinity
\exists	existential quantifier
\notin	not a member of
$[]$	closed interval
$\{ \}$	unordered set

1 INTRODUCTION

Remote sensing images acquired from aircraft and spacecraft platforms provide much more useful information of the earth's surface and atmosphere, and play an increasingly important role in a broad range of applications ranging from geology (Reeves, 1999), geography (Bo et al., 2001), agriculture (Richards, 1993), forestry (Neville and Till, 1991; Goodenough et al., 2003), environmental monitoring (Ehlers et al., 2003), transportation (Georgopoulos et al., 1995), and so on. Consequently, remote sensing image processing techniques to extract, analyze, process, and interpret the information included in remote sensing images require knowledge from several disciplines such as computer vision, digital image processing and pattern recognition (Richards, 1999).

1.1 Motivations

Since the early 1960s, numerous satellite sensors have been launched into orbit around the earth to observe and monitor the Earth and its environment (Fu and Cazenave, 2001). Most early satellite sensors acquired data for meteorological purposes (Carleton, 1991; Bader, 1995). The advent of earth resources satellite sensors (those with a primary objective of mapping and monitoring land cover) occurred when the first Landsat satellite was launched in 1972 (Short, 1982). Currently, many types of orbiting satellites provide data to improve the knowledge of the earth's atmosphere, oceans, ice and snow, and land (Lowman, 2002; Verstraete, 2000). With the development of satellite imaging sensor

techniques for earth observation (Jacobsen, 1998; Kilston, 1998), the new generation of very high spatial resolution commercial imaging satellite sensors such as Ikonos (Dial et al., 2003) and QuickBird (<http://www.digitalglobe.com>) has shown that images acquired from these satellite sensors can provide a viable alternative to aerial images for mapping the earth's surface. However, due to the lack of intelligent and fast image processing algorithms and tools, it is difficult to apply these data to landuse management, urban mapping, city planning, environmental study and transportation planning (Stafford, 1991).

The work presented in this thesis was motivated by developing efficient image processing techniques to analyze and interpret high-resolution remote sensing images.

1.2 Goals and Key Issues

In this thesis, three aims are focused on. First of all, a mathematic foundation for other works in this thesis is attempted to establish. This work is accomplished by studying the similarity among vectors in a vector space and defining the fuzzy similarity measure (FSM) between two vectors. The second aim of this thesis is to develop efficient and powerful tools for high-resolution remote sensing image processing tasks such as colour morphology, fuzzy clustering and multivariate filtering. The last one is to solve some applied problems in Geomatics such as colour edge extraction, road and building extraction and noise reduction from high-resolution remote sensing images such as Ikonos, QuickBird, and aerial images.

The following key issues will be studied in this thesis.

- Fuzzy similarity measure (FSM)
 - Definition of the FSM
 - Analysis of numerical properties of the FSM
 - Case study: colour similarity
- Colour morphology
 - Definition of colour morphology based on the FSM
 - Analysis of properties of the colour morphology
 - Case study: color edge extractor based on the colour morphology
- Fuzzy Clustering
 - The fuzzy c-partition algorithm based on the FSM
 - Definition of colour histogram
 - Colour image segmentation method based the fuzzy c-partition algorithm and colour histogram
 - Case study: road and building extraction
- Multivariate filtering
 - Definition of the multivariate filtering method based on the FSM
 - Analysis of properties of the proposed filtering technique
 - Case study: noise reduction

1.3 Methodologies

Remote sensing images are generally available in discrete digital format and represent the spatial distribution of energy emanating from the earth's surface in a sensible range of wavelengths. Consequently, remote sensing images are usually originated in multivariate forms such as multispectral and multitemporal images. As a result, processing multivariate images is much more complicated due to the increased dimensions and the needs for extracting and exchanging information from and among all components. Therefore, it is important to organize components as one entity because both within and between components correlations will be used. Toward this end, it is convenient to treat all components of each pixel in a multivariate image as a vector, called the feature vector corresponding to the pixel. Mathematically, all possible feature vectors form a vector space, called feature vector space.

In vector-based multivariate image processing, an important measure between two vectors is the similarity measure that can be used to compare two vectors and determine whether and how they are related to each other. The fuzzy similarity measure (FSM) that computes the fuzzy-based similarity of two vectors in a feature vector space is defined by using a fuzzy similarity function, which uses the distance and angle of two vectors and is based on two basic assumptions, i.e., the short-range ordering and fuzzification on vector similarity.

The first application of the FSM is to define colour morphology. The developed morphology is under following assumption, i.e., the pixels of an object in a colour image have the similar colours. The purpose of the defined colour morphology is to recognize the shape of objects in a colour image by smoothing the colours in each object and shrinking or expanding objects.

In fuzzy clustering algorithm based on the FSM, the FSM is used to compute the fuzzy c-partition matrix. The colour histogram defined in this thesis is employed to determinate the number of the clusters in a colour image. The segmentation algorithm based on the fuzzy clustering and colour histogram can be modeled a combinational optimum problem.

Following the FSM, a fuzzy similarity filter (FSF) is developed. Unlike the commonly used vector-based filtering techniques which always select so-called the most central vector as the output of filters, the FSF chose the most central vector or the original vectors as the output if the late is similar to the most central vector under a given threshold.

1.4 Organization of the Thesis

The thesis is organized as follows. Chapter 2 provides basic knowledge which will be used throughout this thesis, for example, the background notions on colour spaces, similarity measure, mathematical morphology, fuzzy set theory, and vector-based filter.

In Chapter 3, the discussion will be focused on the definition of the FSM and the analysis of its properties. An example is provided to show how to apply the proposed similarity measure to compare colour similarity in RGB colour space. In chapter 4, the basic colour morphological operations such as dilation, erosion, closing, and opening based on the FSM will be introduced. And the application of the colour morphology to colour edge extraction will also be given. In Chapter 5, the FSM is applied to designing a fuzzy clustering algorithm. A histogram-based colour segmentation method is also introduced and is employed to design object extractor to extract the road networks and building roofs. In Chapter 6, a novel multivariate filter based on the FSM, called fuzzy similarity filter (FSF), is introduced. The application of the FSF to detecting and removing noise from corrupted remote sensing images is also described. The performances of the FSF and other vector-based filters such as vector median filter (VMF), vector directional filter (VDF), and distance-direction filter (DDF) are compared in Chapter 6. Chapter 7 draws conclusions on the findings from the research and gives some recommendations for future research.

2 PRELIMINARIES

In this chapter, some basic knowledge which will be used throughout this thesis is mentioned. In particular, colour space, similarity measure, mathematical morphology, fuzzy set theory, and vector based filtering technique are discussed.

2.1 Colour Space

Colour is the perceptual result of light in the visible region of the electromagnetic spectrum, having wavelengths in the region of $0.4 - 0.7 \mu m$, as shown in Figure 2.1 (Wyszecki and Stiles, 1967; Gonzalez and Woods, 1992; Fairchild, 1998).

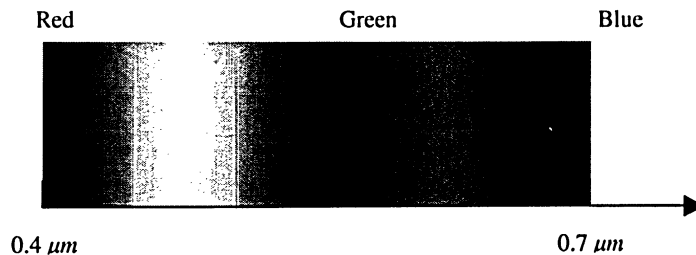


Fig. 2.1 Visible electromagnetic spectrum.

Psychophysiology studies have shown that colour information is generally tri-variant (Boynton, 1979). The reason is that the human retina has three types of colour photoreceptor cells, called cones, which have peak sensitivities in the red, green and blue portions of the electromagnetic spectrum, respectively. Therefore, a colour can be specified by a tri-components vector. The set of all colours forms a vector space, called

colour space or colour model. Three components of colours can be defined in many different ways, which lead to various colour spaces such as RGB (Red, Green, Blue), HSI (Hue, Saturation, Intensity), CMY (Cyan, Magenta, Yellow), $L^*u^*v^*$, and $L^*a^*b^*$, etc. For simplification, only RGB and $L^*u^*v^*$ colour spaces are introduced in this section because they will be used later.

2.1.1 RGB Colour Space

In RGB colour space, a colour is represented by the combination of its three primaries (Red, Green, Blue). This model uses a rectangular coordinate system with three coordinate axes assigned to each of three primaries to indicate their intensities which start at the origin and increase along each axis (Wyszecki and Stiles, 1967). This colour space is illustrated in Figure 2.2.

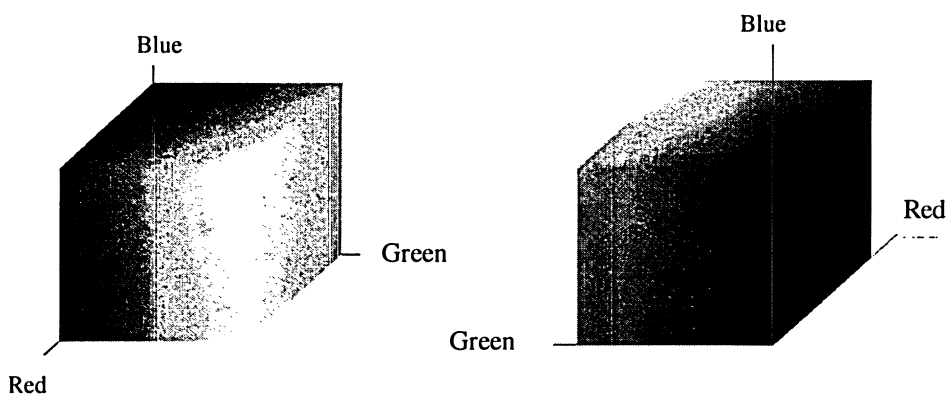


Fig. 2.2 RGB colour space.

Because each colour in RGB colour space can only have discrete values between zero and some maximum intensity (255 for 8-bit length), the resulting structure of this colour space is a cube. Any colour can be simply defined by giving its red, green, and blue

values or coordinates within the colour cube. These coordinates are usually represented as an ordered triplet (r, g, b) .

RGB colour space is an additive colour space. Its origin starts at black and all other colours are derived by adding various amounts of the primary colours. It is the natural choice for computer display where black or no light intensity is the starting point and the increasing intensities of the red, green, and blue electron guns provide the range of colours. RGB colour system is also used as a physical colour model which is utilized to digitize colour images. Recently, many colour image processing algorithms have been developed for this space. However, RGB representation is far from the one used for the human sensation of colours and colour features in RGB colour space are highly correlative.

2.1.2 Uniform Colour Space

In spite of all useful characteristics of the chromaticity diagram, it lacks a very important characteristic. That is, even though the spatial distance between two colour points in this diagram equals that between other two colour points, their perceived distances must not be the same. In the worst case, for two pairs of colour points in this diagram with the same perceived distance, their spatial distances can differ as much as 20 times. In order to correct this difference, researchers have been trying to find a perceptually uniform colour space. Unfortunately, it has still not been found. Commission Internationale de l'Eclairage (CIE) proposed two alternatives as improvements compared with CIE XYZ

space. They are $L^*u^*v^*$ and $L^*a^*b^*$ colour spaces. Although the two colour spaces are referred to as perceptually uniform colour spaces by some authors (Wyszecki and Stiles, 1967), they are not. Just for comparison, two pairs of colour points with an equal distance in perceptual can differ in the $L^*u^*v^*$ distance as much as four times. This is a significant improvement compared to twenty times in the original space, but it is still not perfect.

Converting the representation of colours from the linear RGB colour space to $L^*u^*v^*$ colour space is based on CIE XYZ space and a white reference, see Jain (1989) and Pratt (1991) for details.

The RGB values in the range $[0, 1]$ can be converted to the corresponding CIE XYZ values in the range $[0, 1]$ by using the following matrix transformation (Pratt, 1991):

$$\begin{bmatrix} X \\ Y \\ Z \end{bmatrix} = \begin{bmatrix} 0.4125 & 0.3576 & 0.1804 \\ 0.2127 & 0.7152 & 0.0722 \\ 0.0193 & 0.1192 & 0.9502 \end{bmatrix} \begin{bmatrix} r \\ g \\ b \end{bmatrix} \quad (2.1)$$

And the reference point $[X_n, Y_n, Z_n]$ to express the special XYZ value when $(r, g, b) = (1, 1, 1)$ should be used (see Pratt, 1991).

The conversion between CIE XYZ and $L^*u^*v^*$ is defined with the formulas, which can be described as follow.

The lightness component L^* of $L^*u^*v^*$ colour space is defined by CIE as the modified cube root of luminance Y in CIE XYZ space (Hill et al, 1997; Hall, 1999):

$$L^* = \begin{cases} 116 \left(\frac{Y}{Y_n} \right)^{\frac{1}{3}} - 16, & \text{if } \frac{Y}{Y_n} > 0.008856 \\ 903.3 \left(\frac{Y}{Y_n} \right), & \text{otherwise} \end{cases} \quad (2.2)$$

Computations of u^* and v^* involve the intermediates u' , v' , u_n' , and v_n' defined by

$$u' = \frac{4X}{X + 15Y + 3Z} \quad (2.3)$$

$$v' = \frac{9Y}{X + 15Y + 3Z} \quad (2.4)$$

$$u_n' = \frac{4Y_n}{X_n + 15Y_n + 3Z_n} \quad (2.5)$$

$$v_n' = \frac{9Y_n}{X_n + 15Y_n + 3Z_n} \quad (2.6)$$

The formulas for u^* and v^* are given by

$$u^* = 13L^*(u' - u_n') \quad (2.7)$$

$$v^* = 13L^*(v' - v_n')$$
(2.8)

2.2 Similarity Measures among Vectors

To determine the relationship between two objects or events is of importance in various applications such as information retrieval (Frakes and Baeza, 1992), pattern recognition (Li and Cheng, 2002), data mining (Erlich et al., 2002), image retrieval (Zhao et al., 2003), and so on. The most important and useful relationships among objects include the degree to which they are similar, called similarity measure, the degree to which they differ, called dissimilarity measure, and the degree to which the features of one object completely encompass those of another, called compatibility measure (Cross and Sudkamp, 2002). Among these measures, similarity measure is often used and is difficultly quantified. In vector analysis, the spatial distance and the relative direction of two vectors are often used to measure and judge similarity (Stark and Yang, 1998).

Let V be a vector space and R be the set of real numbers. A norm on V is a function that assigns a real number, denoted by $\|v\|$, to each vector v in V such that

- $\|v\| \geq 0$ and $\|v\| = 0$ if and only if $v = 0$
- $\|av\| = |a| \|v\|$, $\forall a \in R$ and $v \in V$
- $\|v + u\| \leq \|v\| + \|u\|$, $\forall v, u \in V$

The vector space V together with the norm $\| \cdot \|$ is called a normed vector space, denoted by $(V, \| \cdot \|)$.

Let $1 \leq p \leq \infty$ and $V_i = [V_{i1}, V_{i2}, \Lambda, V_{im}]^T \in R^m$, the p -norm of V_i is defined by

$$\|V_i\|_p = \left(\sum_{k=1}^m |V_{ik}|^p \right)^{1/p} \quad (2.9)$$

and

$$\|V_i\|_\infty = \max\{|V_{i1}|, |V_{i2}|, \Lambda, |V_{im}|\} \quad (2.10)$$

then $(R^m, \| \cdot \|_p)$ is a normed vector space. When $p = 2$, the norm $\| \cdot \|_2$ is called the Euclidean norm.

It is obvious that the norms defined in Equations (2.9) and (2.10) can be considered as the measures of the magnitude of vectors in a normed vector space.

Let $V_i, V_j \in (V, \| \cdot \|)$, the distance between V_i and V_j can be defined by

$$d(V_i, V_j) = \|V_i - V_j\| \quad (2.11)$$

Let $V_i, V_j \in (R^m, \| \cdot \|_p)$, the distance between V_i and V_j can be defined by

$$d_p(V_i, V_j) = \left(\sum_{k=1}^m |V_{ik} - V_{jk}|^p \right)^{1/p} \quad (2.12)$$

and

$$d_\infty(V_i, V_j) = \max\{|V_{i1} - V_{j1}|, |V_{i2} - V_{j2}|, \Lambda, |V_{im} - V_{jm}|\} \quad (2.13)$$

When $p = 1$, $d_1(V_i, V_j)$ is the sum of absolute displacements, called city block distance.

When $p = 2$, $d_2(V_i, V_j)$ is the straight line distance, called Euclidean distance. When $p =$

∞ , $d_\infty(V_i, V_j)$ is the so-called chessboard distance.

Another useful distance measure is the weighted distance measure. Let

$w_1, w_2, \Lambda, w_m \in R$, then the weighted distance measure is defined as,

$$d_{wp}(V_i, V_j) = \left(\sum_{k=1}^m w_k |V_{ik} - V_{jk}|^p \right)^{1/p} \quad (2.14)$$

where w_1, w_2, \dots, w_m are called the weighting factor and satisfy $\sum_{i=1}^m w_i = 1$.

It is obvious that the distance measures defined above can be used as similarity measures between two vectors. In this case, the shorter distance between two vectors means the larger similarity between them.

The angle between two vectors can also be used as a similarity measure.

Let $\langle V_i, V_j \rangle$ be the inner product between V_i and V_j , $\|V_i\|$ and $\|V_j\|$ be the norms of V_i and V_j , respectively. The correlation of V_i and V_j , $r(V_i, V_j)$, is defined by

$$r(V_i, V_j) = \frac{\langle V_i, V_j \rangle}{\|V_i\| \|V_j\|} \quad (2.15)$$

The inner product in R^m is defined by

$$\langle V_i, V_j \rangle = \sum_{k=1}^m V_{ik} V_{jk} \quad (2.16)$$

where $V_i = [V_{i1}, V_{i2}, \dots, V_{im}]^T$, $V_j = [V_{j1}, V_{j2}, \dots, V_{jm}]^T \in R^m$

It is clear that $\langle V_i, V_i \rangle = \|V_i\|^2$ for $V_i \in R^m$.

Let θ be the angle between V_i and V_j in R^m , then

$$\cos \theta = r(V_i, V_j) = \frac{\langle V_i, V_j \rangle}{\|V_i\|_2 \|V_j\|_2} = \frac{\sum_{k=1}^m V_{ik} V_{jk}}{\left(\sum_{i=1}^m |V_{ik}|^2 \right)^{1/2} \left(\sum_{j=1}^m |V_{jk}|^2 \right)^{1/2}} \quad (2.17)$$

where $\theta \in [0, \pi)$

It is worthy of note that as a similarity measure, the angle measure, $r(V_i, V_j) = \cos(\theta)$, only considers the relative direction of the two vectors and neglects the distance of them.

2.3 Mathematical Morphology

Mathematical morphology was developed by Matheron (1975) and Serra (1982) as a geometry-based technique for image processing and analysis. This section briefly introduces some basic concepts of mathematical morphology which are often used in binary morphology, grayscale morphology, fuzzy-based grayscale morphology, and colour morphology.

2.3.1 Binary Morphology

Mathematical morphology was initially developed for binary imagery, called binary morphology, which uses the set operators such as union, intersection, complementation, and translation, while a binary image is represented as a set.

Let E be the Euclidean space R^m or the discrete integer space Z^m , a binary image can be represented as a subset of E or a mapping $f: E \rightarrow \{0, 1\}$.

The translation operator, T_a , which translates the set of object vectors, $OV \subset E$, by a constant vector, $a \in E$, is defined as

$$T_a(OV) = \{ov + a : ov \in OV\} \quad (2.18)$$

The reflection or symmetry operator, $-$, of OV is defined as

$$-OV = \{-ov : ov \in OV\} \quad (2.19)$$

Definition 2.1 Let $BI \subset E$ be a binary image and $SE \subset E$ be a binary structuring element. The binary dilation δ_{SE}^T , erosion ε_{SE}^T , closing χ_{SE}^T , and opening o_{SE}^T of BI by SE are binary images given by:

$$\delta_{SE}^T(BI) = \{a \in E : T_a(-SE) \cap BI \neq \Phi\} \quad (2.20)$$

$$\varepsilon_{SE}^T(BI) = \{a \in E : T_a(SE) \subseteq BI\} \quad (2.21)$$

$$\chi_{SE}^T(BI) = \varepsilon_{SE}^T(\delta_{SE}^T(BI)) \quad (2.22)$$

$$o_{SE}^T(BI) = \delta_{SE}^T(\varepsilon_{SE}^T(BI)) \quad (2.23)$$

Generally, the binary dilation typically will extend the contours of the objects in an binary image, while the binary erosion will reduce them. Furthermore, the dilation will fill up small gaps and narrow channels, while the erosion will eliminate small foreground details, enlarge gaps and broadens channels. The binary opening will suppress small peaks and eliminates other small details, while the binary closing will fill up narrow channels and small gaps. It is notable that in contrast to the binary dilation and binary erosion, the size of larger structures or objects isn't really affected by binary closing and binary opening.

2.3.2 Grayscale Morphology

Binary morphology has been successfully extended to grayscale morphology. Such extension requires rules for the combination of different grayscale values. There are several approaches which are used to extent binary morphology to grayscale morphology, for example, the umbra approach (Heijmans, 1996), the threshold set approach (Maragos and Ziff, 1990), the complete lattice approach (Ronse, 1990), and the fuzzy logic approach (Goetcherian, 1980).

For the complete lattice approach, its mathematical fundament is the complete lattice theory. This grayscale morphology follows on the assumption that the set of all possible grayscale images constitutes a complete lattice.

A nonempty set L with a partial ordering \leq is called a complete lattice if every subset $M \subseteq L$ has an infimum $\sqcap M$ and a supremum $\sqcup M$ in L . Suppose that L and M are two complete lattices, an operator $\psi : L \rightarrow M$ is said to be increasing if $L_1 \leq L_2$ implies that $\psi(L_1) \leq \psi(L_2)$, for $L_1, L_2 \sqsubseteq L$.

Definition 2.2 An operator $\delta: M \rightarrow L$ is called dilation if $\delta(\bigvee_{j \in J} M_j) = \bigvee_{j \in J} \delta(M_j)$ for every collection $\{M_j \mid j \in J, M_j \subseteq M\}$. An operator $\varepsilon: L \rightarrow M$ is called erosion if $\varepsilon(\bigwedge_{j \in J} L_j) = \bigwedge_{j \in J} \varepsilon(L_j)$ for every collection $\{L_j \mid j \in J, L_j \subseteq L\}$. Two operators $\varepsilon: L \rightarrow M$ and $\delta: M \rightarrow L$ are said to be an adjunction between L and M if $\delta(M_i) \leq L_i \leftrightarrow M_i \leq \varepsilon(L_i)$, for any $L_i \sqsubseteq L$ and $M_i \sqsubseteq M$, i.e., $\delta(M_i)$ is an infimum of L if and only if M_i is an infimum of M . (ε, δ) is used to denote an adjunction between L and M .

Definition 2.3 If (ε, δ) is an adjunction between L and M , then the composition $\varepsilon\delta$ is a closing on M and $\delta\varepsilon$ is an opening on L .

2.3.3 Fuzzy Morphology

Fuzzy morphology means the grayscale morphology defined on fuzzy logical and fuzzy sets. It is another alternative extension of binary morphology to grayscale morphology. In this technique, concepts from fuzzy logic and fuzzy sets are used for designing morphological operators rather than representing grayscale image as a fuzzy set.

Several researchers have made their contributions to fuzzy morphology. Goetcherian (1980) first applied the concepts from fuzzy logic to grayscale morphology. This technique has also been advocated by several other researchers, for example, Sinha and Dougherty (1993), Bloch and Maitre (1995), De Baets (1997), and Nachtegaal and Kerre (2001). De Baets (1997) developed a general logical framework which induces previous results as special cases. His idea was to fuzzificate the logical operations, i.e., Boolean conjunction and Boolean implication, to obtain a successful fuzzification. In other words, his work was based on the notions of negator, conjunctive and implicative on the unit interval.

Definition 2.4 A unary operator $Neg: [0, 1] \rightarrow [0, 1]$ is called a negator if it is decreasing on $[0, 1]$ and satisfies $Neg(0) = 1$ and $Neg(1) = 0$ (De Baets, 1997).

Definition 2.5 A binary operator $Conj: [0, 1] \times [0, 1] \rightarrow [0, 1]$ is a conjunctive if it is increasing on $[0, 1]$ and satisfies $Conj(0, 0) = Conj(0, 1) = Conj(1, 0) = 0$ and $Conj(1, 1) = 1$ (De Baets, 1997).

Definition 2.6 A binary operator $Imp: [0, 1] \times [0, 1] \rightarrow [0, 1]$ is called an implicative if it is hybrid monotonous on $[0, 1]$, that is, decreasing with first argument and increasing with second argument, and satisfies $Imp(0, 0) = Imp(0, 1) = Imp(1, 1) = 1$ and $Imp(1, 0) = 0$ (De Baets, 1997).

According to the above definitions, every impicator Imp induces the negator Neg_I defined by $Neg_I(x) = Imp(x, 0), \forall x \in [0, 1]$. Similarly, given a conjunctor one can construct an implication from the conjunctor, and vice versa (De Baets, 1997). Using these extended logical operators, the basic fuzzy morphological operators are defined as follows.

Definition 2.7 Let $Conj$ be a conjunctor on $[0, 1]^2$, Imp be an impicator on $[0, 1]^2$, GI be a grayscale image ($GI: R^m \rightarrow [0, 1]$), and SE be a grayscale structuring element ($SE: R^m \rightarrow [0, 1]$). The fuzzy dilation δ_{Conj}^{SE} and the fuzzy erosion ε_{Imp}^{SE} are the grayscale images defined by

$$\delta_{Conj}^{SE}(y \in d_A) = \sup_{x \in T_y(d_B)} Conj(SE(x - y), GI(y)) \quad (2.24)$$

$$\varepsilon_{Imp}^{SE}(y \in d_A) = \sup_{x \in T_y(d_B)} Imp(SE(x - y), GI(y)) \quad (2.25)$$

where d_A and d_B are the domains of image GI and structuring element SE , respectively, and are defined by

$$d_A = \{z \in R^m \mid (\exists t \in [0, 1])(GI(z) = t)\} \quad (2.26)$$

$$d_B = \{z \in R^m \mid (\exists t \in [0, 1])(SE(z) = t)\} \quad (2.27)$$

$T_y(d_B)$ is the translation operation of d_B by the vector $w \in R^m$,

$$T_y(d_B) = \{z \in R^m \mid z - w \in SE\} \quad (2.28)$$

Definition 2.8 Let $Conj$ be a conjunctor on $[0, 1]^2$, Imp be an implicator on $[0, 1]^2$, GI be a grayscale image, and SE be a grayscale structuring element. The fuzzy closing $\chi_{Conj, Imp}^{SE}$ and the fuzzy opening $o_{Conj, Imp}^{SE}$ are the grayscale images defined by

$$\chi_{Conj, Imp}^{SE} = \varepsilon_{Imp}^{SE}(\delta_{Conj}^{SE}) \quad (2.29)$$

$$o_{Imp, Conj}^{SE} = \delta_{Conj}^{SE}(\varepsilon_{Imp}^{SE}) \quad (2.30)$$

2.3.4 Colour Morphology

Similar to the extension from binary morphology to grayscale morphology, in order to extend the concepts of grayscale morphology to colour morphology, one needs some rules to organize colour values. The complete lattice has been used in colour morphology, because it retains the basic properties of its grayscale counterpart. However, when employing the theory of complete lattice, an inherent difficulty is that there is no obvious and unambiguous method of fully ordering colours (vectors).

So far, there is no unified colour morphology theory, due to the variety of vector ordering schemes and colour spaces that can be used. Approaches to defining colour morphology can be categorised by the vector ordering schemes. They are marginal morphology (Beacher, 1996), partial morphology (Meyer, 1996), and reduced morphology (Serra, 1982).

2.4 Fuzzy Set Theory

This section reviews some basic notions about fuzzy set theory, which will be used later. More information on fuzzy set theory can be found in Gottwald (1979), Dubois and Prade, (1980), Zhang, (1980), George and Bo (1995).

The concepts of fuzzy sets and fuzzy logic were first introduced by Zadeh (1965) to deal with problems involving knowledge expressed in vague, linguistic terms. Classically, a set is defined by its members. In traditional (crisp or point) set theory, an object (or element) may be either a member or a non-member of a set. Mathematically, the set U , called universe of discourse, can be represented by its indicator function, or characteristic function, μ

$$\mu(u) = \begin{cases} 1 & \text{if } u \in U \\ 0 & \text{if } u \notin U \end{cases} \quad (2.31)$$

As an extension of classical set theory, a fuzzy set can also be characterized by its characteristic function, called membership degree function, which maps U into the interval

$[0, 1]$. The value 0 of the membership degree means that the member is not included in the given set. The value 1 of the membership degree describes a fully included member (these behaviours correspond to classical set theory). A value between 0 and 1 characterizes the degree to which a member belongs to the universe.

Definition 2.9 A fuzzy subset F on U can be described by its characteristic function μ_F which is a mapping from U to $[0, 1]$, i.e.,

$$\mu_F: U \rightarrow [0, 1] \quad (2.32)$$

Generally, there are two notations for fuzzy set, F stands for the actual fuzzy set, while μ_F , which is always a function from U to $[0, 1]$, means a degree assigned to each member of U , called the membership degree. All fuzzy sets on U form a set denoted by $F(U)$. Like the crisp set theory, some operations between two fuzzy sets on $F(U)$, such as union, intersection, and complement, can be defined by using their characteristic functions.

Definition 2.10 Let U be a universal set, F_1 and F_2 be two fuzzy subsets on U , and their characteristic functions be μ_{F_1} and μ_{F_2} , then union \vee , intersection \wedge of F_1 and F_2 , and complement $'$ on F_1 are defined by

$$\mu_{(F_1 \vee F_2)}(x) = \max\{\mu_{F_1}(x), \mu_{F_2}(x)\}, \forall x \in U \quad (2.33)$$

$$\mu_{(F_1 \wedge F_2)}(x) = \min\{\mu_{F_1}(x), \mu_{F_2}(x)\}, \forall x \in U \quad (2.34)$$

$$\mu_{F_1^c}(x) = 1 - \mu_{F_1}(x), \forall x \in U \quad (2.35)$$

2.5 Vector-based Filters

Let n m -dimensional vectors in the vector set $V = \{V_1, V_2, \dots, V_n\}$ be arranged in ascending order according to some ordering criterion as follows

$$V_{(1)} \leq V_{(2)} \leq \Lambda \leq V_{(i)} \leq \Lambda \leq V_{(n)} \quad (2.36)$$

the i th vector $V_{(i)}$ in this sequence is called i th order statistic. The minimum vector $V_{(1)}$, maximum vector $V_{(n)}$, and median vector $V_{(n/2)}$ are the most important order statistics, resulting in the min, max, and median filters, respectively.

Unfortunately, ordering multivariate vectors is not straightforward, because there is no notion of the natural order in a vector space as in one dimension case. Although there is no unambiguous scheme for ordering multivariate vectors, many works have been done to order multivariate data. Barnett (1976) proposed the sub-ordering principles to rule the ordering. In general, the sub-ordering principles are divided into four classes: marginal ordering (M-ordering), condition ordering (C-ordering), partial ordering (P-ordering), and reduced ordering (R-ordering) or aggregate ordering.

In the M-ordering scheme, vectors in V are ordered along each of components independently. The i th marginal order statistic is the vector $V_{(i)} = [V_{(i)1}, V_{(i)2}, \dots, V_{(i)j}, \dots, V_{(i)m}]^T$, where $V_{(i)j}$ is the i th largest element in the j th component. The marginal order statistic $V_{(i)}$ may not correspond to any original vector in V as it does in the one dimension case. This ordering scheme is equivalent to a separating method in which each component of a vector is processed independently and new vectors may be resulted in.

In the P-ordering scheme, the objective is to partition vectors into groups such that these groups can be distinguished with respect to order, rank, or extremeness. For example, subsets of vectors are grouped together forming minimum convex hulls. The first convex hull is formed such that its perimeter contains a minimum number of vectors and the final hull contains all other vectors in V . However, to determine the convex hull is a difficult task if the dimensions of V are more than two. Another drawback associated with P-ordering scheme is that there is no ordering within the groups and this scheme is not easily expressed in analytical terms. Thus, P-ordering is still rather infeasible for implementation in color image processing.

In the C-ordering scheme, vectors are ordered conditionally on some specified component. Thus, after the component is ranked other components of each vector are listed according to the position of the ranked component. This scheme has a disadvantage in multivariate image processing, i.e., only the information in one channel is used. It seems that this ordering scheme is suitable for ordering colours in HSI colour space in which the components of colours have less correlation.

In general, the R-ordering scheme reduces a vector to a scalar value according to a given criterion. Mardia (1976) further developed the subclasses of R-ordering scheme: measure ordering and projection ordering. The measure ordering refers to the use of any specific measures among vectors, such as distance and angle measures. It is obvious that R-ordering scheme is easier to be used in multivariate image processing than other vector ordering schemes.

By using the distance measure $d(V_i, V_j)$ defined in Section 2.2 for two vectors V_i and V_j in V , the aggregation distance $D(V_i)$ associated with each vector V_i can be calculated by

$$D(V_i) = \sum_{j=1}^n d(V_i, V_j), \quad \text{for } i = 1, 2, \dots, n \quad (2.37)$$

If the aggregation distances of all vectors in V are arranged in ascending order, i.e.,

$$D(V_{(1)}) \leq D(V_{(2)}) \leq \Lambda \leq D(V_{(i)}) \leq \Lambda \leq D(V_{(n)}) \quad (2.38)$$

then the same ordering to all vectors in V is implied, i.e.,

$$V_{(1)} \leq V_{(2)} \leq \Lambda \leq V_{(i)} \leq \Lambda \leq V_{(n)} \quad (2.39)$$

In the ordered sequence presented in Equation (2.39), $V_{(1)}$ is the minimum vector. It is defined as the vector in V whose aggregation distance is minimum. This ordering results in the vector median filter (VMF).

Like distance measure of vectors, the angle measure between two vectors can also be used to order the vectors in V . Using the angle measure $a(V_i, V_j)$ described in Section 2.2, the aggregation angle $A(V_i)$ associated with the vector V_i can be calculated as follows

$$A(V_i) = \sum_{j=1}^n a(V_i, V_j), \quad \text{for } i = 1, 2, \dots, n \quad (2.40)$$

Similarly, the order of the vectors in Equation (2.39) can also be implied, if the aggregation angle defined in Equation (2.40) follows the order,

$$A(V_{(1)}) \leq A(V_{(2)}) \leq \dots \leq A(V_{(i)}) \leq \dots \leq A(V_{(n)}) \quad (2.41)$$

In this case, $V_{(1)}$ in Equation (2.39) results in another kind of vector filter, the basic vector directional filter (BVDF).

To take advantage of both distance and angle measures, the R-ordering scheme based on the so-called distance-angle measure is introduced.

Generally, the product of the aggregation distance and aggregation angle for V_i is defined as

$$DA(V_i) = \sum_{j=1}^n a(V_i, V_j) \sum_{j=1}^n d(V_i, V_j) \quad (2.42)$$

where $d(X_i, X_j)$ and $a(V_i, V_j)$ are the angle and distance measures between V_i and V_j , respectively.

From Equation (2.42), an ascending ordering of the products $DA(V_i)$'s is assumed, i.e.,

$$DA(V_{(1)}) \leq DA(V_{(2)}) \leq \Lambda \leq DA(V_{(i)}) \leq \Lambda \leq DA(V_{(n)}) \quad (2.43)$$

then the order implies the same ascending order to the corresponding vectors V_i 's, i.e.,

$$V_{(1)} \leq V_{(2)} \leq \Lambda \leq V_{(i)} \leq \Lambda \leq V_{(n)} \quad (2.44)$$

By using $V_{(1)}$ in Equation (2.44), the filter, called directional-distance filter (DDF), can be constructed.

3 FUZZY SIMILARITY MEASURE

The similarity measure is an important concept in multivariate data analysis (Bouchon et al., 1996; Santini and Jain, 1999; Yeung and Tsang, 1997). Such a measure can be used to compare two vectors in a vector space and to determine how they are similar to each other. In a vector space, both the spatial distance and the relative direction of two vectors are the similarity measures (Stark and Yang, 1998).

In this chapter, a new similarity measure between two vectors in a vector space, called fuzzy similarity measure (FSM), is introduced. It is based on both distance and direction of vectors and address the rationale of the proposed measure from the short-range ordering and fuzzification perspectives.

This chapter consists of four sections. In Section 3.1, the definition of the FSM is given. In Section 3.2, the numerical properties of the FSM are analyzed. In Section 3.3, an example to show how to use the FSM to compare the colour similarity in RGB colour space is presented. A summary about the study is given in Section 3.4.

3.1 Definition of FSM

The FSM is based on two basic assumptions: (1) short-range ordering, and (2) fuzzification on similarity relationships among vectors. The idea behind the short-range

ordering similarity among vectors is sparked by the same concept from solid physics. It is well known that the atom structure in an amorphous is short-range ordering. This phenomenon can be explained as that the interaction among atoms in an amorphous just exists among those atoms that are concentrated in a small neighbor. In other words, an atom in the amorphous is just correlated with those atoms in a neighbor around it. Similarly, this phenomenon also happens for vectors in some feature vector spaces. For example, depending on the human perception, similar colours in RGB colour space concentrate on a small neighbourhood. In addition to the short-range ordering, the similarity among vectors in some feature vector spaces is difficult to quantify and shows much more uncertainty, so the best way to characterize the similarity is to use a fuzzy based measure.

Instead of directly using both distance and angle between two vectors as their similarity measures like stated in Chapter 2, this chapter introduces the FSM which uses the distance and angle of two vectors simultaneously and models the concept of the short rank ordering and fuzzification on similarity among vectors.

Definition 3.1 Let V be a vector set. A fuzzy membership function μ ,

$$\mu : V \times V \rightarrow [0,1] \tag{3.1}$$

is called a fuzzy-based similarity measure among vectors in V if μ satisfies the following conditions:

- (a) Ascending
- (b) Convex
- (c) Identical
- (d) Symmetric.

For (a) and (c), it is easy to understand that the similarity measure between two vectors should has a larger value if they are more similar (ascending), and the measure value should be equal to 1 when two vectors are the same (identical). Convexity is explained as that given two vectors, if there exist other two vectors that locate between them, then the similarity between the latter is larger than that for the former. Symmetry emphasizes that two vectors should has the same similarity no matter their order.

In order to define a reasonable and reliable similarity measure, it is necessary to indicate the meaning of the similarity between two vectors by considering the contribution of the distance and angle between them. There may be many different ways to explain the similarity. In this study, two vectors in a vector space are considered to be similar if they have both a short distance and a small angle. Based on this idea, the fuzzy membership function described in Equation (3.1) can be defined by a mapping from the distance and angle of two vectors to the unit interval $[0, 1]$, i.e.,

$$\mu(V_i, V_j) : (d(V_i, V_j), \theta(V_i, V_j)) \rightarrow [0, 1], \quad \forall V_i, V_j \in V \quad (3.2)$$

where $d(V_i, V_j)$ and $\theta(V_i, V_j)$ are distance measure and angle measure between V_i and V_j , respectively.

And the above conditions for μ can be further stated as follows

- (e) $\mu(V_i, V_j) \leq \mu(V_k, V_l)$, if $d(V_i, V_j) \geq d(V_k, V_l)$ and $\theta(V_i, V_j) \geq \theta(V_k, V_l)$, $\forall V_i, V_j, V_k, V_l \in V$
- (f) $\mu(V_i, V_j) \leq \mu(V_k, V_l)$, $V_i, V_j, V_k, V_l \in R^m$ and $V_k, V_l \in [V_i, V_j]$
- (g) $\mu(0, 0) = 1$, and $\mu(\infty, \theta) = 0$, and
- (h) $\mu(V_i, V_j) = \mu(V_j, V_i)$, $\forall V_i, V_j \in V$

There exist many convex functions that satisfy the conditions (e)-(h) and can be selected as the fuzzy membership functions. The following equation is used in this study as the FSM.

$$\mu(V_i, V_j) = e^{-k_1 d(V_i, V_j)} \cos(k_2 \theta(V_i, V_j)) \quad (3.3)$$

where $k_1 = [0, \infty)$ and $k_2 = [0, 1]$, and $d(V_i, V_j)$ and $\theta(V_i, V_j)$ are distance and angle between V_i and V_j defined in Equations (2.15) and (2.21), respectively.

It is obvious that Equation (3.3) satisfies the above conditions (e) and (g) directly. It is also worthy of note that if Equation (3.3) is used as the definition of the FSM the condition (h) is also naturally satisfied.

Figure 3.1 explains the convexity of the FSM in 2-D case. For any two vectors V_i and V_j corresponding to points A and B in quadrant I with the distance $|AB|$ and angle ΔAOB between them. If there are other two vectors V_k and V_l corresponding to points C and D on AB, it is obvious that the distance $|CD|$ and the angle ΔCOD between V_k and V_l are less than $|AB|$ and ΔAOB , i.e., $d(V_k, V_l) \leq d(V_i, V_j)$ and $\theta(V_k, V_l) \leq \theta(V_i, V_j)$, respectively. By Equation (3.3), it can be concluded that $\mu(V_i, V_j) \leq \mu(V_k, V_l)$. It means that V_k and V_l are more similar than V_i and V_j are. Then the convexity is proved.

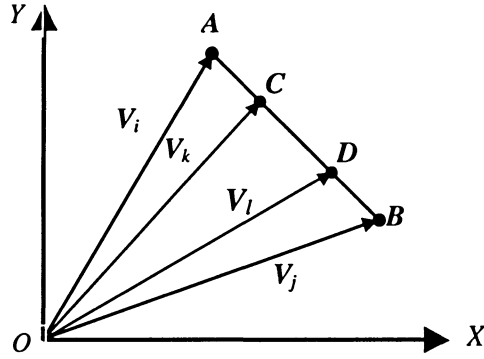


Fig. 3.1 Convexity of FSM in 2-D case.

3.2 Numerical Properties of FSM

In this section the numerical properties of the FSM is discussed. The impact of the parameter k_1 on the FSM when $k_2 = 1$ is illustrated in Figure 3.2.

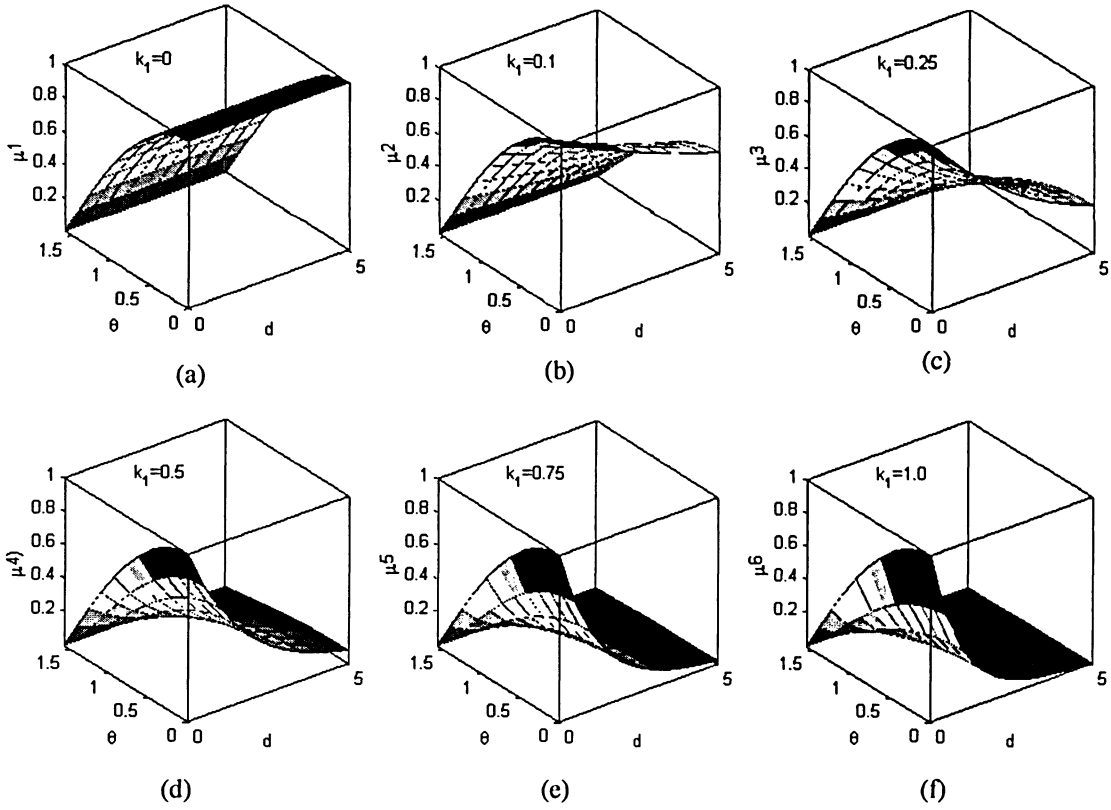


Fig. 3.2 Impact of k_1 on FSM when $k_2 = 1$.

When $k_1 = 0$, the FSM defined in (3. 3) depends only on the angle and is decreasing on θ . This case is shown in Figure 3.2(a). Figure 3.2 also illustrates that the value of the FSM is sensitive to the change of k_1 . It implies that the values of the FSM have a rapid attenuation with the slight increase of k_1 as shown in Figures 3.2(b)-(f). So the parameter k_1 can be used to decide how two vectors are similar when they are gapped by a distance d .

Figure 3.3 illustrates the impact of the parameter k_2 on the FSM when $k_1 = 1$.

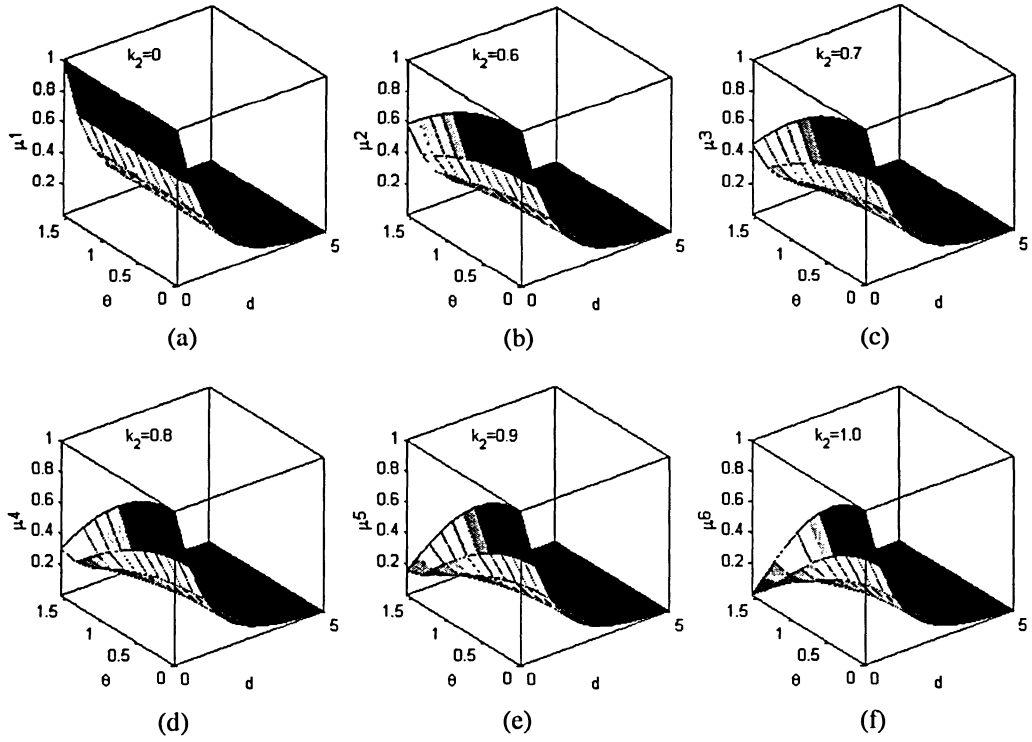


Fig. 3.3 Impact of k_2 on FSM when $k_1 = 1$.

When $k_2 = 0$, the fuzzy similarity measure depends only on the distance, which is shown in Figure 3.3(a). In this case, the values of the FSM have no relation to the angle measure θ . Figure 3.3 shows that the FSM decreases as the angle and k_2 increase.

Figure 3.4 shows the change of the FSM with the change of the parameters k_1 and k_2 , where $d = 0.5$ and $\theta = \pi/4$. Comparing with Figure 3.3, it can be observed that the value of the FSM is much more sensitive to the change of k_1 because μ has more pronounced attenuation with the increase of k_1 .

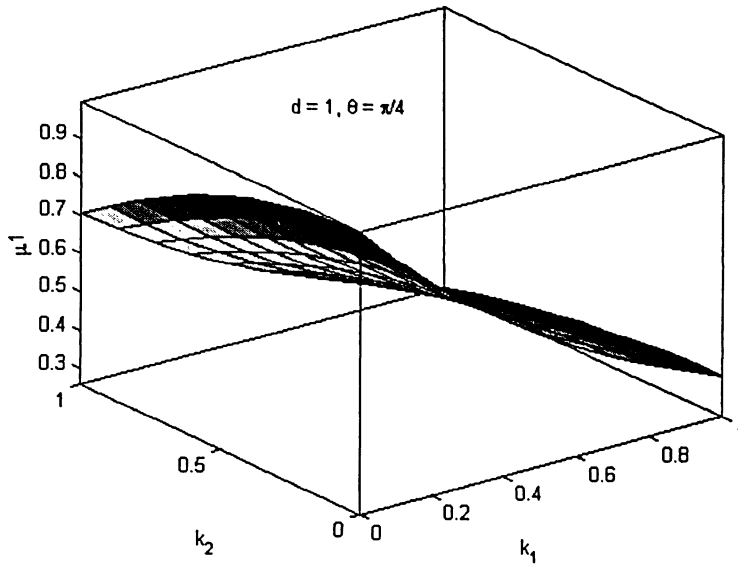


Fig. 3.4 Impact of k_1 and k_2 on FSM, when $d = 1$, $\theta = \pi/4$.

It can be concluded from the analysis of the numerical properties that the FSM can adequately characterize the short-range ordering and fuzzification of the similarity. The short-range ordering of the similarity can be explained by selecting a threshold to characterize the degree under which vectors are considered to be dissimilar or non-correlative. For each vector in a vector space there is its neighbour in which its similarity values to other vectors are larger than the given threshold. As a result, the neighbour can be called the range in which the vectors are similar. On the other hand, the range of the neighbour can be determined by the parameters k_1 and k_2 . It means that the neighbor restricted by a certain threshold will change with the different combinations of the parameters k_1 and k_2 . This can be explained as the uncertainty of the similarity.

3.3 Colour Similarity in RGB Colour Space: An Example

In this section, the FSM is applied to measure the colour similarity in RGB colour space. RGB colour space is an additive colour space. Its three primary colours (r , g , b) are combined additively to produce any desired colour. Each component of a colour is represented by a value between 0 and 255. For example, RGB value (255, 255, 255) indicates white, and (0, 0, 0) indicates black. This representation leads itself to be easily manipulated by computer systems. It also means that 16,777,216 ($=255^3 = 255 \times 255 \times 255$) colours can be represented in such a RGB colour space.

In order to demonstrate the similarity among colours, the similarity measures between the colour (204, 102, 153) and colours in three typical groups (see Figures 3.5-3.7) in RGB colour space are calculated.

The colours in Group 1 are sampled from whole RGB space by evenly dividing the RGB cube into eight bins and taking colours corresponding to the nodes of each bin. In Figure 3.5, the gray cube denotes the RGB cube, the planes surrounded by white lines are the slicing planes to cut the cube, and the planes I, II, and III are the colour planes consisted of those selected colours.

The colours in Group 2 are from a colour subspace in which the red changes from 153 to 255, the green from 51 to 153, and the blue from 102 to 204. It means that the colour subspace is a 102^3 cube. By evenly dividing the RGB colour subspace into eight bins and

taking colours according to the nodes of each bin the colours for Group 2 can be obtained. In Figure 3.6, the gray cube denotes the RGB colour subspace, the planes rounded by white lines are the slicing planes to divide the cube, and the planes, II, and III are the colour planes consisted of selected colours.

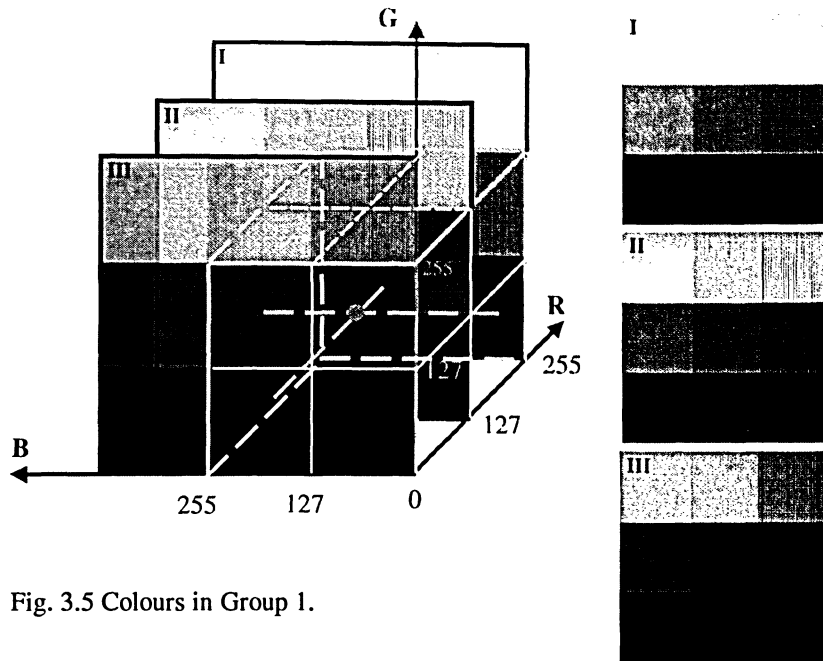


Fig. 3.5 Colours in Group 1.

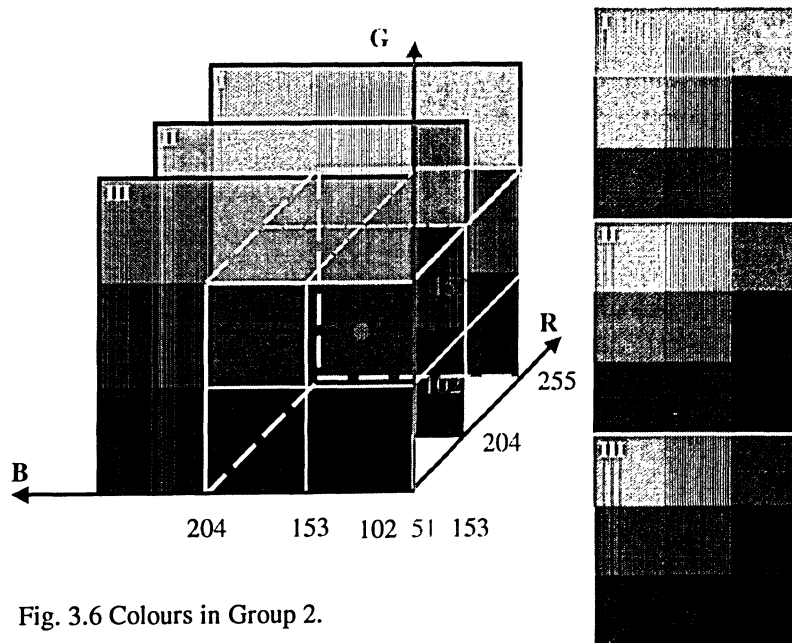


Fig. 3.6 Colours in Group 2.

The colours in Group 3 are obtained with the same way as for Group 2. The only difference is that the colour subspace for Group 3 locates from 187 to 221 for red, from 85 to 119 for green, and from 134 to 170 for blue, see Figure3.7.

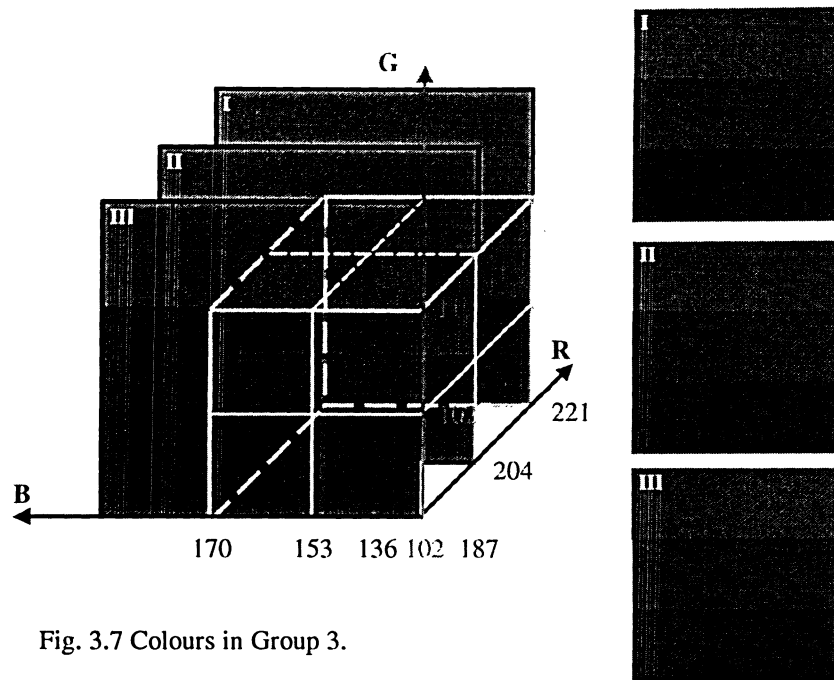


Fig. 3.7 Colours in Group 3.

The similarities between the colour (204, 102, 153) and each of selected colours are measured by the FSM. The computational results are given in Tables 3.1 and 3.2.

For all selected colours, the similarities are first computed with parameters $k_1 = 0.001$ and $k_2 = 0.2$. The results are listed in Table 3.1. The aim of this experiment is to examine whether colours similarity measured by the proposed similarity measure conforms to the human perception. Table 3.1 also shows those selected colours. By observation, the results obtained in general conform to the human perception. Of course, the human perception on colour similarity is subjective and sometimes application dependent. In Table 3.1, the colours in Group 3 have larger similarity values to the colour (204, 102,

153) than that of the colours in Group 2, since the colour subspace from which colours in Group 3 are obtained is totally embedded in that colour subspace from which colours in Group 2 are taken. As a result, the colours in Group 3 are more similar to the colour (204, 102, 153) than those in Group 2 in vision.

Table 3.1 Similarity measure values and colours in Groups 1, 2, and 3.

Group 3			Group 2			Group 1		
S	R, G, B	C	S	R, G, B	C	S	R, G, B	C
1.0000	204, 102, 153		1.0000	204, 102, 153		0.9389	255, 127, 127	
0.9831	221, 102, 153		0.9501	255, 102, 153		0.9172	127, 127, 127	
0.9831	187, 102, 153		0.9499	204, 102, 204		0.8895	255, 127, 255	
0.9831	204, 102, 170		0.9499	153, 102, 153		0.8865	255, 0, 127	
0.9831	204, 102, 136		0.9498	204, 153, 153		0.8749	127, 0, 127	
0.9831	204, 119, 153		0.9497	204, 102, 102		0.8747	127, 127, 255	
0.9831	204, 85, 153		0.9496	204, 51, 153		0.8553	255, 0, 255	
0.9762	221, 102, 170		0.9303	255, 102, 204		0.8468	255, 255, 127	
0.9762	187, 102, 136		0.9301	255, 153, 153		0.8435	255, 127, 0	
0.9762	221, 119, 153		0.9301	153, 102, 102		0.8432	127, 0, 255	
0.9762	187, 85, 153		0.9299	204, 153, 204		0.8352	127, 255, 127	
0.9762	204, 119, 170		0.9297	153, 51, 153		0.8337	127, 127, 0	
0.9761	204, 85, 136		0.9294	255, 51, 153		0.8251	255, 255, 255	
0.9761	221, 85, 153		0.9294	204, 51, 102		0.8174	255, 0, 0	
0.9761	204, 85, 170		0.9293	204, 51, 204		0.8148	127, 255, 255	
0.9761	221, 102, 136		0.9293	255, 102, 102		0.8105	127, 0, 0	
0.9761	187, 119, 153		0.9291	153, 102, 204		0.8010	0, 127, 127	
0.9761	187, 102, 170		0.9291	204, 153, 102		0.7936	255, 255, 0	
0.9761	204, 119, 136		0.9291	153, 153, 153		0.7837	0, 127, 255	
0.9710	221, 119, 170		0.9154	255, 153, 204		0.7835	127, 255, 0	
0.9710	187, 85, 136		0.9152	153, 51, 102		0.7797	0, 0, 127	
0.9708	221, 85, 170		0.9145	255, 51, 204		0.7640	0, 0, 255	
0.9708	187, 119, 136		0.9141	255, 153, 102		0.7599	0, 255, 127	
0.9708	221, 119, 136		0.9138	153, 153, 204		0.7588	0, 0, 0	
0.9708	187, 85, 170		0.9136	153, 153, 102		0.7521	0, 127, 0	
0.9708	187, 119, 170		0.9136	255, 51, 102		0.7488	0, 255, 255	
0.9708	221, 85, 136		0.9135	153, 51, 204		0.7218	0, 255, 0	

Table 3.2 lists the values of the similarities between colour (204, 102, 153) and each colour in Group 3 with the different combinations of the parameters k_1 and k_2 , i.e., $k_1 = 0.001$ and $k_2 = 0.2$, $k_1 = 0.01$ and $k_2 = 0.2$, and $k_1 = 0.0001$ and $k_2 = 0.8$. The results in Table 3.2 indicate that the similarity measure decreases as k_1 (or k_2) is increasing and more detail can be identified.

Table 3.2 Similarity measure values and colours in Group3.

$k_1 = 0.001, k_2 = 0.2$		$k_1 = 0.1, k_2 = 0.2$		$k_1 = 0.001, k_2 = 0.8$		Colours
*S	*R, *G, *B	S	R, G, B	S	R, G, B	
1.0000	204, 102, 153	1.0000	204, 102, 153	1.0000	204, 102, 153	
0.9831	221, 102, 153	0.1827	221, 102, 153	0.9827	221, 102, 153	
0.9831	187, 102, 153	0.1827	187, 102, 153	0.9826	187, 102, 153	
0.9831	204, 102, 170	0.1827	204, 102, 170	0.9824	204, 102, 170	
0.9831	204, 102, 136	0.1827	204, 102, 136	0.9823	204, 102, 136	
0.9831	204, 119, 153	0.1827	204, 119, 153	0.9822	204, 119, 153	
0.9831	204, 85, 153	0.1827	204, 85, 153	0.9821	204, 85, 153	
0.9762	221, 102, 170	0.0903	221, 102, 170	0.9759	221, 102, 170	
0.9762	187, 102, 136	0.0903	187, 102, 136	0.9758	187, 102, 136	
0.9762	221, 119, 153	0.0903	221, 119, 153	0.9755	221, 119, 153	
0.9762	187, 85, 153	0.0903	187, 85, 153	0.9752	187, 85, 153	
0.9762	204, 119, 170	0.0903	204, 119, 170	0.9750	204, 119, 170	
0.9761	204, 85, 136	0.0903	204, 85, 136	0.9747	204, 85, 136	
0.9761	221, 85, 153	0.0903	221, 85, 153	0.9741	221, 85, 153	
0.9761	204, 85, 170	0.0903	204, 85, 170	0.9740	221, 102, 136	
0.9761	221, 102, 136	0.0903	221, 102, 136	0.9740	204, 85, 170	
0.9761	187, 119, 153	0.0903	187, 119, 153	0.9739	187, 119, 153	
0.9761	187, 102, 170	0.0903	187, 102, 170	0.9739	187, 102, 170	
0.9761	204, 119, 136	0.0903	204, 119, 136	0.9739	204, 119, 136	
0.9710	221, 119, 170	0.0526	221, 119, 170	0.9708	221, 119, 170	
0.9710	187, 85, 136	0.0526	187, 85, 136	0.9707	187, 85, 136	
0.9708	221, 85, 170	0.0526	221, 85, 170	0.9687	221, 85, 170	
0.9708	187, 119, 136	0.0526	187, 119, 136	0.9681	187, 119, 136	
0.9708	221, 119, 136	0.0526	221, 119, 136	0.9680	221, 119, 136	
0.9708	187, 85, 170	0.0526	187, 85, 170	0.9676	187, 85, 170	
0.9708	187, 119, 170	0.0526	187, 119, 170	0.9676	187, 119, 170	
0.9708	221, 85, 136	0.0526	221, 85, 136	0.9674	221, 85, 136	
* S = Similarity; R = Red; G = Green; B = Blue.						

Comparing the similarity values of columns 1, 4, and 7 in Table 3.1 and selecting a threshold (for example, 0.97), if the values of the similarities is smaller than this threshold the colours are considered to be dissimilar, then the range of short-range ordering for the similarity can be determined to be the cube corresponding to the colours in Group 1. And by observing the similarity measures in columns 1, 3, and 5 in Table 3.2,

the similarity measures change for the same colour. The phenomenon indicates the fuzzification of the FSM.

3.4 Chapter Summary

In this chapter, the scheme for measuring the similarity among vectors in a feature vector space has been presented. Under two basic assumptions on similar relationship of vectors: short-range ordering and fuzzification and by using both distance and angle of vectors, the similarity measure between two vectors is defined and its numerical properties are studied. Experimental results have shown that the similarities for colours in RGB colour space obtained by the similarity measure coincide with that from human perception. In the following chapters of this thesis the proposed similarity measure will be used to define colour morphology, fuzzy clustering and multivariate filtering algorithms.

4 COLOUR MORPHOLOGY BASED ON FSM

In this chapter, the colour morphology is defined by using the FSM proposed in the previous chapter. The properties of the colour morphology are also given. To demonstrate the application of the colour morphology to colour image processing, an edge extractor focused on the detection of colour edges is designed.

4.1 Introduction

Mathematical morphology has been widely used in image processing community (Serra, 1982; Sternberg, 1986; Dougherty, 1992; 1994; Haralick et al., 1992). This is not only due to its rigorous mathematical theory (Heijmans and Ronse, 1990), such as set theory (Tourelakis, 2003), fuzzy set theory (George and Bo, 1995; Klir and Yuan, 1995), topology (Cain, 1994), and lattice theory (Wechler, 1992), but also its powerful utilities in image analyses, such as image filtering (Heijmans, 1996b; Pessoa and Maragos, 1996; Schonfeld, 1996; Mehnert and Jackway, 2000), image segmentation (Beacher, 1996; Meyer, 1996; Bieniek and Moga, 1998; D'Ornellas and Boomgaard, 2000; Pesaresi and Benediktsson, 2000), image measurement (Serra, 1982), image sequence analysis (Demarty, 1996; Gu, 1996), and image texture analysis (Auber et al., 2000). Generally speaking, mathematical morphology uses morphological operations to analyze and recognize geometric properties and structures of objects in images. Mathematical morphology has been well developed and used as a complete and efficient tool to analyze

the spatial organization in binary and grayscale images. It can be categorized into binary morphology and grayscale morphology.

From both practical and theoretical point of view, colour morphology should be of great interest. Firstly, it is well known that colours play a significant role in human visual perception and is heavily relevant to remote sensing image processing when multi-spectral and hyper-spectral images become widely available (Sharma and Trussel, 1997). By contrast with binary and grayscale imagery, colour imagery contains more information which can be used to simplify image analysis, e.g., object identification and extraction based on colour attributes (Ohta et al., 1980). Therefore, it is necessary to develop efficient techniques to analyze colour images directly. Secondly, since both binary and grayscale morphology are intended to analyze binary and grayscale imagery, respectively, it would be of interest, from the theoretical point of view, to extend morphological theory to colour morphology for directly processing of colour imagery.

The simplest scheme for extending grayscale morphology to colour morphology is to treat a colour image as three independent monochrome images corresponding to its three components, and then to utilize grayscale morphological operators to deal with each colour component. Unfortunately, this procedure has some drawbacks. For example, it produces new colours that are not contained in the original image and loses the correlations among the components. Vector morphological techniques involving these correlations have been developed (Comer and Del, 1998; Talbot et al., 1998; Vardavoulia et al., 2002). These algorithms are based on the concepts of ranking multivariate data

(Barnett, 1976; Mardia, 1976; Mardia et al., 1979). In other words, they require an appropriate colour ordering scheme to define colour morphological operations that can retain the basic properties of their grayscale counterparts. Unfortunately, ordering vectors is not straightforward, because there is no notion of the natural ordering in a vector space as in one dimension case. On the other hand, it seems that the similarity is more essential and significant than the order to characterize the correlation between vectors in a feature vector space.

In this chapter, novel colour morphology is introduced. The proposed colour morphology is based on the assumption, i.e., the colours represent an object in colour imagery are much more similar than those for other objects. In fact, it is true for most of scenes. Under the above assumption, the proposed morphological operations should be able to smooth the colours in the same object and at the same time “shrink” or “expand” the objects to detect their geometric structure. By using the FSM proposed in Chapter 3, the infimum and supremum operations are firstly defined. On the basis of the infimum and supremum operators, the fundamental colour morphological operations (erosion, dilation, opening, and closing) are defined. As an application of the proposed colour morphology, edge detectors for extracting edges in colour images are designed by using the colour morphological operations and post-processing algorithms.

4.2 Infimum and Supremum Operators Based on FSM

Let X represent an arbitrary m -dimensional vector subset of a vector set V on R^m , which includes n vectors, i.e., $X = \{X_1, X_2, \dots, X_i, \dots, X_n\}$, $X_i = [X_{i1}, X_{i2}, \dots, X_{im}]$. The most dissimilar vector pair, called max-min vector pair (X_{max}, X_{min}) , induced in X , consists of two vectors between which the value of the FSM is minimum comparing to the values for all possible vector pairs in $X \times X$, that is,

$$(X_{max}, X_{min}) = (X_i, X_j) \left| \mu(X_i, X_j) = \min_{1 \leq k, l \leq n} \mu(X_k, X_l) \right. \quad (4.1)$$

The maximum vector X_{max} and minimum vector X_{min} in the max-min vector pair (X_{max}, X_{min}) are defined as one with larger magnitude and another with smaller magnitude, i.e.,

$$X_{max} = X_i \left| X_i, X_j \in (X_{max}, X_{min}), \|X_i\| \geq \|X_j\| \right. \quad (4.2)$$

$$X_{min} = X_i \left| X_i, X_j \in (X_{max}, X_{min}), \|X_i\| \leq \|X_j\| \right. \quad (4.3)$$

where $\|\cdot\|$ is a norm chosen as the measure of the magnitude of a vector.

According to the FSM proposed in Chapter 3 and the maximum and minimum vectors defined above, all vectors in X can be classified as two classes $CL1$ and $CL2$, called the similar vector class. For any vector $X_i \in X$, if the value of the FSM between X_i and X_{min}

is larger than that between X_i and X_{max} , then X_i belongs to $CL1$. Otherwise, the vector belongs to $CL2$, i.e.,

$$CL1 = \{X_i \mid \mu(X_i, X_{min}) \geq \mu(X_i, X_{max}), \forall X_i \in X\} \quad (4.4)$$

$$CL2 = \{X_i \mid \mu(X_i, X_{max}) \geq \mu(X_i, X_{min}), \forall X_i \in X\} \quad (4.5)$$

The most similar vectors X_{CL1} in $CL1$ and X_{CL2} in $CL2$ are determined by

$$X_{CL1} = X_i \mid X_i \in CL1 \text{ and } \sum_{j=1}^{|CL1|} \mu(X_i, X_j) = \max_{1 \leq k \leq |CL1|} \left\{ \sum_{j=1}^{|CL1|} \mu(X_k, X_j) \right\} \quad (4.6)$$

$$X_{CL2} = X_i \mid X_i \in CL2 \text{ and } \sum_{j=1}^{|CL2|} \mu(X_i, X_j) = \max_{1 \leq k \leq |CL2|} \left\{ \sum_{j=1}^{|CL2|} \mu(X_k, X_j) \right\} \quad (4.7)$$

where $|CL1|$ and $|CL2|$ are the numbers of vectors in $CL1$ and $CL2$, respectively.

Figure 4.1 provides the illustration of above definitions on max-min vector pair, similar vector classes, and the most similar vectors. The vector subset used in this example consists of 16 2-D vectors. In this example, only the direction and length of vectors are considered as the features to judge the similarity. The colours of vectors are just for the purpose of the explanation.

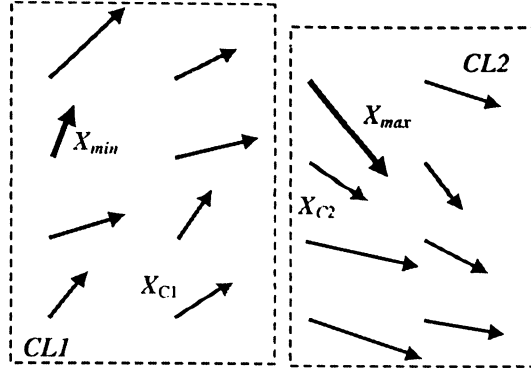


Fig. 4.1 Definitions of max-min vector pair, similar vector classes, and the most similar vectors.

As shown in Figure 4.1, the bold blue and bold red vectors are two most dissimilar vectors in terms of their length and direction in all possible vector pairs. Then the two vectors are selected as the max-min vector pair. In this vector pair, the red vector is longer than the blue one, so the red vector is defined as the maximum vector and blue one as the minimum vector. It is obvious that all blue vectors are more similar to the minimum vector and all red ones are more similar to the maximum vector with respect to both their lengths and directions. Therefore, all blue vectors belong to $CL1$ and all red vectors belong to $CL2$. According to the defined similarity measure, the light blue vector has the maximum aggregation similarity with all other seven vectors in $CL1$, so the vector is the most similar vector in $CL1$. Similarly, the light red vector is the most similar vector in $CL2$.

Using the most similarity vectors in two vector classes described above, the infimum operator \wedge in X can be defined by

$$\wedge X = \wedge\{X_1, X_2, \dots, X_n\} = X_{CL1} \quad (4.8)$$

From Equation (4.8), it is obvious that the operator \wedge outputs the so-called “most centrally located” vector in $CL1$, which has the maximum sum of the values of the FSM between X_{CL1} and each vector in $CL1$.

In the same way, the supremum operator \vee is defined by

$$\vee X = \vee\{X_1, X_2, \dots, X_N\} = X_{CL2} \quad (4.9)$$

Thus, the \vee operator results in the most centrically located vector in $CL2$, which has the minimal sum for the values of the FSM between X_{CL2} and each vector in $CL2$.

The infimum and supremum operators defined above are vector preserving, i.e.,

$$\forall X \subseteq V, \exists X_{CL1}, X_{CL2} \in X, \text{ such that } \wedge X = X_{CL1} \text{ and } \vee X = X_{CL2} \quad (4.10)$$

Furthermore, the two operators can be used to define the colour morphological operations, which will be discussed in next section.

4.3 Colour Morphological Operations

4.3.1 Definition

According to the supremum and infimum operators defined above, the colour morphological operations can be defined as follows.

Definition 4.1 Let CI be a colour image and W be a window centered at pixel p and the colours of all pixels in W form the vector subset W_p . The colour dilation δ_{CI}^{wp} , erosion ε_{CI}^{wp} , closing χ_{CI}^{wp} , and opening o_{CI}^{wp} of CI are the colour images given respectively by

$$\delta_{CI}^{wp} = \{\vee W_p, \forall p \in CI\} \quad (4.11)$$

$$\varepsilon_{CI}^{wp} = \{\wedge W_p, \forall p \in CI\} \quad (4.12)$$

$$\chi_{CI}^{wp} = \varepsilon_{CI}^{wp}(\delta_{CI}^{wp}) \quad (4.13)$$

$$o_{CI}^{wp} = \delta_{CI}^{wp}(\varepsilon_{CI}^{wp}) \quad (4.14)$$

The overall characteristics of the colour morphological operations are similar to that in grayscale case. For example, the colour erosion eliminates ‘dark’ details, enhances ‘light’ details, reduces ‘dark’ objects and enlarges ‘light’ objects, while the colour dilation

eliminates 'light' details, enhances 'dark' details, reduces 'light' objects, and enlarges 'dark' objects. The colour opening typically eliminates 'dark' details, and the colour closing eliminates 'light' objects

4.3.2 Illustration

In this section, the proposed morphological operations are illustrated (see Figure 4.2). For simplification, all operations are just used on a small region. The window size for all morphological operations is 3×3 . The parameters k_1 and k_2 for the FSM are 0.001 and 0.8, respectively.

Figure 4.2a shows a colour aerial image with the size of 150×150 pixels and 1 *m* resolution. Figure 4.2b1 is the small region centred at pixel point (30, 100) with the size of 15×15 pixels framed by the red square shown in Figure 4.2a. This region is enlarged by increasing the area of each pixel to $10 \times 10 = 100$ times (see Figure 4.2b2) and increasing the number of pixels to $10 \times 10 = 100$ pixels by interpolating pixels (see Figure 4.2b3). The scene in this small region consists of four colour objects. The gray corresponds to roads, the white to curbs, the dark green to trees, and the black to shadows. Figures 4.2c1, d1, e1, and f1 show the results of the colour morphological operations: dilation, erosion, closing, and opening, respectively. And also, these images are enlarged by the same ways as Figure 4.2b1 and the enlarged images are shown in Figures 4.2c2 and c3, d2 and d3, e2 and e3, and f2 and f3, respectively.

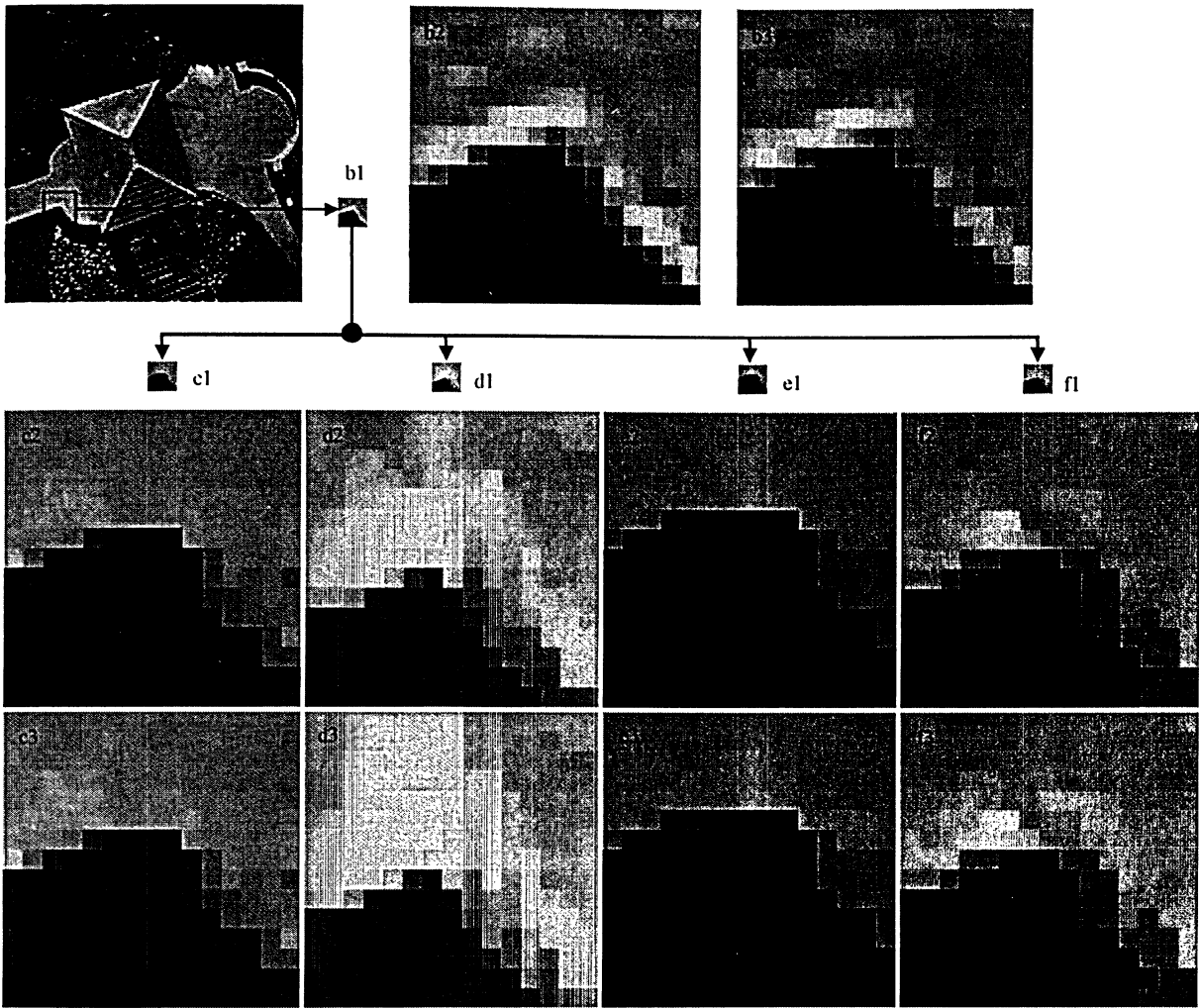


Fig. 4.2 Illustration of proposed morphological operations

It is observed from Figures 4.2c1, c2, and c3 that after dilation shadows (in black) expand toward trees (in green), trees expand toward curbs (in white), and roads (in gray) also expand toward curbs. As a result, curbs are compressed. On the other hand, the colours of each object look much smoother. Figures 4.2d1, d2, and d3 show the results from the erosion operation that is the reverse process from the dilation operation. Curbs expand toward both roads and trees, and trees expand toward shadows. It can also be observed that the colours become smoother in each object. The closing (opening) operation is similar to the dilation (erosion) operation (see Figures 4.2e1, e2, e3, 3f1, f2, and f3).

4.3.3 Properties

In order to evaluate the impact of the parameters k_1 and k_2 in Equation (3.3) on the performance of the colour morphological operators, the different combinations of the parameters k_1 and k_2 are used for all colour morphological operators.

Figure 4.3 shows a colour Ikonos image with the size of 150×150 pixels and 1 m resolution, which covers a typical residential area in Toronto, Ontario.



Fig. 4.3 Colour Ikonos image.

Figures 4.4 - 4.7 show the results obtained by using the colour morphological operations on Figure 4.3 with the different combinations of the parameters k_1 and k_2 listed in Table 4.1.

Table 4.1 Parameters used in colour morphological operators

Parameters	Figures 4.4 - 4.7								
	a1	a2	a3	b1	b2	b3	c1	c2	c3
k_1	0.01	0.01	0.01	0.005	0.005	0.005	0.001	0.001	0.001
k_2	0.2	0.5	0.8	0.2	0.5	0.8	0.2	0.5	0.8

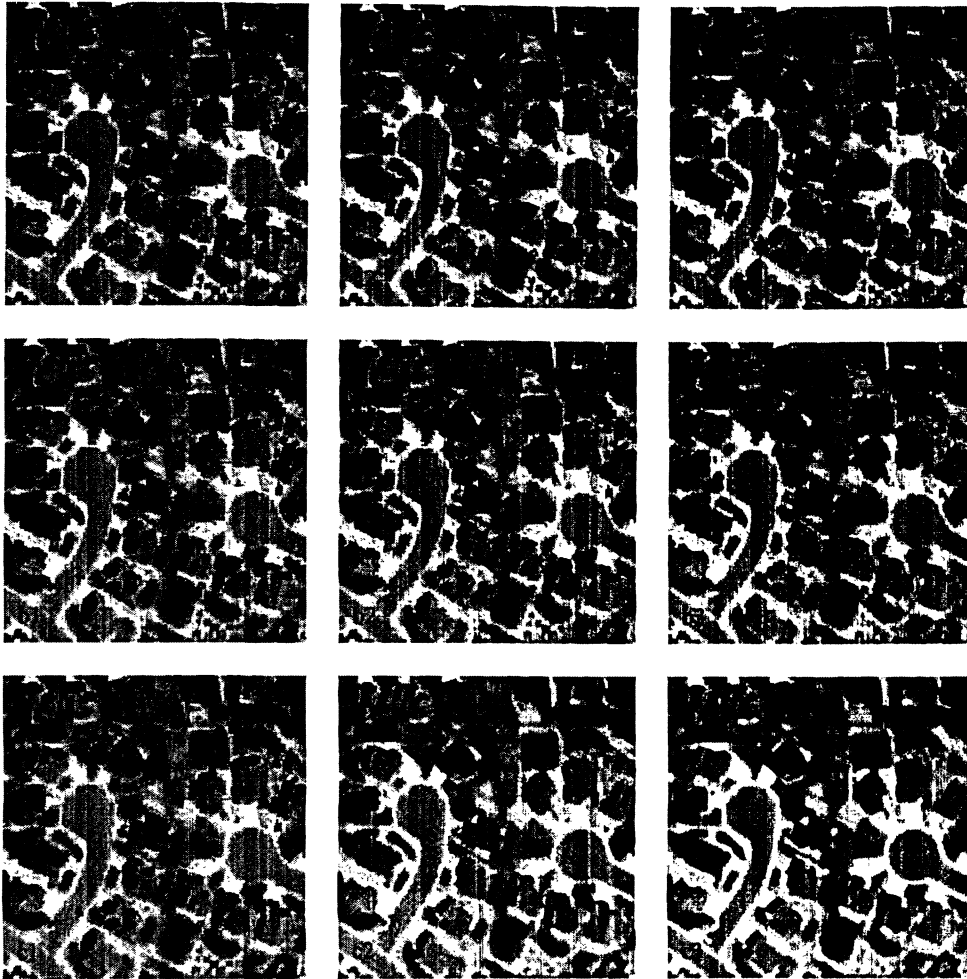


Fig. 4.4 Dilation with parameters in Table 4.1.

The results reveal the effects of the parameters k_1 and k_2 on the colour morphological operators. Though the colour morphological operators are based on the same concept, they have different results when using different parameters. The simple reason is that the different similarity degrees can be available under different combinations of the parameters to quantify similarity among the colour vectors.

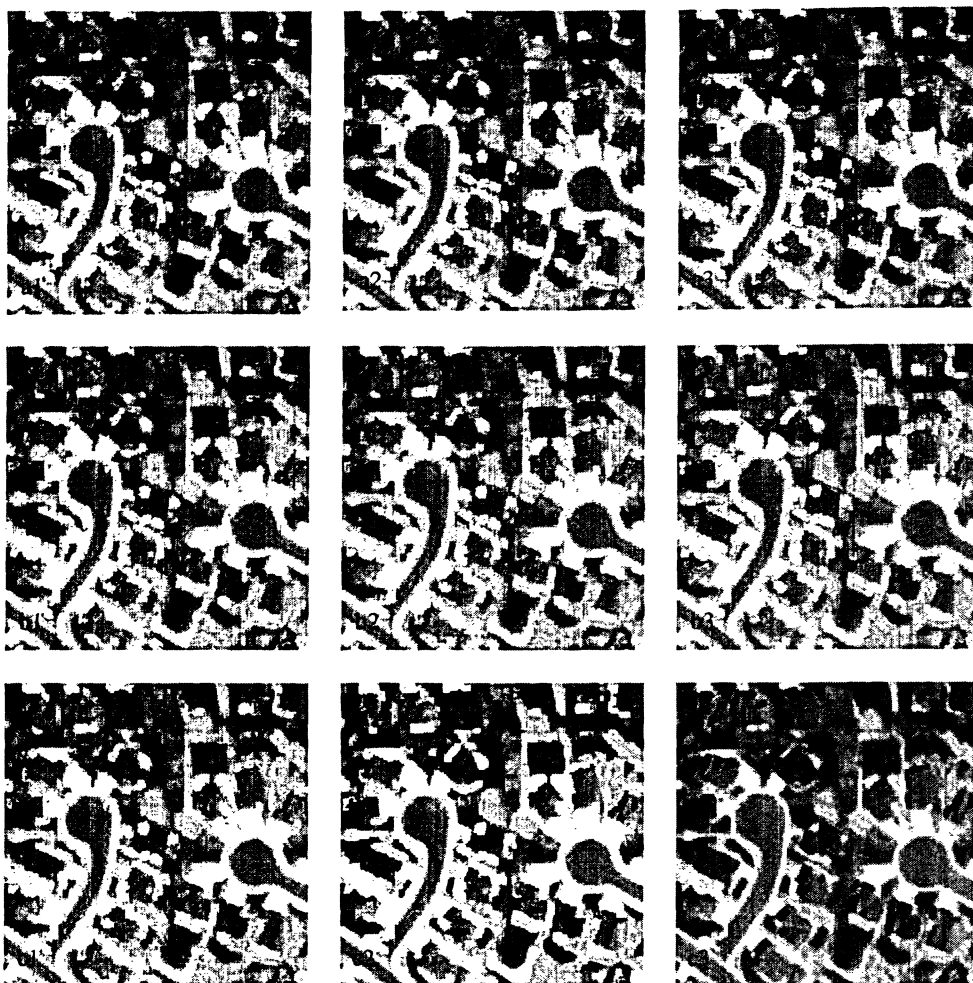


Fig. 4.5 Erosion with parameters in Table 4.1.

For the results presented in Figures 4.4 - 4.7, the following conclusions can be drawn by subjective evaluation.

- All four morphological operators (dilation, erosion, closing, and opening) are optimum when $k_1 = 0.001$, $k_2 = 0.8$ (see Figures 4.4 (c3) - 4.7 (c3)) from the point of view of smoothing objects and preserving edges.

- With the decrease of k_1 and the increase of k_2 , the performances of all morphological operators can be improved evidently and they are more sensitive to the change of k_1 than the change of k_2 .
- With decrease of k_1 and the increase of k_2 the similarity between the dilation image and erosion image increases.
- The objects are shrunk or expanded and the colours in an object become smoother after the colour morphological operations.

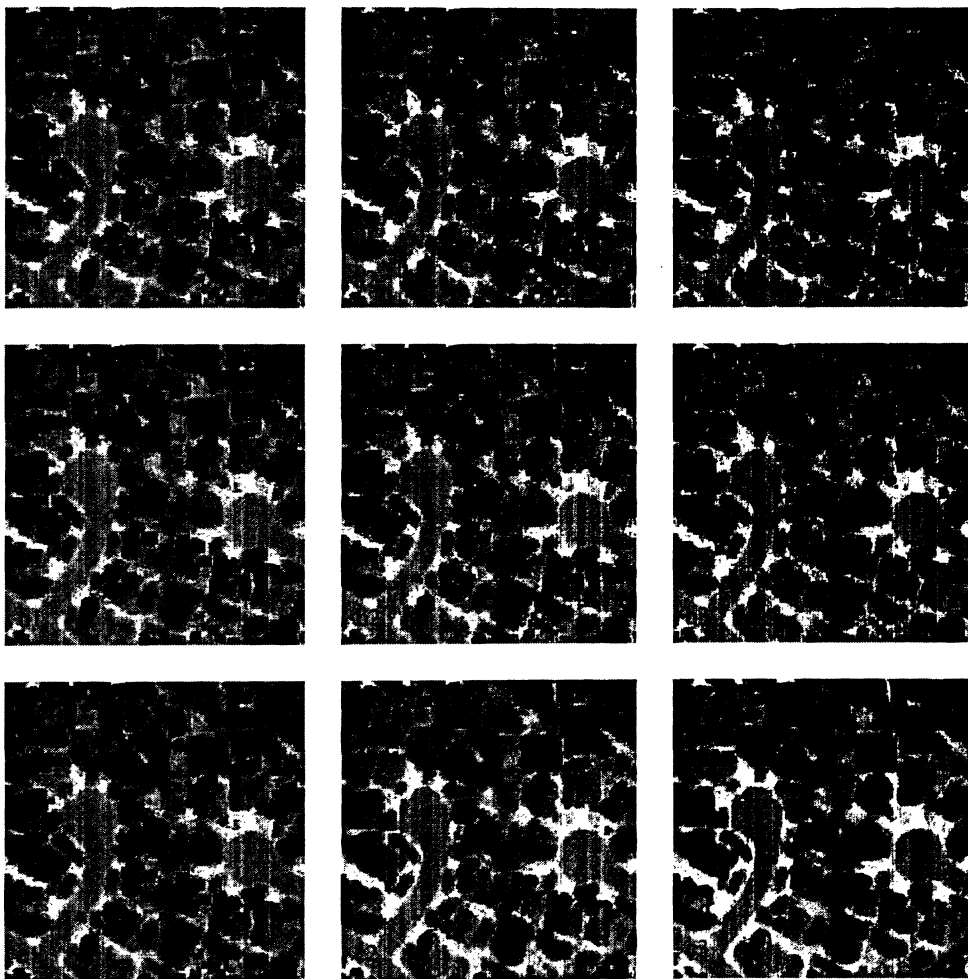


Fig. 4.6 Closing with different parameters listed in Table 4.1.

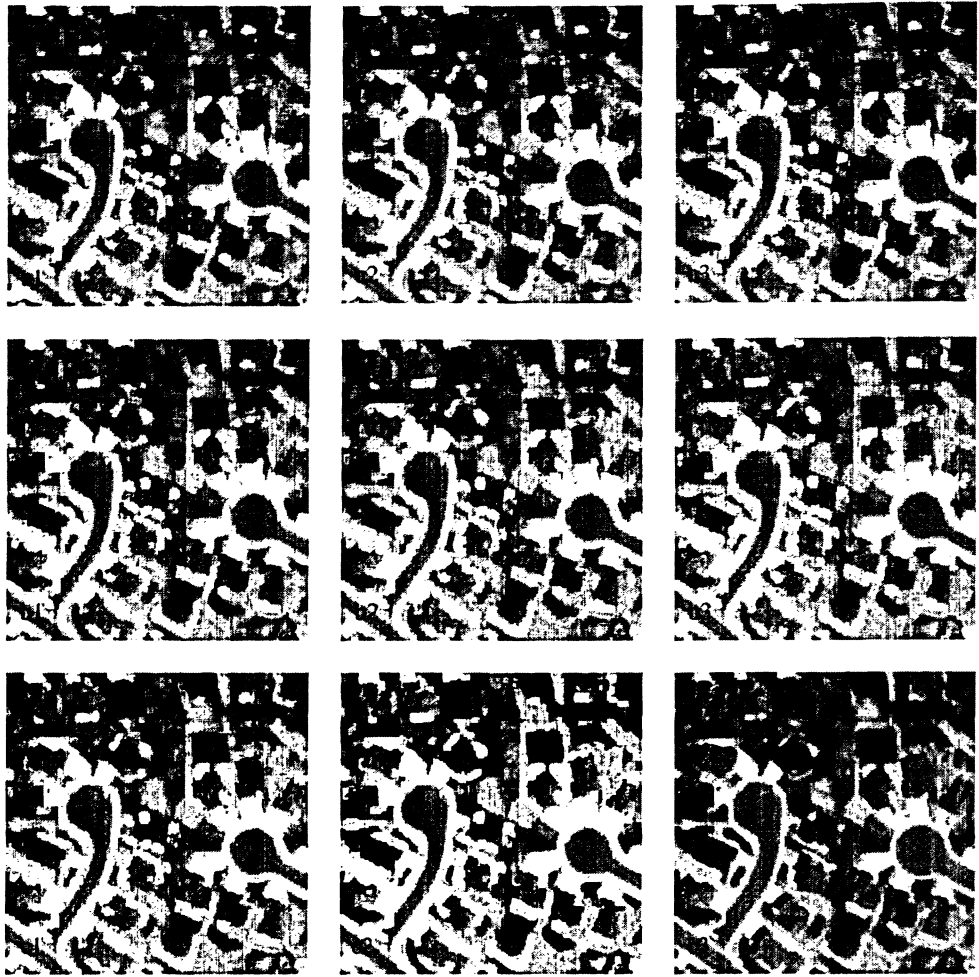


Fig. 4.7 Opening with parameters in Table 4.1.

4.4 Colour Edge Detection

In this section, a colour edge detection method based on the colour morphological operations is presented. The proposed method creates a binary edge image that results from the similarity between a pair of morphological images. In this method, colour edges are detected by three consequent stages. In the first stage, a pair of morphological operations are chosen, which extends and reduces the contours of objects in the colour image efficiently. In the second stage, the similarity between the resultant images of two

chosen operations is calculated by using the FSM between two colour images. In the last stage, a threshold, which controls the dissimilarity between two colour vectors, is determined to extract colour edges. A block diagram for the proposed colour edge extractor is shown in Figure 4.8.

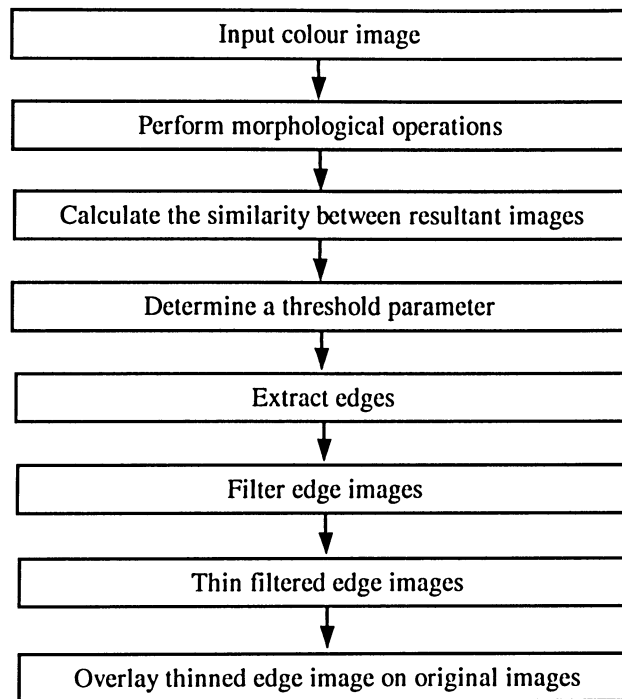


Fig. 4.8 Block diagram of the colour edge extractor.

4.4.1 Definition of Colour Edge

Generally, the edges of the objects in a grayscale image can be defined as the discontinuities of the brightness. However, the situation is different in colour images. Several definitions of colour edges have been proposed (Pratt, 1991). First, a colour edge can be said to exist if and only if the luminance field contains an edge, i.e., the discontinuities of the luminances. This definition ignores discontinuities in the hue and

saturation that occur in regions of constant luminance. The second way to define colour edges is to check if the edges exist in any primary components. The third definition is based on forming the sum of the gradients of the primary values. A colour edge is said to exist if the gradient exceeds a threshold. In this study, a potential colour edge is defined as the discontinuities of neighbor vectors in the vector field representing the colour image shown in Figure 4.9, in which pink line and orange line indicate two typical colour edges.

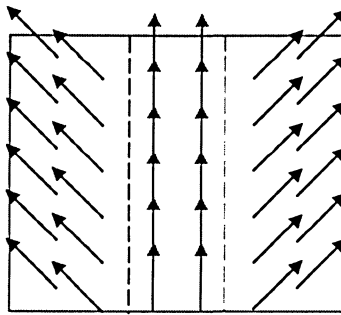


Fig. 4.9 Definition of colour edge.

Grayscale erosion and dilation have been successfully applied to extract the edges in grayscale images based on the subtraction of these two morphological images (Lee et al., 1987; Dougherty, 1994). However, these algorithms cannot be applied directly to colour images by means of the difference of colour erosion and dilation, since the subtraction of two colours in RGB colour space does not make sense. In order to define an efficient colour edge extractor by using the colour morphological results, it is necessary to introduce the method to compare two colour images.

4.4.2 Similarity Measure between Two Colour Images

According to the similarity measure between two colour vectors, the similarity measure between two images can be stated as follows.

Let $\mu(V_i, V_j)$ be the value of the FSM between two colour vectors V_i and V_j in RGB colour space and $CI1$ and $CI2$ be two colour images with n pixels denoted by the vector sets $V_{CI1} = \{V_{CI1}^1, V_{CI1}^2, \Lambda, V_{CI1}^n\}$ and $V_{CI2} = \{V_{CI2}^1, V_{CI2}^2, \Lambda, V_{CI2}^n\}$, respectively. The similarity measure between V_{CI1} and V_{CI2} is defined as a scalar set on $[0, 1]$, called similarity set M .

$$\begin{aligned} M(V_{CI1}, V_{CI2}) &= \{M_1, M_2, \Lambda, M_n\} \\ &= \{\mu(V_{CI1}^1, V_{CI2}^1), \mu(V_{CI1}^2, V_{CI2}^2), \Lambda, \mu(V_{CI1}^n, V_{CI2}^n), \} \end{aligned} \quad (4.15)$$

where M_p , $p = 1, 2, \dots, n$, is the value of the FSM between two colour vectors from $CI1$ and $CI2$ for pixel p .

4.4.3 Fuzzy Similarity Edge Extractor

Based on the previous discussion on the similarity measure between two colour images, the fuzzy similarity edge extractor (FSEE) is constructed by thresholding the values of the similarity measure between two morphological images.

Let $\alpha \in [0,1]$ be the threshold to indicate the similarity between two colour vectors. The FSEE is defined as the scalar set as follows.

$$FSEE = \{FSEE_i | FSEE_i = 1, \text{ if } M_i \leq \alpha; \text{ and } FSEE_i = 0, \text{ if } M_i > \alpha\} \quad (4.16)$$

where $FSEE_i = 1$ indicates colour edges.

Figure 4.10 illustrates the rationality of the extractor. The colour image shown in Figure 4.10a consists of two objects (one in red and another in blue). Though the colours of the single object are not very smooth, they still have much more similarities to each other compared to the colours of another object. The green line is the edge or boundary of two objects. When considering an edge, the pixels corresponding to the edge is dependent upon the size of a used window. For example, if a 3×3 window is used those pixels beside the two sides of a boundary will be processed as the so-called edge pixels (for example, pixels 2 and 3 in Figure 4.10). Other pixels except for edge pixels are called object pixels (pixels 1 and 4). For simplification, four typical pixels, framed by light blue lines, are chosen to make the illustration. Figures 4.10b and 4.10c show the results of dilation and erosion, respectively. For object pixels, though the two dual morphological operations chose different pixels in the windows around the object pixels (for example, the windows framed by yellow lines in Figure 4.10) as their outputs, the two kinds of resultant pixels are still very similar because they belong to the same object, for example, the pixel 1b (see Figure 4.10b) and the pixel 1c (see Figure 4.10c), the pixel 4b (see Figure 4.10b) and the pixel 4c (see Figure 4.10c). For edge pixels, the situation would be

totally different. If a morphological operation tries to select the pixel belonging to one object its dual one will select other one belonging to another object, because the pixels in the window corresponding to an edge pixel come from two objects separated by the edge. As a result, the resultant pixels of two dual operations have less similarity to each other. The examples are the pixel 2b (see Figure 4.10b) and the pixel 2c (see Figure 4.10c), the pixel 3b (see Figure 4.10b) and pixel 3c (see Figure 4.10c).

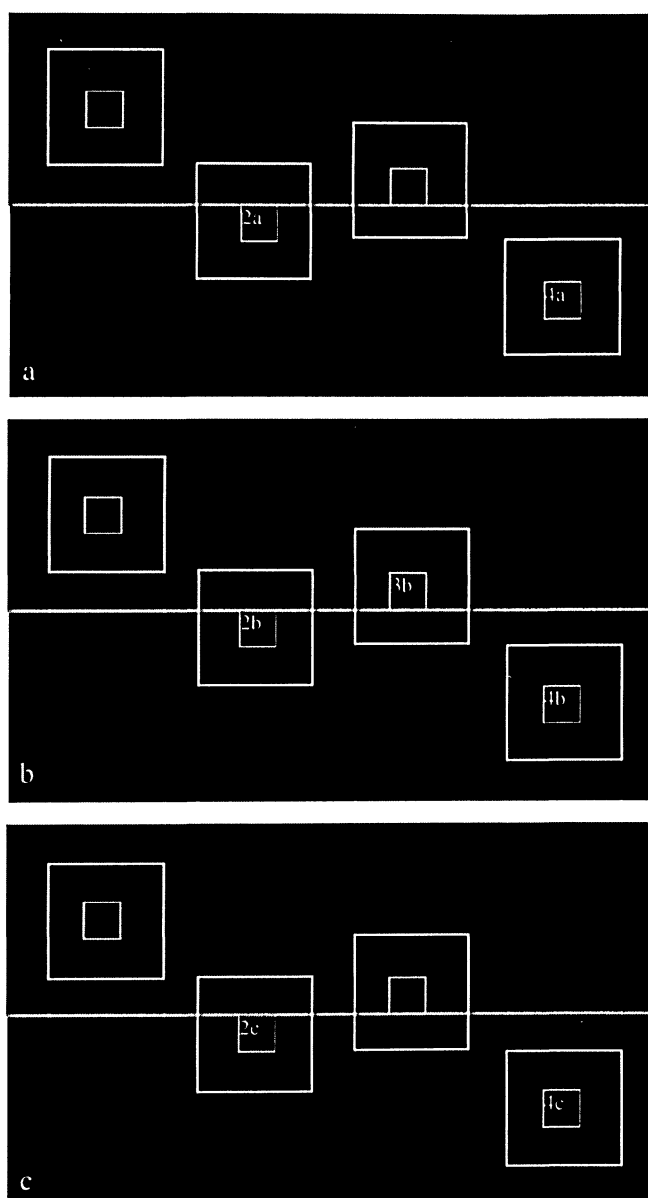


Fig. 4.10 Illustration of FSEE.

4.4.4 Experimental Results and Discussions

Experiments using QuickBird, Ikonos, and aerial images have been conducted. Three test images are shown in Figure 4.11. Each has 24 bits per pixel and 150×150 in size. The window size for morphological operations is 3×3.

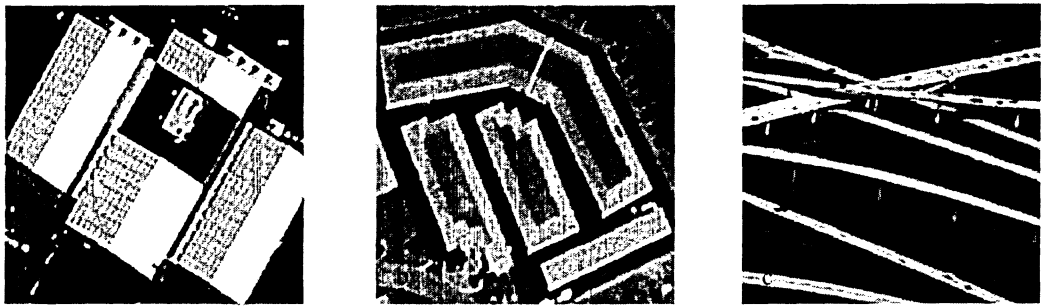


Fig. 4.11 Original images: (a) QuickBird, (b) Ikonos, and (c) aerial images.

In this experiment, parameters k_1 and k_2 for all morphological operators are taken as 0.001 and 0.2, and k_1 and k_2 for similarity measures between images are also set as 0.001 and 0.2, respectively, to design the FSEE.

To design an edge detector, the first step is to select a pair of suitable morphological operations. According to the resultant images of morphological operations shown in Figure 4.12, the pair of dilation-original images is chosen to construct the FSEE. In Figure 4.12, (a), (b), and (c) show QuickBird, Ikonos, and aerial images, respectively, while (1), (2), (3), and (4) show the results of dilation, erosion, closing, and opening, respectively.

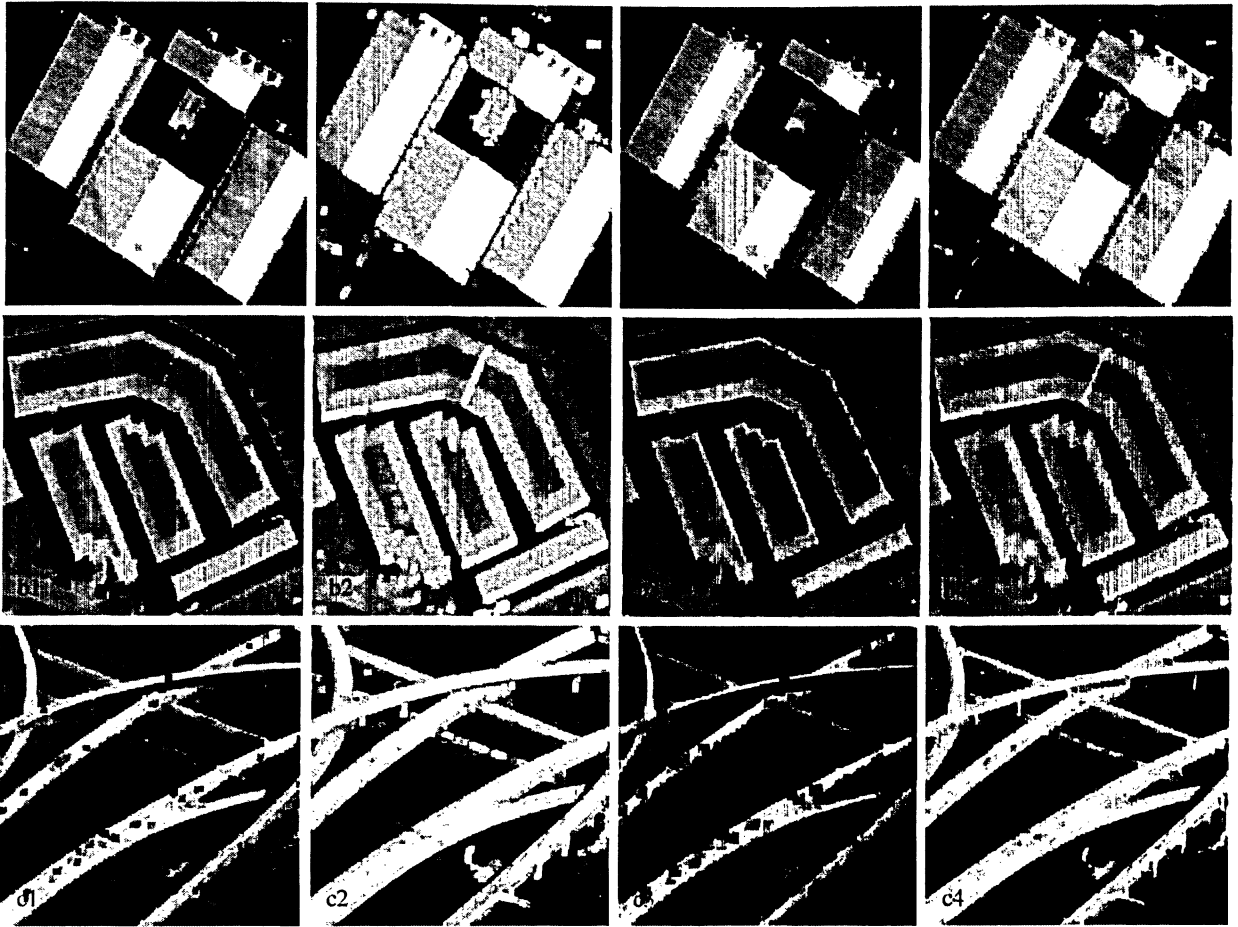


Fig. 4.12 Result of morphological operations.

By using Equation (4.15), the similarity set for the selected image pair can be calculated. Actually, this set includes all information about the edges in the processed image from similarity point of view. The set is shown in two ways. In the profile curve (see Figure 4.13), the value of the colour similarity corresponding to each pixel is demonstrated by a height. In the grayscale image (see Figure 4.14), the values are used to indicate a grayscale.

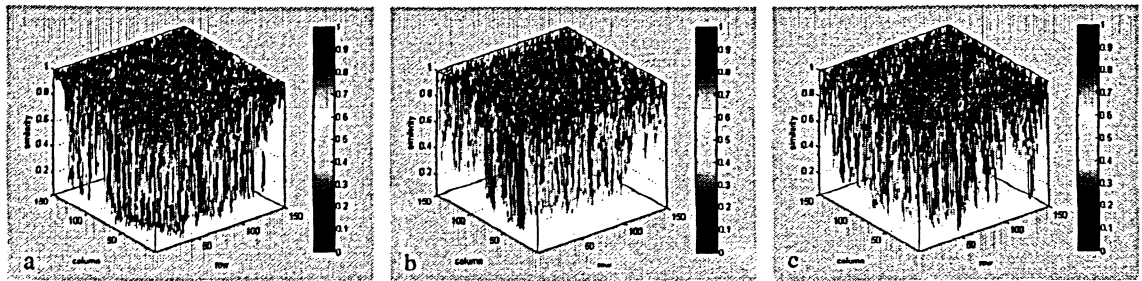


Fig. 4.13 Profile curves of similarity measure between selected images pair for (a) QuickBird, (b) Ikonos, and (c) aerial images.



Fig. 4.14 Grayscale images of similarity measure between selected images pair for (a) QuickBird, (b) Ikonos, and (c) aerial images.

In order to extract the edges of interest, it is necessary to give a suitable threshold. For comparison, three thresholds are chosen to extract different edge details. Table 4.2 lists the selected morphological operation pairs and thresholds obtained by analyzing the results illustrated in Figures 4.13 and 4.14.

Table 4.2 Morphological operation pairs and thresholds

Colour images	Morphological operation pair	Thresholds
QuickBird	Dilation-Original	0.5, 0.6, and 0.7
Ikonos	Dilation-Original	0.5, 0.6, and 0.7
Aerial	Dilation-Original	0.5, 0.6, and 0.7

Using these thresholds listed in Table 4.2 to Equation (4.16), the FSEE can be constructed. The edge images of the test images obtained by the FSEE are shown in Figures 4.15. It can be observed from Figure 4.15 that more and more edges can be detected with the increase of the thresholds. In Figures 4.15, 4.16, and 4.17, (a), (b), and (c) show the results on QuickBird, Ikonos, and aerial images, respectively, and the results of (1), (2), and (3) are obtained by using thresholds 0.5, 0.6, and 0.7, respectively.

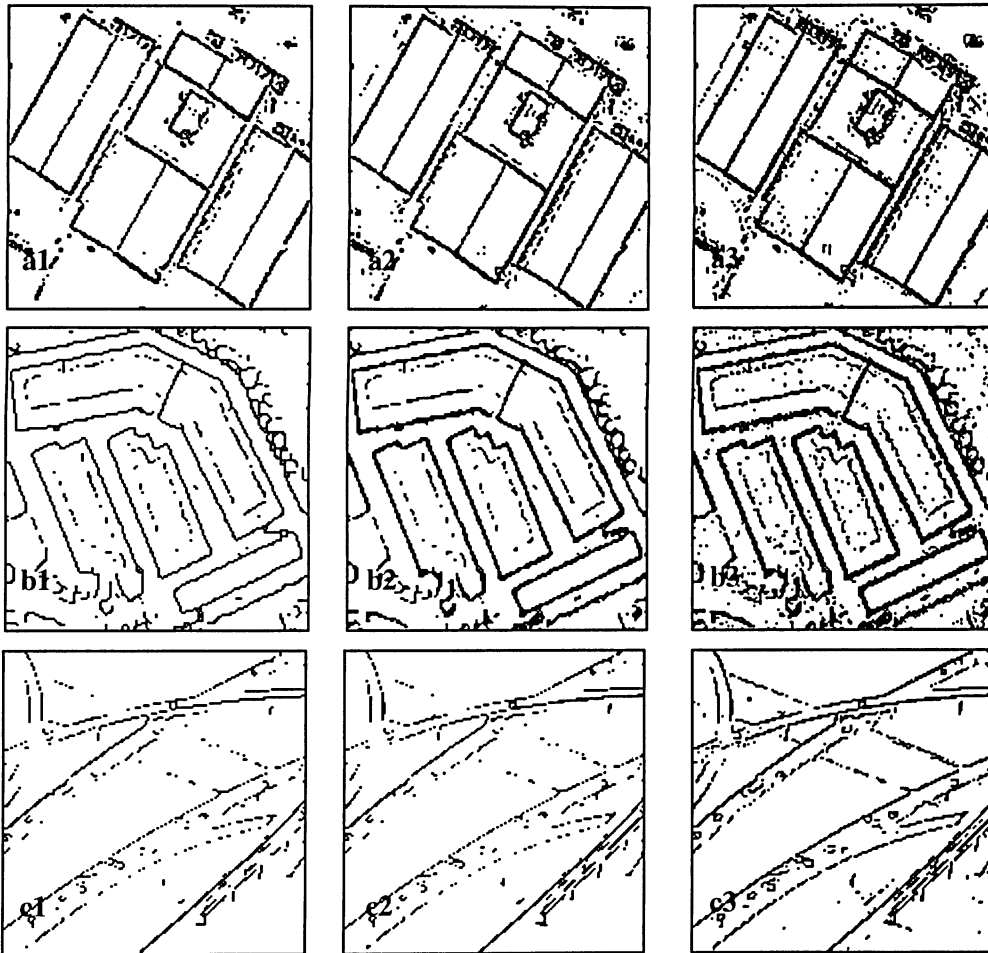


Fig. 4.15 Binary edge images.

In order to eliminate noises (i.e., non-edge pixels), the directly binary morphological dilation operator using a structuring element of 3×1 pixels is applied (Li et al., 2002).

This operation deletes isolated pixels. The results are shown in Figure 4.16, which are obtained by filtering the binary images shown in Figure 4.15.

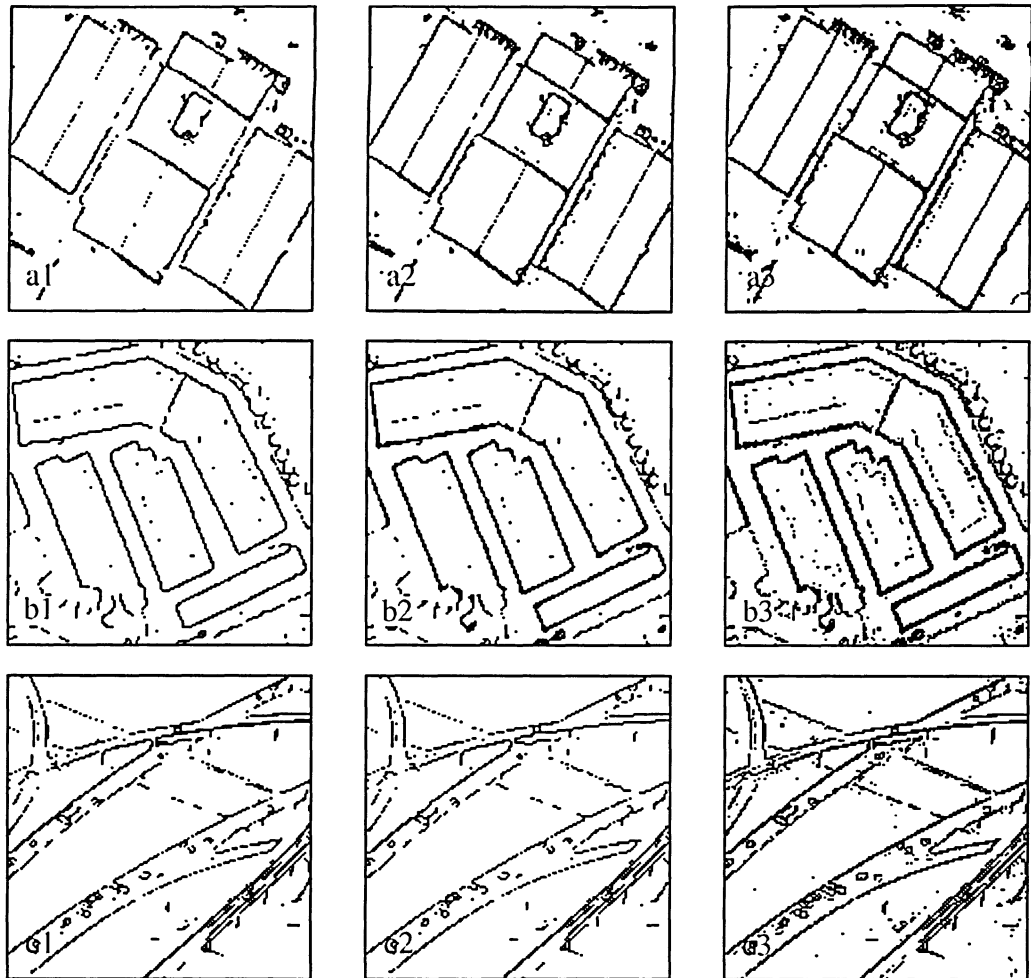


Fig. 4.16 Results of directly binary morphological dilation of edge images.

To recognize exact edges, a thinning algorithm (Zhang and Suen, 1984) is used. Figure 4.17 shows the extracted object edges after applying the thinning algorithm.

In image processing, the subjective evaluation constitutes a very important criterion to assess the performance of any operator. Consequently, the extracted edges (see Figure 4.17) are overlaid on the original images for the verification purpose (see Figure 4.18). A visual evaluation gives the impression that the FSEE performs well for edge detection and is less sensitive to small texture variations. In all cases the extracted edges are in good agreement with the subjective criteria for colour edges.

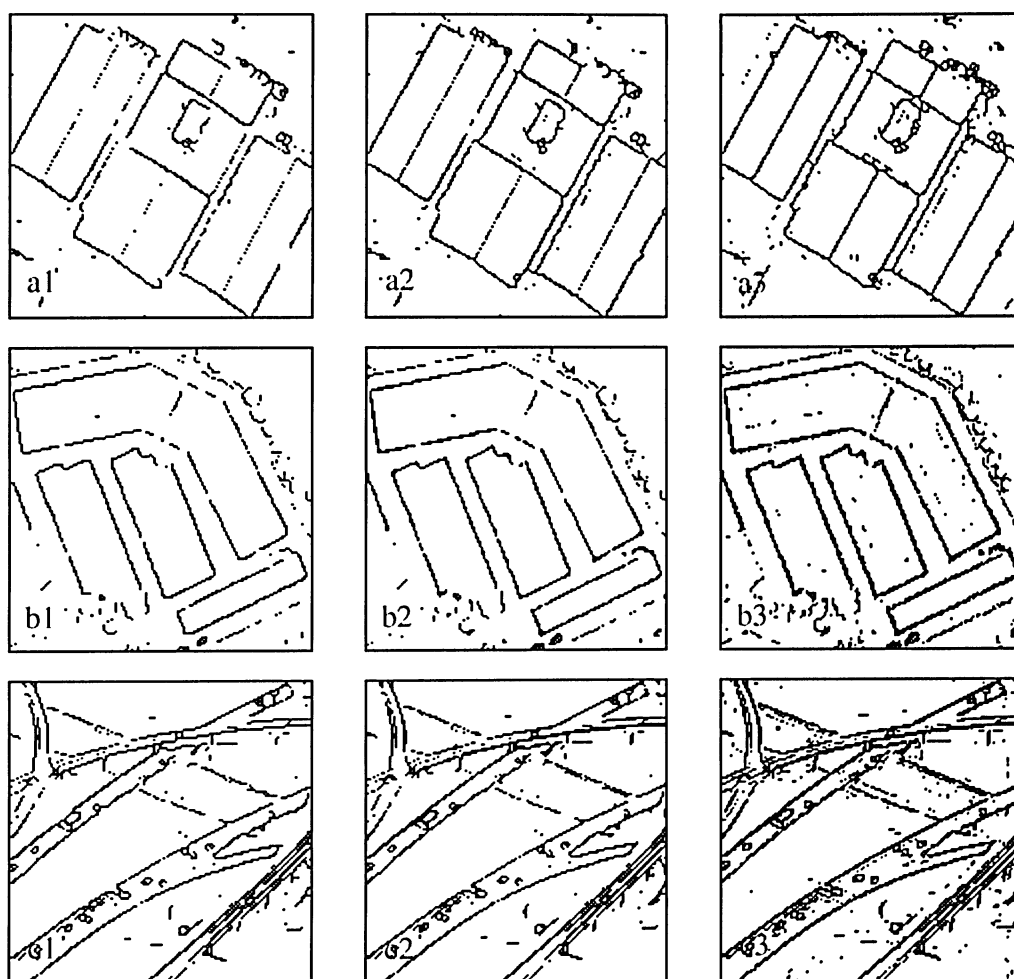


Fig. 4.17 Extracted object edges.

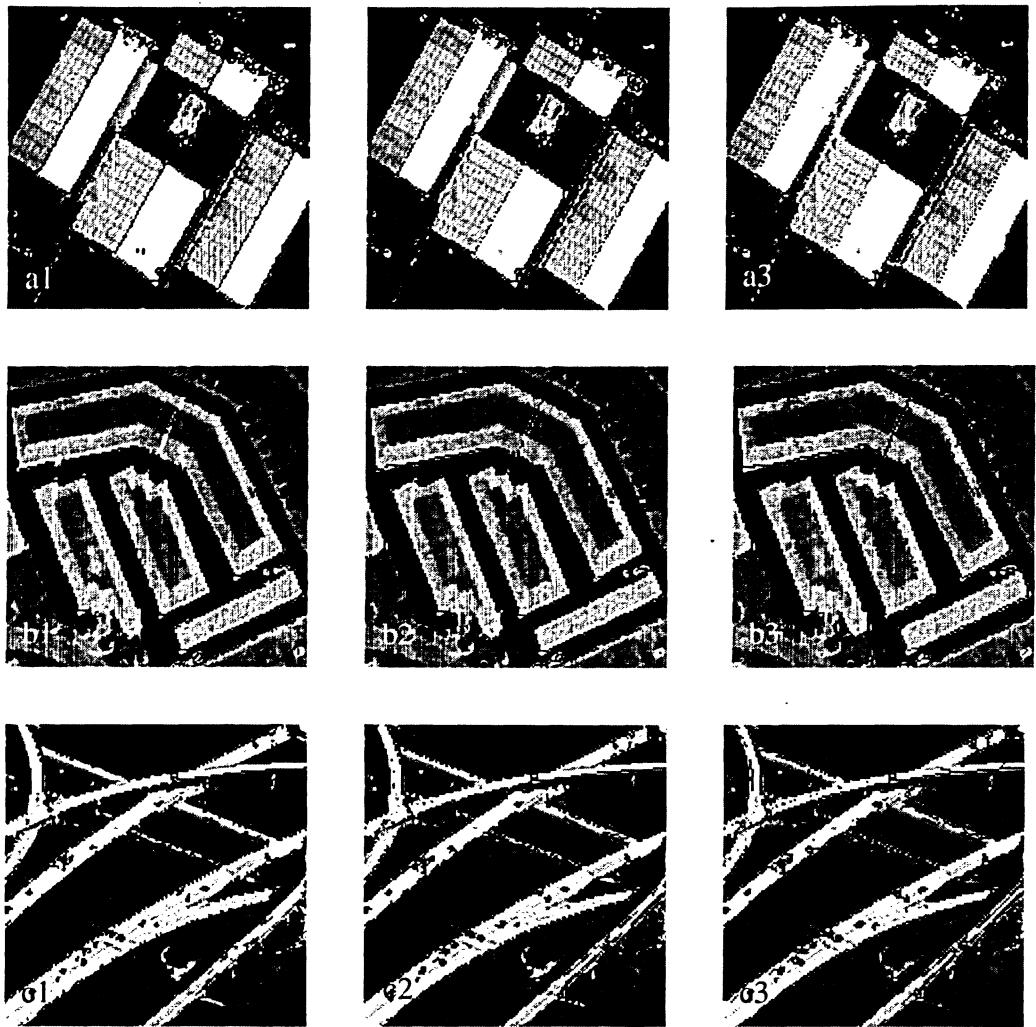


Fig. 4.18 Overlaying edges (in red) on original images.

4.5 Chapter Summary

In this chapter, a new framework that extends the concepts of morphology to colour image processing based on the FSM has been presented. Its foundational and secondary operations, colour erosion, dilation, opening, and closing have been defined, and their basic properties have been examined. The new approach is vector preserving. The defined morphological operations have been used to design colour edge extractor and the results of the extractor have revealed the applicability and efficiency of the colour morphology.

5 FUZZY CLUSTERING BASED ON FSM

Clustering is one of the most fundamental problems in pattern recognition (Tou and Gonzalez, 1974; Zeng and Starzyk, 2001), image segmentation (Liew and Yan, 2001), unsupervised learning (Langan et al., 1998), and data compression (Zhong et al., 2000). It plays a key role in assessing the relationships among the patterns of data sets.

Given a finite vector set, a clustering procedure organizes the vectors in the vector set into groups or clusters based on similarity or dissimilarity among vectors such that the vectors within a cluster show a greater similarity. There are two distinct families of clustering schemes. One is the crisp-based clustering algorithm (Anderberg, 1973; Hartigan, 1975) and the other is the fuzzy-based clustering algorithm (Bezdek, 1981; Sato et al., 1997; Hoppner et al., 1999). The latter has been proved to be well suited to deal with the imprecise and uncertain nature of vector sets, such as multivariate remote sensing images. This chapter presents a fuzzy clustering method based on the FSM. In this method the clustering procedure is modeled as a combinational optimum problem. And then a colour image segmentation method is proposed by using the fuzzy cluster algorithm. The use of the proposed segmentation algorithm for automated extraction of roads and buildings from high-resolution remote sensing imagery has also been investigated

This chapter consists of five sections. In Section 5.1, the fuzzy c-partition algorithm based on the FSM is proposed. In Section 5.2, the colour histogram is defined. In Section

3, the segmentation method based on the proposed fuzzy c-partition algorithm and the defined colour histogram is developed. In section 5.4, the segmentation method is used to design the road and building extractors, respectively. The section 5.5 is the summary of this chapter.

5.1 Fuzzy C-Partition Algorithm Based on FSM

Consider a vector set V formed by n vectors in m -dimensional real number space R^m , i.e., $V = \{V_1, V_2, \dots, V_n\}$, $V_j = [V_{j1}, V_{j2}, \dots, V_{jm}]$ and $j = 1, 2, \dots, n$, a fuzzy c -partition on V is represented by

$$P = [p_{ij}], \quad i=1, 2, \dots, c \quad \text{and} \quad j=1, 2, \dots, n \quad (5.1)$$

where P is a fuzzy partition matrix and satisfies

$$\sum_{i=1}^c p_{ij} = 1, \quad \text{for all } j = 1, 2, \dots, n \quad (5.2)$$

$$0 < \sum_{j=1}^n p_{ij} < n, \quad \text{for all } i = 1, 2, \dots, c \quad (5.3)$$

where c is the positive integer to indicate the number of the clusters in the partition, and $p_{ij} \in [0,1]$ is the fuzzy membership value of V_j belonging to i th cluster (George and Bo, 1995).

The above clustering process is generally completed as follows. First, each cluster is associated with a vector, called centre vector, and all c centre vectors form a vector set, called centre vectors set $VC = \{VC_1, VC_2, \dots, VC_c\}$. Second, the similarity between VC_i and V_j to characterize the fuzzy membership value of V_j belonging to i th cluster is calculated by

$$p_{ij} = \frac{\mu(VC_i, V_j)^{\frac{1}{m-1}}}{\sum_{k=1}^c \mu(VC_k, V_j)^{\frac{1}{m-1}}} \quad (5.4)$$

where $\mu(VC_i, V_j)$ is a similarity measure between two vectors defined on R^m and represents a similarity relationship between them, $m \in [1, \infty)$ is the weighting exponent on each fuzzy membership. The larger m is the fuzzier the partition is.

Briefly, fuzzy clustering can be considered to find an associated centre vector set and calculate a fuzzy c -partition matrix by using this set. To evaluate the effectiveness of a fuzzy c -partition, an objective function is required. Generally, the objective function expresses that the relationship among the vectors is strong if these vectors are within the same cluster and it would be weak if they are in different clusters. Give a fuzzy c -

partition matrix P and a centre vector set VC , the objective function, $J_m(P, VC)$, is defined by

$$J_m(P, VC) = \sum_{i=1}^c \sum_{j=1}^n p_{ij} \mu(VC_i, V_j) \quad (5.5)$$

where p_{ij} is the weight of similarity measure $\mu(VC_i, V_j)$ and calculated by Equation (5.4).

In order to obtain the best fuzzy c -partition, the number of the clusters should be first given, and then a searching process controlled by J_m should be designed carefully to find the best VC corresponding to the best fuzzy c -partition. In this study, the former is accomplished by a histogram-based method and the later is modeled as an integer programming (IP) problem.

Given a vector set $V = \{V_1, V_2, \dots, V_n\}$, and the number of the clusters c ,

Max

$$J_m(P, VC) = \sum_{i=1}^c \sum_{j=1}^n p_{ij} \mu(VC_i, V_j) \quad (5.6)$$

Subject to

$$VC_i \in V \quad (5.7)$$

$$\mu(VC_i, V_j) = e^{-k_1 d(VC_i, V_j)} \cos(k_2 \theta(VC_i, V_j)) \quad (5.8)$$

$$d(VC_i, V_j) = \left(\sum_{k=1}^m |VC_{ik} - V_{jk}|^2 \right)^{1/2} \quad (5.9)$$

$$\theta(VC_i, V_j) = \arccos \left(\frac{\sum_{k=1}^m VC_{ik} V_{jk}}{\sqrt{\sum_{k=1}^m VC_{ik}^2} \sqrt{\sum_{k=1}^m V_{jk}^2}} \right) \quad (5.10)$$

where $j (= 1, 2, \dots, n)$ is the index of vectors in V , $i (= 1, 2, \dots, c)$ is the index of vectors in VC , and $k (= 1, 2, \dots, m)$ is the index of vector's dimensions in V_j .

After finding the best centre vector set $VC_b = \{VC_{b1}, VC_{b2}, \Lambda, VC_{bc}\}$, the best fuzzy c-partition matrix is calculated as follows

$$P_b = [p_{bij}], \quad i = 1, 2, \Lambda, c \quad \text{and} \quad j = 1, 2, \Lambda, n \quad (5.11)$$

$$p_{bij} = \frac{\mu(VC_{bi}, V_{bj})^{\frac{1}{m-1}}}{\sum_{k=1}^c \mu(VC_{bk}, V_{bj})^{\frac{1}{m-1}}} \quad (5.12)$$

As stated early, the fuzzy c-partition algorithm requires the desired number of clusters specified in advance. Unfortunately, in most of situations, the number of clusters is unknown a prior and sometimes it is difficult to specify any desired number of clusters. For example, the situations often happen in the segmentations of remote sensing images, because the ground truth is always not available for these images. In the following segmentation method, a histogram-based procedure is used to obtain the number of the cluster c and the initial centre vector set VC_0 .

5.2 Colour Histogram

Colour histogram is an important technique in colour image analysis, because of its efficiency, effectiveness and triviality in computation (Pratt, 1991). Generally speaking, a colour histogram represents the statistical distribution of the colours in a colour image on all colours in a colour space. From the view of the applicability and computation, this kind of histogram is unnecessary and impossible. The general way is to divide a colour space into some bins and calculate the colour distribution on those bins.

Given a colour space divided into I colour bins, the colour histogram of the colour image CI with n pixels is represented as a vector $H = [h_0, h_1, \dots, h_{I-1}]$, in which each entry h_i indicates the statistical figures of the colours in the colour image which belong to the i th bin, i.e.,

$$h_i = \frac{n_i}{n}, i = 0, 1, \dots, I-1 \quad (5.13)$$

where n_i is the number of pixels with colours in the i th colour bin.

In this chapter, RGB colour space is represented with 24 bits (8 bits for each component). Each colour corresponds to a point in RGB colour space. In order to obtain a colour histogram, pixels of a colour image distributed on all bins should be accounted for.

Let RGB colour space be discretized along the R, G, and B axes by the numbers N_R , N_G , and N_B , respectively. Then the total $N (= N_R \times N_G \times N_B)$ bins are available. These bins are coded in such a sequence from R to G and then from G to B. According to the specified discretizing and coding scheme the index of each bin can be represented as

$$i = R + N_G \times G + N_B^2 \times B \quad (5.14)$$

where $R = 0, 1, \dots, N_R-1$, $G = 0, 1, \dots, N_G-1$, and $B = 0, 1, \dots, N_B-1$.

Then the pixel (r_p, g_p, b_p) will be in the bin with the index i_p ,

$$i_p = \left\lfloor \frac{r_p N_R}{256} \right\rfloor + N_G \times \left\lfloor \frac{g_p N_G}{256} \right\rfloor + N_B^2 \times \left\lfloor \frac{b_p N_B}{256} \right\rfloor \quad (5.15)$$

where $\lfloor \rfloor$ is an integral operator.

Figure 5.1 shows an example of the divided RGB colour space with $N_R = N_G = N_B = 4$ and the codes of all bins. In this example, a total of 64 ($=4 \times 4 \times 4$) bins can be obtained.

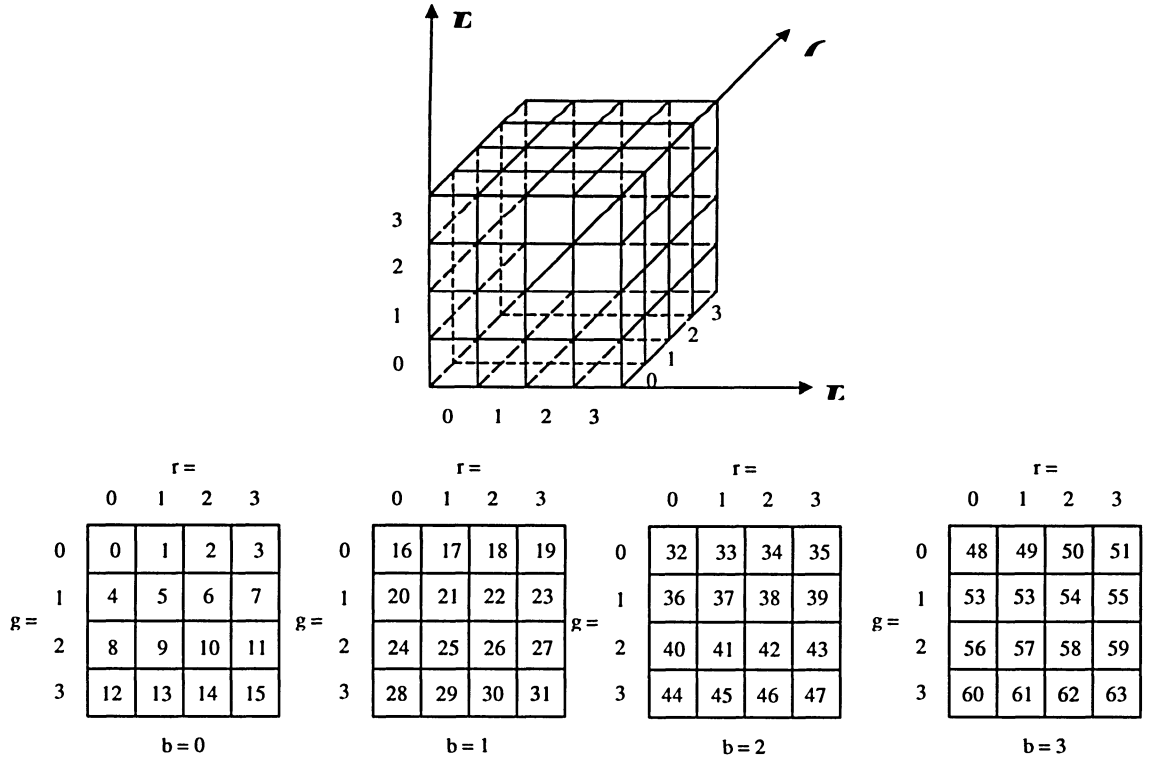


Fig.5.1 Discretization of RGB colour space and codes of bins.

5.3 Segmentation Based on Fuzzy C-Partition Algorithm

To solve the optimization model introduced in the previous section, there are many methods, such as a branch-and-bound approach (Winston, 1991), and genetic algorithms (Goldberg, 1989). However, they are very time consuming and not practical in the real world. Therefore, the use of a heuristic, which gives a good but sometimes not optimal or the best solution, is necessary. The approach consists of three steps: (1) Pre-clustering.

This process includes determining of the number of clusters, finding an initial centre vector set VC_0 , and indicating the ranges in which the centre vectors are chosen in the following optimal procedure. This procedure is finished by using a histogram-based technique. (2) Searching the best fuzzy c-partition. It is realized by solving an integer programming problem to find a good fuzzy c-partition. (3) Post-processing. It means a defuzzification procedure to convert the fuzzy c-partition matrix to the crisp c-partition matrix. In this section, only steps (1) and (3) are emphasized.

5.3.1 Pre-clustering Procedure

For the given colour image CI , the colour histogram $H(CI)$ can be obtained in terms of the definition of colour histogram discussed in the previous section. It is obvious that if an image is composed of distinct objects with different colours, its colour histogram usually shows different peaks. Each peak corresponds to one object and adjacent peaks are likely to be separated by a valley. The height of a peak implies the number of the pixels falling in the bin corresponding to the location of the peak.

The pre-clustering procedure is carried out by thresholding the colour histogram of a colour image. For a selected threshold, the peaks having higher magnitudes than the threshold can be detected. The number of all detected peaks is chosen as the number of clusters, and the bins corresponding to the detected peaks determine the ranges in which the centre vectors are investigated for the purpose of the optimization. The initial centre

vectors consist of the minimum vectors of all bins. On the other hand, they can also be produced randomly, as long as they are located in the selected bins.

The threshold is determined by either a manual or an automatic way. In the manual case, the number of clusters is determined by observing the colour image and the colour histogram of the image. In the automatic case, the criterion to determine the threshold should be given first. For example, the mean of all peaks can be used as the criterion. It means that the peaks with the higher magnitudes than the mean are valid.

5.3.2 Post-processing Procedure

In order to obtain the segmented image, it is necessary to transform the fuzzy c-partition matrix to the crisp partition matrix. In this study, the following defuzzification scheme is used.

Let $\mathbf{P} = [p_{ij}]$ $i = 1, 2, \dots, c$ and $j = 1, 2, \dots, n$ be the fuzzy c -partition matrix, it is well known that p_{ij} presents the membership grade for pixel j belonging to cluster i . A percent partition matrix, \mathbf{P}_p , is defined as

$$\mathbf{P}_p = [p_{p_{ij}}], p_{p_{ij}} = \frac{P_{ij}}{\sum_{j=1}^n P_{ij}} \quad (5.16)$$

In terms of the percent partition, the crisp partition matrix, \mathbf{P}_c , is defined as

$$P_c = [p_{cij}] \mid p_{cij} = 1, \text{ if } p_{pij} = \max_{i=1}^c(p_{pij}), \text{ else } p_{cij} = 0 \quad (5.17)$$

It is clear that in the crisp-partition matrix each pixel belongs to a certain cluster.

5.3.3 Experiment and Results

The purpose of the experiment is to illustrate the procedure of the segmentation method and show its performance. In this experiment, colour QuickBird, Ikonos, and aerial images are used. They are shown in Figure 5.2. Each colour image has 24 bits per pixel and 128×128 pixels in size and 1 *m* resolution.

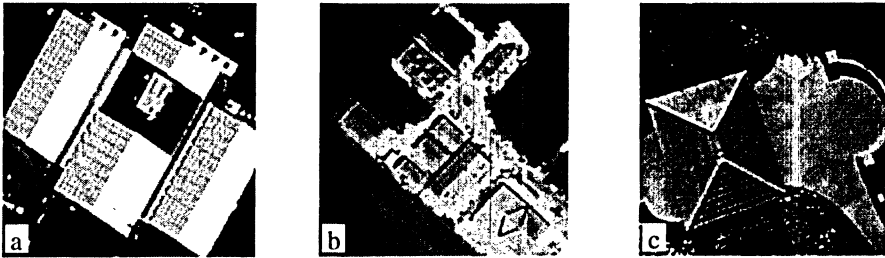


Fig. 5.2 Test images: (a) QuickBird, (b) Ikonos, and (c) aerial images.

The pre-clustering procedure determines the number of clusters, finds the appropriate initial centre vector for each cluster, and gives the ranges (bins) in which the optimal centre vectors corresponding to the clusters are searched. This procedure is completed by using the histogram-based technique discussed in the previous section. In colour histogram analysis, a suitable discretization is crucial. It depends on the compromise

between the appropriate initial centre vectors and the adequate search space, of course, and the search time. In this experiment, the interval for discretizing each colour component is 32. It means that the total 512 ($= (256/32)^3 = 8^3$) bins can be obtained.

Figure 5.3 shows the colour histograms for the three types of colour images shown in Figure 5.2. It is observed from Figure 5.3 that the colour histograms are multimodal with planes. In this case, the bins can be grouped into different regions by those planes. For example, in Figure 5.3 (a), the bins are divided in 8 regions, i.e., [0, 49], [50, 99], [100, 199], [200, 249], [250, 349], [350, 399], [400, 499], and [500, 511]. The number of all segmented regions is taken as the number of clusters.

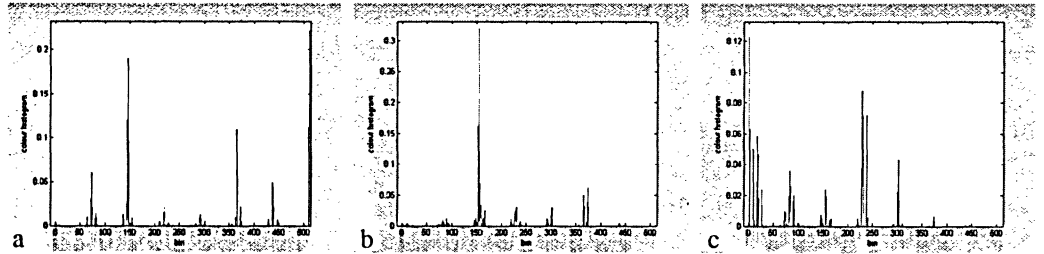



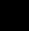

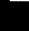












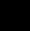
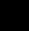



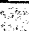








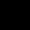
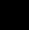

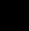








Fig. 5.3 Colour histograms of (a) QuickBird, (b) Ikonos, and (c) aerial images.

In each given region, the bin with the maximum peak is selected as the searching range of centre vector corresponding to the cluster. The minimum vectors in selected bins are taken as the initial centre vectors. The number of clusters, the selected bins, and the initial centre vectors are summarized in Table 5.1.

After searching the best centre vector set, the optimal centre vectors and the corresponding fuzzy c-partition are obtained. The optimal centre vectors for the different

test images are listed in the last column of Table 5.1. Figures 5.4 - 5.9 show the profile curves and the pseudo-colour images of fuzzy c-partition matrix of different clusters for the test images, where (a)-(h) are the results of Clusters 1-8, respectively. They indicate the membership degree of each pixel belonging to corresponding clusters. In profile curves, the membership values are denoted by the heights of curves. In pseudo colour images, they are represented by some specified colours. It seems that the pseudo colours give a much more intuitive representation of the fuzzy c-partition matrix.

Table 5.1 Results of pro-clustering and optimal centre vectors

Image	Number of cluster	Bins for searching centre vectors	Initial centre vectors		Optimal centre vectors	
QuickBird	8	$BIN_1^* = \{(32, 0, 0), (63, 31, 31)\}$	$V_{10} = (32, 0, 0)$		$V_1 = (41, 20, 16)$	
		$BIN_2 = \{(224, 64, 0), (255, 95, 31)\}$	$V_{20} = (224, 64, 0)$		$V_2 = (233, 78, 4)$	
		$BIN_3 = \{(224, 160, 0), (255, 191, 31)\}$	$V_{30} = (224, 160, 0)$		$V_3 = (248, 164, 13)$	
		$BIN_4 = \{(128, 64, 0), (159, 95, 31)\}$	$V_{40} = (128, 64, 0)$		$V_4 = (155, 78, 9)$	
		$BIN_5 = \{(96, 160, 0), (127, 191, 31)\}$	$V_{50} = (96, 160, 0)$		$V_5 = (98, 181, 20)$	
		$BIN_6 = \{(0, 64, 0), (31, 95, 31)\}$	$V_{60} = (0, 64, 0)$		$V_6 = (23, 94, 11)$	
		$BIN_7 = \{(192, 128, 0), (223, 159, 31)\}$	$V_{70} = (192, 128, 0)$		$V_7 = (194, 155, 9)$	
		$BIN_8 = \{(160, 224, 0), (191, 255, 31)\}$	$V_{80} = (160, 224, 0)$		$V_8 = (177, 249, 2)$	
Ikonos	7	$BIN_1 = \{(96, 32, 0), (127, 63, 31)\}$	$V_{10} = (96, 32, 0)$		$V_1 = (97, 41, 23)$	
		$BIN_2 = \{(32, 160, 0), (63, 191, 31)\}$	$V_{20} = (32, 160, 0)$		$V_2 = (35, 189, 14)$	
		$BIN_3 = \{(224, 192, 0), (255, 233, 31)\}$	$V_{30} = (224, 192, 0)$		$V_3 = (255, 205, 25)$	
		$BIN_4 = \{(224, 96, 0), (255, 127, 31)\}$	$V_{40} = (224, 96, 0)$		$V_4 = (225, 115, 12)$	
		$BIN_5 = \{(128, 192, 0), (159, 223, 31)\}$	$V_{50} = (128, 192, 0)$		$V_5 = (147, 199, 26)$	
		$BIN_6 = \{(32, 96, 0), (63, 127, 31)\}$	$V_{60} = (32, 96, 0)$		$V_6 = (34, 103, 15)$	
		$BIN_7 = \{(224, 128, 0), (255, 159, 31)\}$	$V_{70} = (224, 128, 0)$		$V_7 = (254, 130, 14)$	
Aerial	6	$BIN_1 = \{(32, 0, 0), (63, 31, 31)\}$	$V_{10} = (32, 0, 0)$		$V_1 = (45, 5, 31)$	
		$BIN_2 = \{(32, 128, 0), (63, 159, 31)\}$	$V_{20} = (32, 128, 0)$		$V_2 = (49, 136, 27)$	
		$BIN_3 = \{(0, 224, 0), (31, 255, 31)\}$	$V_{30} = (0, 224, 0)$		$V_3 = (24, 246, 0)$	
		$BIN_4 = \{(192, 96, 0), (223, 127, 31)\}$	$V_{40} = (192, 96, 0)$		$V_4 = (220, 119, 15)$	
		$BIN_5 = \{(128, 192, 0), (159, 223, 31)\}$	$V_{50} = (128, 192, 0)$		$V_5 = (144, 204, 12)$	
		$BIN_6 = \{(32, 96, 0), (63, 127, 31)\}$	$V_{60} = (32, 96, 0)$		$V_6 = (37, 121, 28)$	

* Each bin is indicated by its left lowest and right highest points.

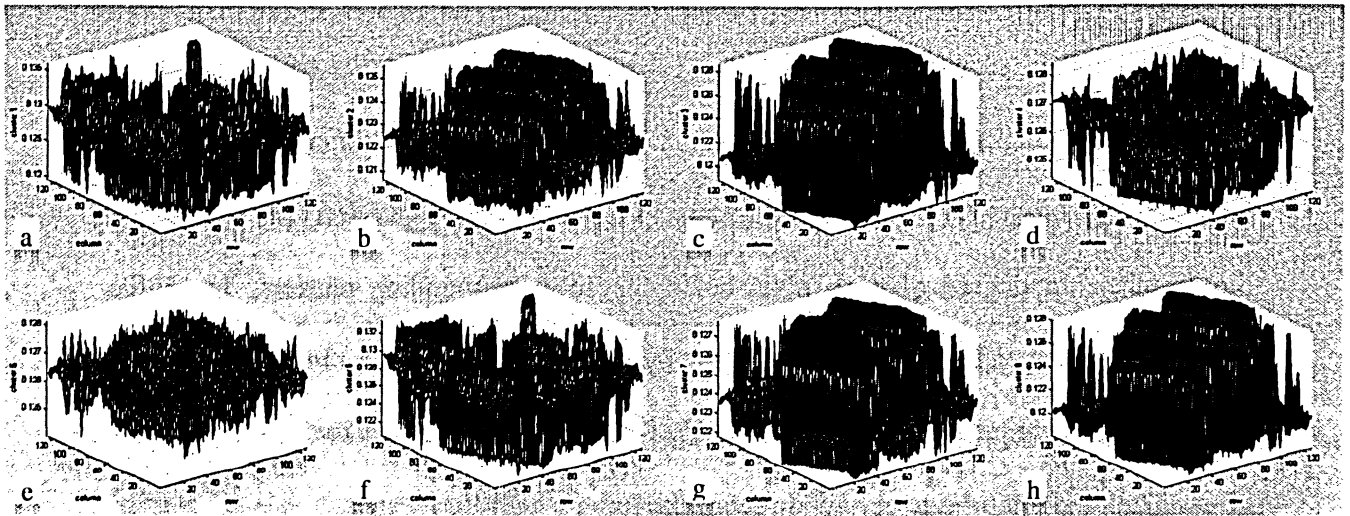


Fig. 5.4 Profile curves of fuzzy c-partition matrix of QuickBird image.

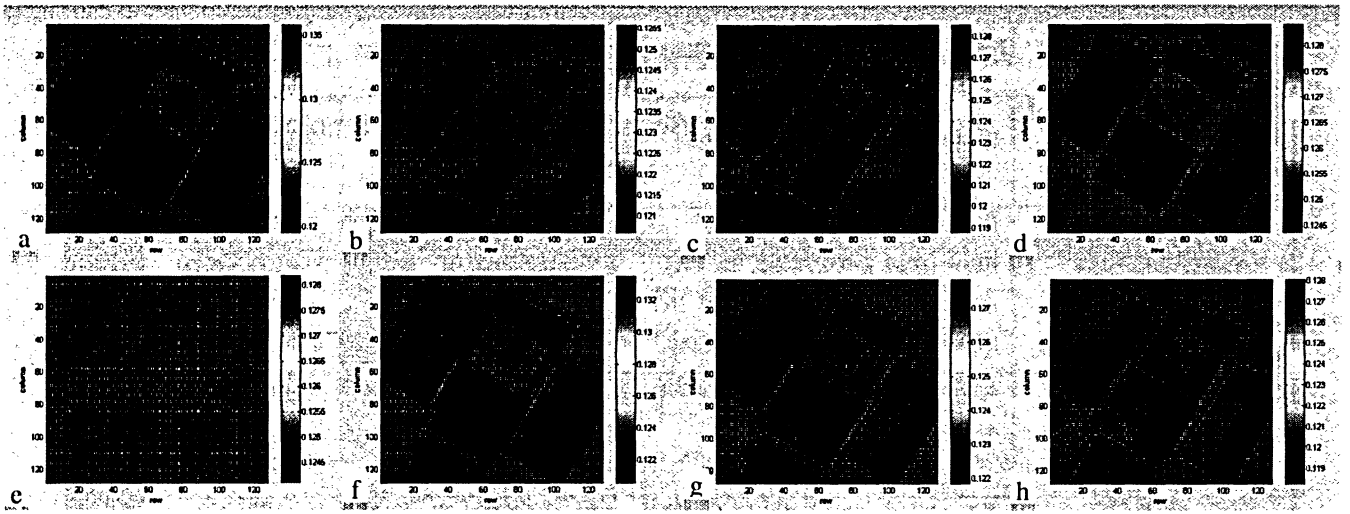


Fig. 5.5 Pseudo colour images of fuzzy c-partition matrix of QuickBird image.

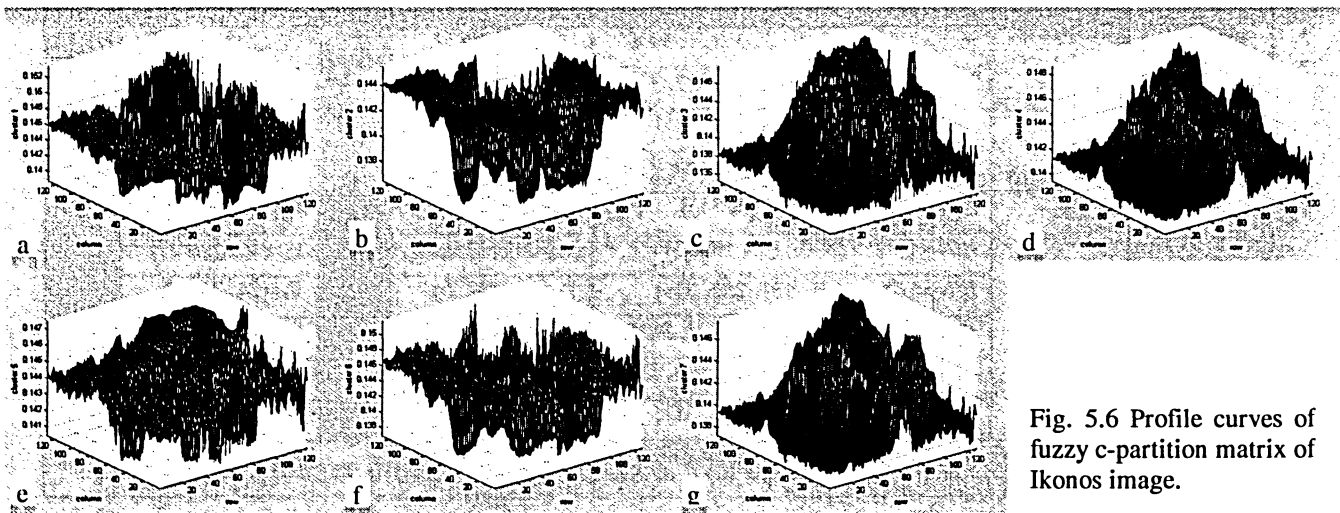


Fig. 5.6 Profile curves of fuzzy c-partition matrix of Ikonos image.

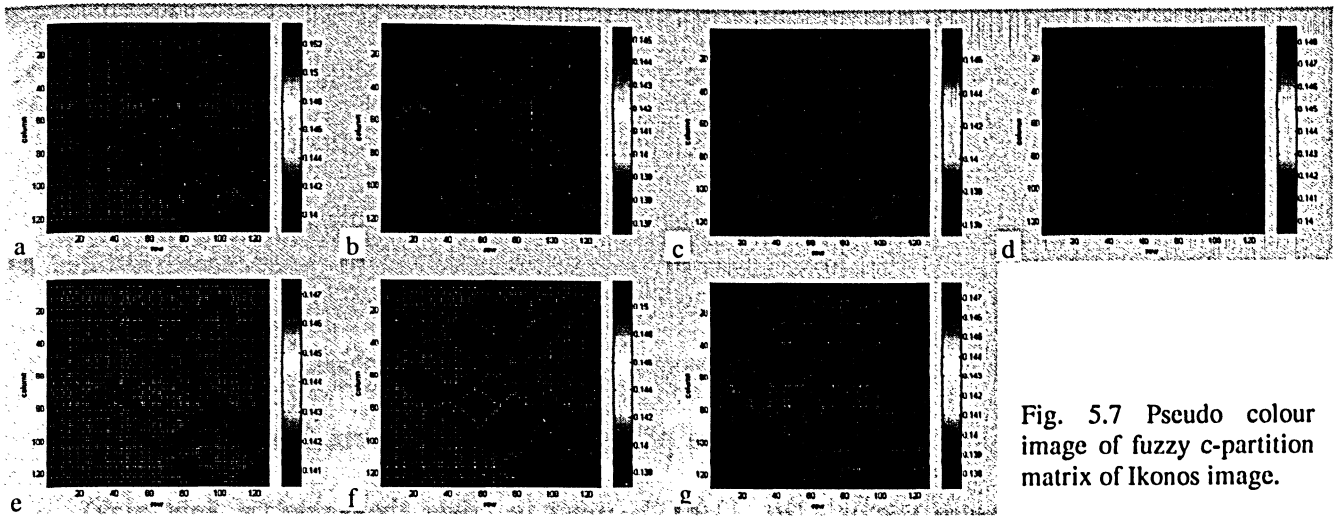


Fig. 5.7 Pseudo colour image of fuzzy c-partition matrix of Ikonos image.

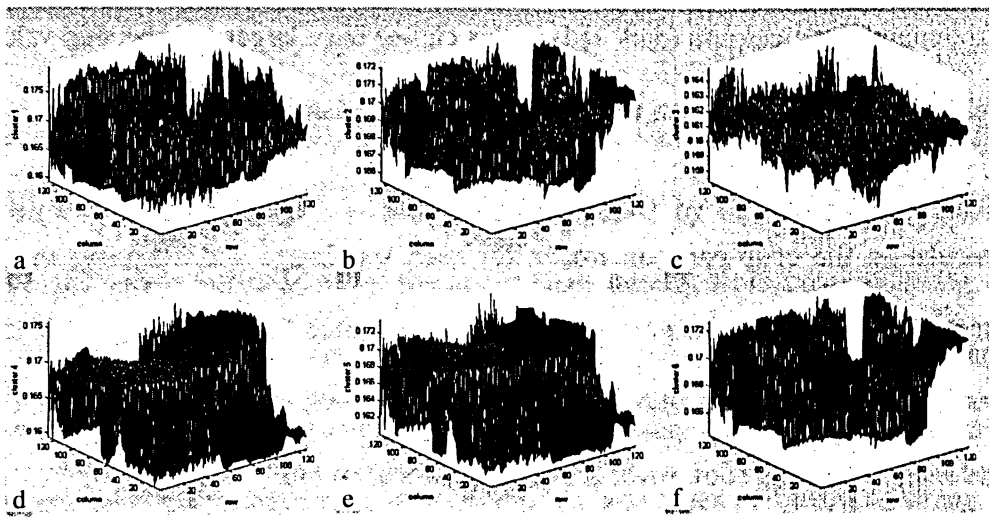


Fig. 5.8 Profile curves of fuzzy c-partition matrix of aerial image.

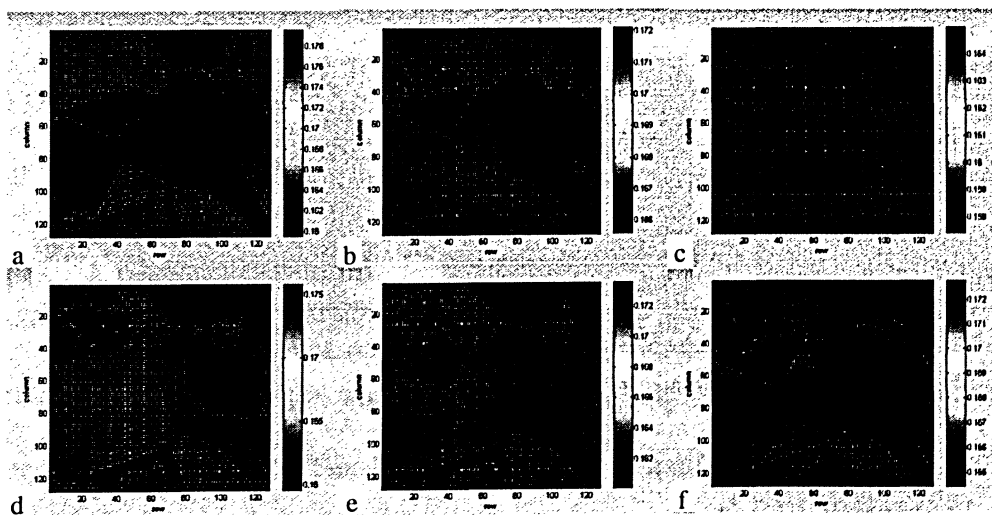


Fig. 5.9 Pseudo colour image of fuzzy c-partition matrix of aerial image.

Referring to Figure 5.2c, optimum centre vectors for the aerial image and their colours listed in Table 5.1, and the pseudo colour image of its fuzzy c-partition matrix (Figure 5.9), the meaning of fuzzy c-partition matrix can be explained as follows. The Cluster 1 centred at the vector (45, 3, 31) include shadow (in black) pixels representing shadows (in black) in original image, since they have larger membership values. These pixels are indicated by red in pseudo colour image of fuzzy c-partition matrix (see Figure 5.9a). Cluster 4 with centre vector (220, 119, 15) trend to cover the circle (in light pink) correspondingly, the colours (dark red) in this cluster have larger membership values (see Figure 5.9d). Other clusters can also be explained in the same way.

By calculating the crisp-partition matrix for each test image and assigning the pseudo colour for each cluster, the segmented images can be obtained (see Figure 5.10). It can be observed that the crisp-partition matrix gives the obvious classifications of different objects such as building roof, road, grass, shadow, and so on.

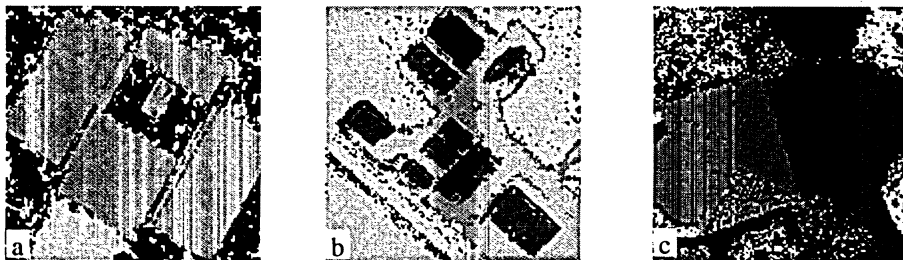


Fig. 5.10 Segmented images: (a) QuickBird, (b) Ikonos, and (c) aerial.

5.4 Object Extraction Application

In this section, the proposed segmenting algorithm is applied to the road and building extraction. The results demonstrate that the proposed method is efficient for high-resolution remote sensing image processing tasks.

5.4.1 Road Centreline Extraction

Extracting road networks from high-resolution remote sensing images, such as Ikonos, QuickBird, and aerial images, is particularly motivated by the increasing demand for accurate and timely information for the applications ranging from urban planning, traffic flow analysis and simulation, estimations of air and noise pollutions, road maintenance and upgrading, and the telecommunication. Many road extraction algorithms using satellite or aerial images have been developed in the past years (Trinder and Wang, 1998; Lee et al., 2000; Dell'Acqua and Gamba, 2001; Hinz et al., 2001).

In this section, the segmentation method based on the fuzzy c-partition algorithm is utilized to extract road centrelines from high-resolution remote sensing images. The overall flow of the extracting procedure is illustrated in Figure 5.11. It consists of three main steps: (1) segmenting colour images based on the above segmentation method; (2) detecting road networks from segmented images; (3) delineating road centrelines from the extracted road networks. The discussions are mainly focused on the Steps 2 and 3.

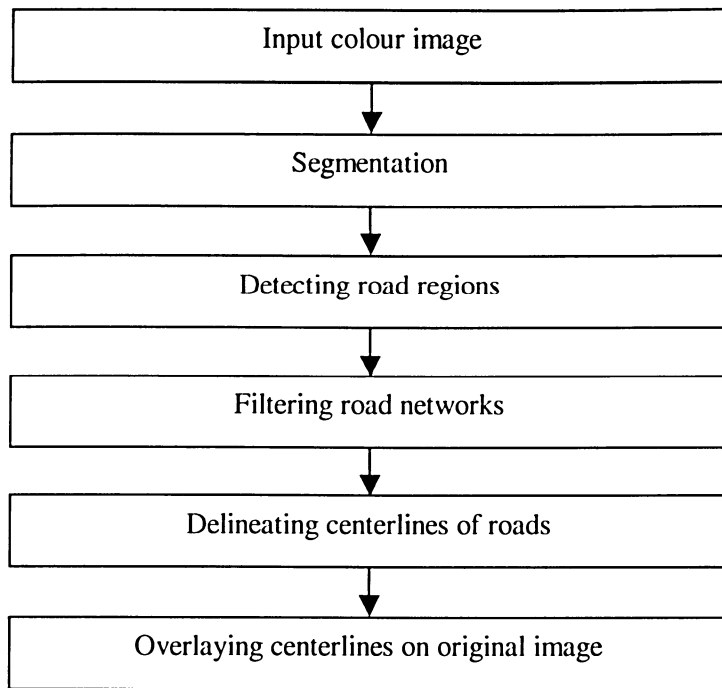


Fig. 5.11 Road extraction strategy.

5.4.1.1 Extraction of Road Networks

Once the pseudo-colour segmented images are obtained by the above segmentation method, the binary road network image can be extracted from it by selecting the pseudo-colour corresponding to the road regions. In general, the roads in the binary image are corrupted by noise objects, which have the similar colours to roads. In order to clear the road regions, it is necessary to filter the corrupted road network image. To this end, binary morphological operations are used. For example, depending on the shapes of noise objects, the appropriate combinations of binary dilation, erosion, opening, and closing should be chosen.

5.4.1.2 Delineation of Road Centrelines

An important process for representing the structural shape of the detected road regions is to reduce it to a graph. This work can be accomplished by a thinning algorithm. The thinning algorithm developed by Zhang and Suen (1984) for thinning binary regions is utilized in this study. It is assumed that the road pixels in the binary road network images have value 1 (black), and those background (non-road) pixels have the value 0 (white). The method consists of the successive passes of two basic steps applied to the contour pixels of the given images, where a contour pixel is any pixel with value 1 and has at least one 8-neighbour value 0. With reference to the 8-neighbourhood definition shown in Figure 5.12, the first step indicates a contour pixel p for deletion (from black to white) if the following conditions are satisfied:

- $2 \leq N(p) \leq 6$
- $S(p) = 1$
- $p_0 \cdot p_1 \cdot p_3 = 0$
- $p_3 \cdot p_5 \cdot p_7 = 0$

where $N(p)$ is the number of nonzero neighbors of p , i.e.,

$$N(p) = \sum_{i=0}^7 p_i \quad (5.18)$$

and $S(p)$ is the number of 0-1 transitions in the ordered sequence of $p_0, p_1, \dots, p_6, p_7$.

p_7	p_0	p_1
p_6	p	p_2
p_5	p_4	p_3

Fig. 5.12 Neighborhood arrangement.

In the second step, first two conditions remain the same, but the last two conditions are changed to

- $p_0 \cdot p_1 \cdot p_7 = 0$
- $p_0 \cdot p_5 \cdot p_7 = 0$

5.4.1.3 Experiments and Results of Road Extraction

The proposed road extraction algorithm has been tested on three types of high-resolution remote sensing images, including (a) QuickBird, (b) Ikonos, and (c) aerial images (see Figure 5.13). All test images have a size of 150×150 pixels and 1 *m* resolution.



Fig.5.13 Original images: (a) aerial, (b) Ikonos, and (c) QuickBird images.

The pseudo-colour segmented images generated from the original images shown in Figure 5.13 are given in Figure 5.14.



Fig.5.14 Segmented images: (a) aerial, (b) Ikonos, and (c) QuickBird images.

Figure 5.15 shows the binary images of the road networks after the segmentation of the colour images shown in Figure 5.14. It can be observed in all three images shown in Figure 5.15 that the segmented road networks are corrupted by the objects with similar colours to roads. For example, the pillars supporting the highways, see Figures 5.13 (a), 5.14a, and 5.15a exhibit this characteristic.



Fig.5.15 Binary images of road regions: (a) aerial, (b) Ikonos, (c) QuickBird from segmented images.

Figure 5.16 shows the road regions obtained after filtering the segmented images depicted in Figure 5.15 using the binary morphological operators. A visual comparison of the images clearly favours the filtered images (see Figure 5.16) over the segmented images (see Figure 5.15). Figure 5.16a shows the results obtained by filtering Figure 5.15a using the combinations of the binary closing, dilating, and erosion, followed by another dilating, where the size of the structuring elements are 2×2 for all morphological operators. Figure 5.16b shows the results obtained by dilating Figure 5.15b with a structuring element of 3×3 , followed by eroding with a structuring element of 5×5 . Figure 5.16c shows the results obtained by dilating Figure 5.15c with a structuring element of 3×3 and eroding with a structuring element of 5×5 .

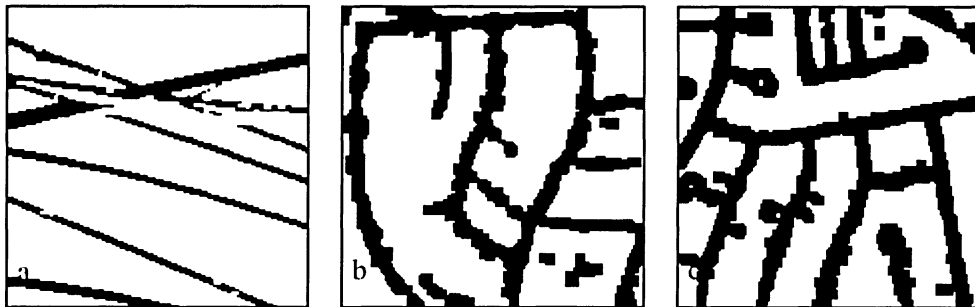


Fig.5.16 Filtered road network images: (a) aerial, (b) Ikonos, and (c) QuickBird images.

The road centrelines are delineated using the thinning algorithm discussed above, and the results are shown in Figure 5.17.

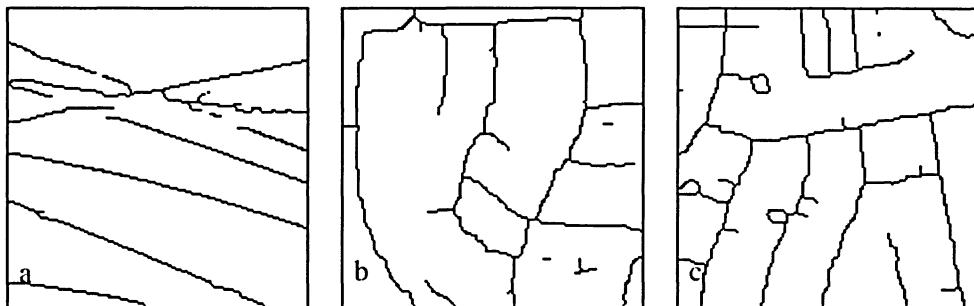


Fig.5.17 Road centerlines: (a) aerial, (b) Ikonos, and (c) QuickBird.

In order to illustrate the accuracy, the extracted road centrelines are overlaid on the original image, see Figure 5.18. In the overlay images the thin red lines indicate the road centerlines, while the narrow white regions indicate the roads. It can be observed in Figure 5.18 that most centrelines match well their roads, though they do not locate accurately on the centres in some parts of the roads. Those situations occur because of either the existence of cars on the road or the irregularities of the roads.



Fig.5.18 Road centerlines (in red) overlaid on original images: (a) aerial, (b) Ikonos, and (c) QuickBird.

5.4.2 Building Extraction

Building extraction from high-resolution remote sensing images is of great practical interest in applications such as data acquisition and update of GIS databases or site models. This section presents the application of the fuzzy c-partition based segmentation method to building roof extraction. Figure 5.19 shows the building extraction strategy. The strategy for extracting building roofs is similar to that for the road extraction described in Section 5.4.1. The difference between the two methods is that the latter extracts the road regions from segmented images according to the colour features of the

roads and then uses a thinning algorithm to decline the extracted roads to the centrelines, but the former needs to extract the building regions according to the colour features of the buildings and uses an edge extraction algorithm to detect the skeletons of the detected buildings. To this end, a boundary extractor is designed and described in this section.

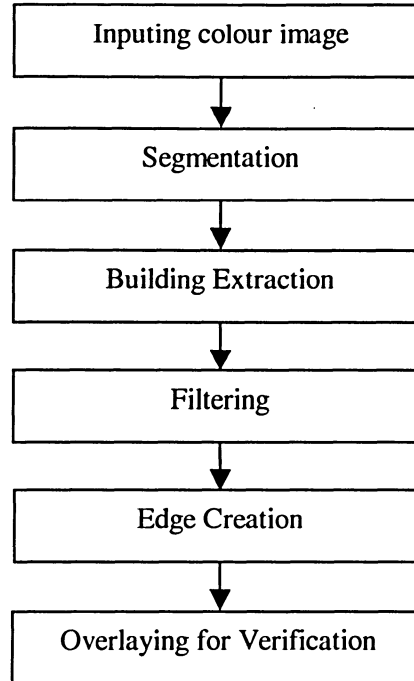


Fig. 5.19 Building extraction strategy

Following the definition of 8-neighborhood shown in Figure 5.12, the boundary pixel for building is determined if it is a contour pixel and satisfies the following condition:

- $0 < N(p) < 8$

where $N(p)$ is the number of nonzero neighbors of pixel p .

Three types of test images, including (a) QuickBird, (b) Ikonos, and (c) aerial images (see Figure 5.20), are used to test the proposed building extraction method. All images have the sizes of 150×150 pixels and 1 *m* resolution.

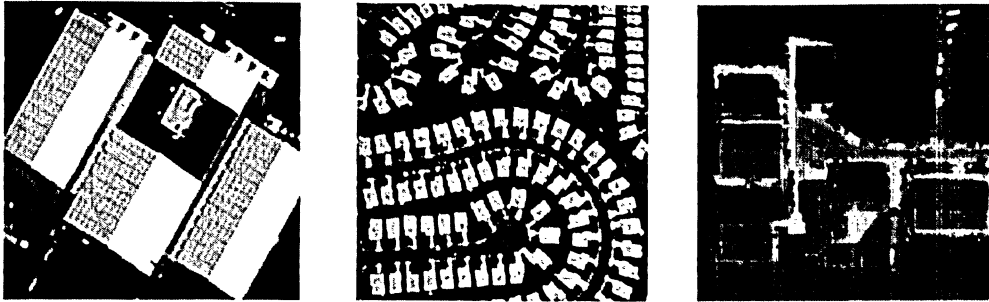


Fig 5.20 Test images: (a) QuickBird, (b) Ikonos, and (c) aerial images.

Figure 5.21 shows the results of the segmentation of the three test images using the proposed segmenting method.



Fig 5.21 Segmented images: (a) QuickBird, (b) Ikonos, and (c) aerial images.

The binary images of building regions generated from the segmented images are shown in Figure 5.22.



Fig 5.22 Detected buildings: (a) QuickBird, (b) Ikonos, and (c) aerial images.

The filtered results of the binary images of the detected building roofs by using the binary morphological operations are shown in Figure 5.23. Figure 5.23a shows the results obtained by erosion with a structuring element of 2×2 followed by dilation with a structuring element of 4×4 . Figure 5.23b shows the results obtained by closing with a structuring element of 4×4 . Figure 5.23c shows the results obtained by erosion with a structuring element of 3×3 followed by closing with a structuring element of 4×4 .

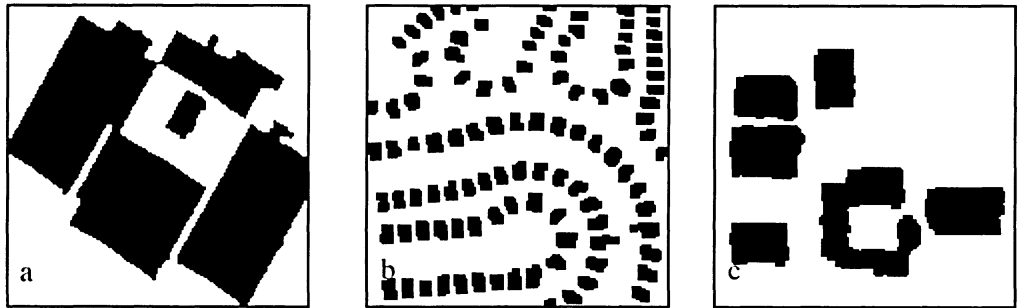


Fig. 5.23 Building roof regions after filtering: (a) QuickBird, (b) Ikonos, and (c) aerial images.

Figure 5.24 shows the edges of the extracted building roofs using the proposed boundary extractor described above.

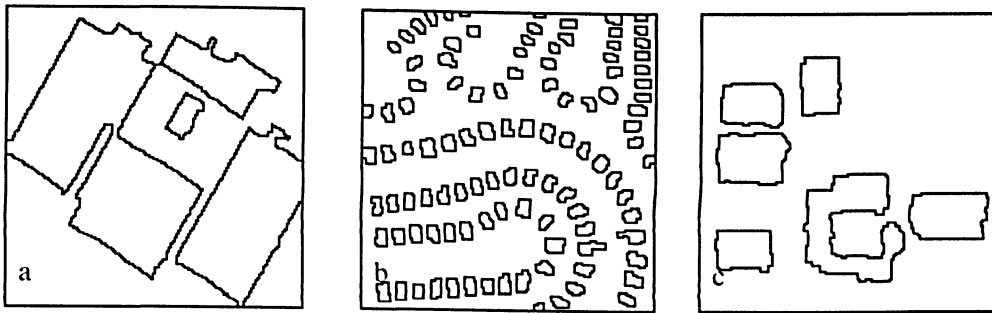


Fig. 5.24 Delineating building roofs: (a) QuickBird, (b) Ikonos, and (c) aerial images.

For the purpose of verification, the extracted building roofs (in red) are overlaid on the corresponding original images shown in Figure 5.25. A visual evaluation gives the impression that the detected building roofs match the shapes of the building very well and the proposed method produces thinner edges.

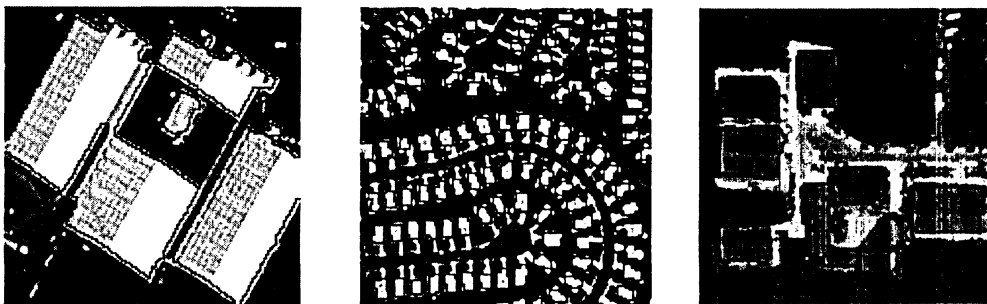


Fig 5.25 Building edges (in red) overlaid on original images: (a) QuickBird, (b) Ikonos, and (c) aerial images.

5.5 Chapter Summary

Colour image segmentation is crucial in many colour image processing applications such as object detection and extraction. Usually, it is the first task of any colour image analysis process, and other steps rely heavily on the quality of segmentation. A new colour image segmentation technique has been presented in this chapter. It is based on the fuzzy similarity measure proposed in Chapter 3. Using the proposed segmentation algorithm,

the approaches of road centrelines and building edges extraction are also proposed. The results of the automated extraction of road centrelines and building roofs show that the proposed colour image segmentation method is very effective.

6 MULTIVARIATE FILTERING BASED ON FSM

Multivariate filtering play a very important role in multichannel remote sensing image processing, especially in reducing noise which is introduced by sensor malfunction, imperfect optics, electronic interference, or flaws in the data transmission procedure (Pitas and Venetsanopoulos, 1990). Recently, a number of non-linear multivariate filters, which utilize the correlations among multivariate vectors, have been proposed. Among them, the vector-based filter is the popular one. Many vector-based filters are designed by ordering vectors in the vector set corresponding to a predefined moving window according to the distance measure and angle measure. The output of these filters is defined as the lowest ranked vectors. Good examples for this kind of filters are vector median filters (VMF) (Astola et al., 1990), vector directional filters (VDF) (Trahanias and Venetsanopoulos, 1993), and directional-distance filters (DDF) (Karakos and Trahanias, 1995). It is no doubt that these standard filters detect and reduce noisy pixels well, but their property of preserving pixels which were not corrupted by the noise processes needs to be improved. The purpose of this chapter is to construct a simple, efficient filter based on the FSM presented in Chapter 3, called fuzzy similarity filter (FSF), which has the ability of generating a compromise between preserving original pixels and removing disturbed pixels.

6.1 Fuzzy Similarity Filter

Unlike the vector-based filters that rely on the distance, angle, or both of them between vectors in a vector space, the fuzzy similarity filter is designed by utilizing the FSM presented in Chapter 3. The fuzzy similarity function to determinate the similarity between two vectors X_i and X_j in a vector set $X = [X_1, X_2, \dots, X_n]$ on R^m can be rewritten as

$$\mu_{ij} = \mu(X_i, X_j) = e^{-k_1 d(X_i, X_j)} \cos(k_2 \theta(X_i, X_j)) \quad (6.1)$$

where $k_1 = [0, \infty)$, $k_2 = [0, 1]$, d and θ are the distance and angle between X_i and X_j , respectively

Based on the FSM, the fuzzy relation FR among vectors in X is constructed as follows

$$FR = [\mu_{ij}(X_i, X_j)]_{n \times n} \quad (6.2)$$

where n is the number of vectors in X .

It is clear that the fuzzy relation defined by Equation (6.2) is a fuzzy compatibility relation because it satisfies the following conditions

- Reflexivity, $\mu_{ii} = 1$, for $i = 1, 2, \dots, n$.

- Symmetry, $\mu_{ij} = \mu_{ji}$, for $i, j = 1, 2, \dots, n$.

The aggregate similarity for the vector X_i in X can be represented as

$$\mu_i(X_i) = \sum_{j=1}^n \mu_{ij}(X_i, X_j) \quad (6.3)$$

It is clearly that the aggregate similarity of X_i describes the degree to which X_i is similar to all vectors in X . According to the aggregate similarity, the maximum similar vector X_{maxs} , which has the maximum aggregate similarity μ_{max} , can be written as

$$X_{maxs} = X_i | \mu_i(X_i) = \mu_{max} = \max\{\mu_k(X_k), \forall X_k \in X\} \quad (6.4)$$

It means that the maximum similar vector most concertedly located in the vector set X according to both distance and direction.

From the definition of the fuzzy compatibility relation in Equation (6.2), it can be noticed that the compatibility class of X_{maxs} induced in terms of a specified membership α defines the crisp subset X_α on X , called α -cut, in which the vectors are similar to X_{maxs} under the degree larger than α , i.e.,

$$X_\alpha = \{X_i | \mu(X_{maxs}, X_i) > \alpha, \forall X_i \in X\} \quad (6.5)$$

Using the compatibility class of X_{maxs} , the FSF is defined as follows.

Definition 6.1 Let W be a window on a multivariate image centred at the pixel p with pixel vector X_p and all pixel vectors in the window form the vector set X . The output of the FSF, $FSF(X)$, is defined as

$$FSF(X) = \begin{cases} X_p, & \text{if } X_p \in X_\alpha \\ X_{maxs}, & \text{if } X_p \notin X_\alpha \end{cases} \quad (6.6)$$

where $0 \leq \alpha \leq 1$, X_{maxs} is the maximum similar vector in X , and X_α is the α -cut.

The most crucial step in the design of the FSF is to select the parameters k_1 and k_2 presented in Equation (6.1) and the parameter α used to determinate the α -cut. These three parameters are the designing parameters and vary in applications.

It is obvious that k_1 determinates the degree to which how the two vectors are similar from the distance point of view. When k_1 is equal to zero, it means that all vectors are the same regardless of the distance between them if they align the same angle. In this case, the designed filter behaviours like a VDF. On the other hand, if $k_1 = \infty$, any two different vectors are totally dissimilarity. Similarly, k_2 determinates the degree to which how the two vectors are similar from the angle point of view. If $k_2 = 0$, the designed filter acts as a VMF. It is expected that α can determinate the degree to which pixels are kept during the filtering process. The following example explains how the FSF works.

Example 6.1 The test image selected (see Figure 6.1) is a pansharpened Ikonos colour image with 1 *m* resolution in Toronto, Ontario. The vector set X taken from the image is formed by the 3×3 window around the pixel at (50, 100) as follows.



Fig. 6.1 Test image.

$$X = \begin{bmatrix} X_1 \\ X_2 \\ X_3 \\ X_4 \\ X_5 \\ X_6 \\ X_7 \\ X_8 \\ X_9 \end{bmatrix} = \begin{bmatrix} 35 & 47 & 49 \\ 232 & 236 & 236 \\ 85 & 97 & 99 \\ 29 & 34 & 43 \\ 143 & 145 & 147 \\ 9 & 23 & 45 \\ 143 & 137 & 146 \\ 56 & 59 & 70 \\ 12 & 18 & 41 \end{bmatrix} \quad (6.7)$$

In X , the centre pixel vector X_p is put on X_1 , that is, $X_p = X_1$.

The fuzzy relation FR induced in X is computed by Equation (6.2) and represented by the membership matrix in Equation (6.8). In this example, $k_1 = 0.001$ and $k_2 = 0.2$.

$$FR = \begin{bmatrix} X_1 & X_2 & X_3 & X_4 & X_5 & X_6 & X_7 & X_8 & X_9 \\ 1.0000 & 0.7180 & 0.9169 & 0.9845 & 0.8386 & 0.9618 & 0.8426 & 0.9683 & 0.9599 \\ 0.7180 & 1.0000 & 0.7832 & 0.7076 & 0.8561 & 0.6920 & 0.8515 & 0.7409 & 0.6903 \\ 0.9169 & 0.7832 & 1.0000 & 0.9035 & 0.9145 & 0.8839 & 0.9187 & 0.9455 & 0.8816 \\ 0.9845 & 0.7076 & 0.9035 & 1.0000 & 0.8265 & 0.9748 & 0.8307 & 0.9553 & 0.9748 \\ 0.8386 & 0.8561 & 0.9145 & 0.8265 & 1.0000 & 0.8080 & 0.9920 & 0.8653 & 0.8061 \\ 0.9618 & 0.6920 & 0.8839 & 0.9748 & 0.8080 & 1.0000 & 0.8121 & 0.9343 & 0.9927 \\ 0.8426 & 0.8515 & 0.9187 & 0.8307 & 0.9920 & 0.8121 & 1.0000 & 0.8698 & 0.8104 \\ 0.9683 & 0.7409 & 0.9455 & 0.9553 & 0.8653 & 0.9343 & 0.8698 & 1.0000 & 0.9326 \\ 0.9599 & 0.6903 & 0.8816 & 0.9748 & 0.8061 & 0.9927 & 0.8104 & 0.9326 & 1.0000 \end{bmatrix} \begin{matrix} X_1 \\ X_2 \\ X_3 \\ X_4 \\ X_5 \\ X_6 \\ X_7 \\ X_8 \\ X_9 \end{matrix} \quad (6.8)$$

After summing all elements of each row vector in FR , the sum vector SV , in which each element corresponds to the aggregate similarity of each pixel vector in X , is given by,

$$SV = [8.1907, 7.0397, 8.1479, 8.1577, 7.9071, 8.0597, 7.9279, 8.2120, 8.0484]^T \quad (6.9)$$

In SV , the maximum aggregate similarity $\mu_{max} = 8.2120$. Corresponding to this maximum aggregate similarity, the maximum similar vector X_{maxs} is determined as $X_{maxs} = X_8$.

For the maximum similar vector X_8 , the similarity measures between X_8 and each vector in X can be obtained from the eighth row of Equation (6. 8), i.e., $\{0.9683, 0.7409, 0.9455, 0.9553, 0.8653, 0.9343, 0.8698, 1.000, 0.9326\}$. If $\alpha = 0.8$, then the compatibility class for X_8 is

$$X_{\alpha=0.8} = \{X_1, X_3, X_4, X_6, X_8, X_9\} \quad (6.10)$$

Because the centre pixel vector X_1 is included in X_a , the filter takes the centre pixel vector X_1 as its output, i.e.,

$$FSF(X) = X_1 \quad (6.11)$$

This result indicates that the FSF chooses the original pixel as output instead of using the most similarity vector X_8 . It shows the FSF's ability of preserving pixels.

If $a = 0.97$, then

$$X_{a=0.8} = \{X_8\} \quad (6.12)$$

In this case, the output of the FSF is

$$FSF(X) = X_8 \quad (6.13)$$

The result shows the ability of the FSF to find the most similar vectors.

6.2 Simulation Results

The evaluation of filtering techniques is a complicated task not only because different criteria employed by filter designers can lead to different assessment results for the performance of designed filters, but also it is difficult to characterize the capabilities of replacing the corrupted pixels and preserving the uncorrupted pixels. The subjective and

objective measures are often used by filter designers to evaluate the performance of their filters (Pratt, 1991).

A variety of objective measures can be utilized for quantitatively comparing the performance of different filters. All of them provide some measures of proximity between two digital images by exploiting the differences in the statistical distributions of the pixel values (Eskicioglu et al., 1995). In this chapter, the normalized mean square error (NMSE) is used as the objective measure of the two compared images and is defined by

$$NMSE = \frac{\sum_{i=1}^{N_1} \sum_{j=1}^{N_2} \|V(i, j) - \hat{V}(i, j)\|^2}{\sum_{i=1}^{N_1} \sum_{j=1}^{N_2} \|V(i, j)\|^2} \quad (6.14)$$

where N_1, N_2 are the dimensions of the images, $V(i, j)$ denotes the pixel vector at the point (i, j) in the original image and $\hat{V}(i, j)$ is its estimation.

Another objective measure, normalized colour difference (NCD) quantifying the perceptual error between images in the perceptually $L^*u^*v^*$ colour space (Wyszecki and Stiles, 1982; Hall, 1999), is also used for the evaluation purpose.

In $L^*u^*v^*$ uniform colour space, the perceptual colour error between two colour vectors is defined as the Euclidean distance given below

$$\|\Delta E_{Luv}\| = [(\Delta L^*)^2 + (\Delta u^*)^2 + (\Delta v^*)^2]^{\frac{1}{2}} \quad (6.15)$$

where $\|\Delta E_{Luv}\|$ is the colour error and ΔL^* , Δu^* , and Δv^* are the differences in the L^* , u^* , and v^* components.

Once each ΔE_{Luv} is calculated, the NCD is estimated according to

$$NCD = \frac{\sum_{i=1}^{N_1} \sum_{j=1}^{N_2} \|\Delta E_{Luv}\|}{\sum_{i=1}^{N_1} \sum_{j=1}^{N_2} \|E_{Luv}^*\|} \quad (6.16)$$

where $\|E_{Luv}^*\| = [(L^*)^2 + (u^*)^2 + (v^*)^2]^{1/2}$ is the norm or magnitude of the uncorrupted pixel vector in an original image.

A set of experiments have been conducted in order to evaluate the FSF and to compare its performance against the performances of the VDF, VMF, and DDF.

The pansharpaned colour Ikonos image (see Figure 6.1) is used in the experiments. In order to evaluate the performance of the FSF under different noise distributions, the test image is contaminated using Gaussian noise, impulsive noise, and both of them. The noise models and their parameters are listed in Table 6.1. The noise images contaminated by different models are shown in Figure 6.2, where Figure 6.2(a)-(d) correspond to noise

models 1-4, respectively. The original image and their noisy versions are represented in RGB colour space.

Table 6.1 Noise models and distributions

Number	Noise Model
1	Gaussian ($\sigma^2 = 200$)
2	Gaussian ($\sigma^2 = 200$), Impulsive (2%)
3	Impulsive (2%)
4	Impulsive (2%), Gaussian ($\sigma^2 = 200$)

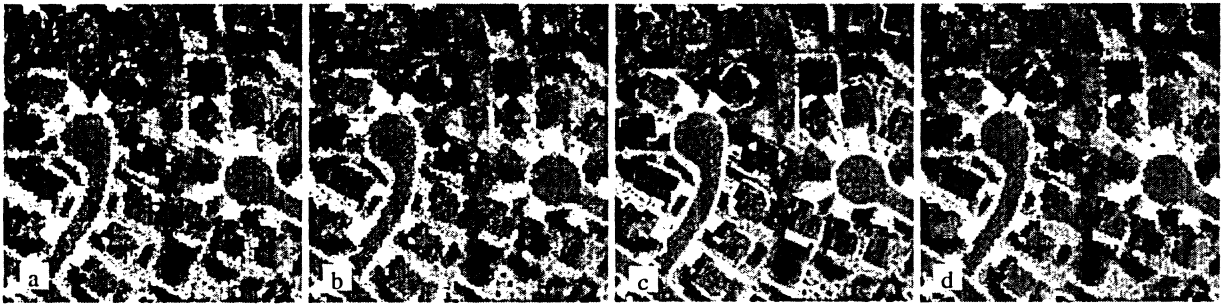


Fig. 6.2 Noisy images.

6.2.1 Impact of Parameters on Performances of FSF

There are three parameters that need to be set in the construction of the FSF before it can be used. They are k_1 , k_2 , and α . In addition, the size of moving window also plays an important role during the design of filters.

In order to evaluate the impact of the parameter k_1 on the performance of the FSF in the presence of different noise models listed in Table 6.1, the simulation experiments are conducted when k_1 varies from 0 to 100 while $k_2 = 0.2$ and $\alpha = 0.9$.

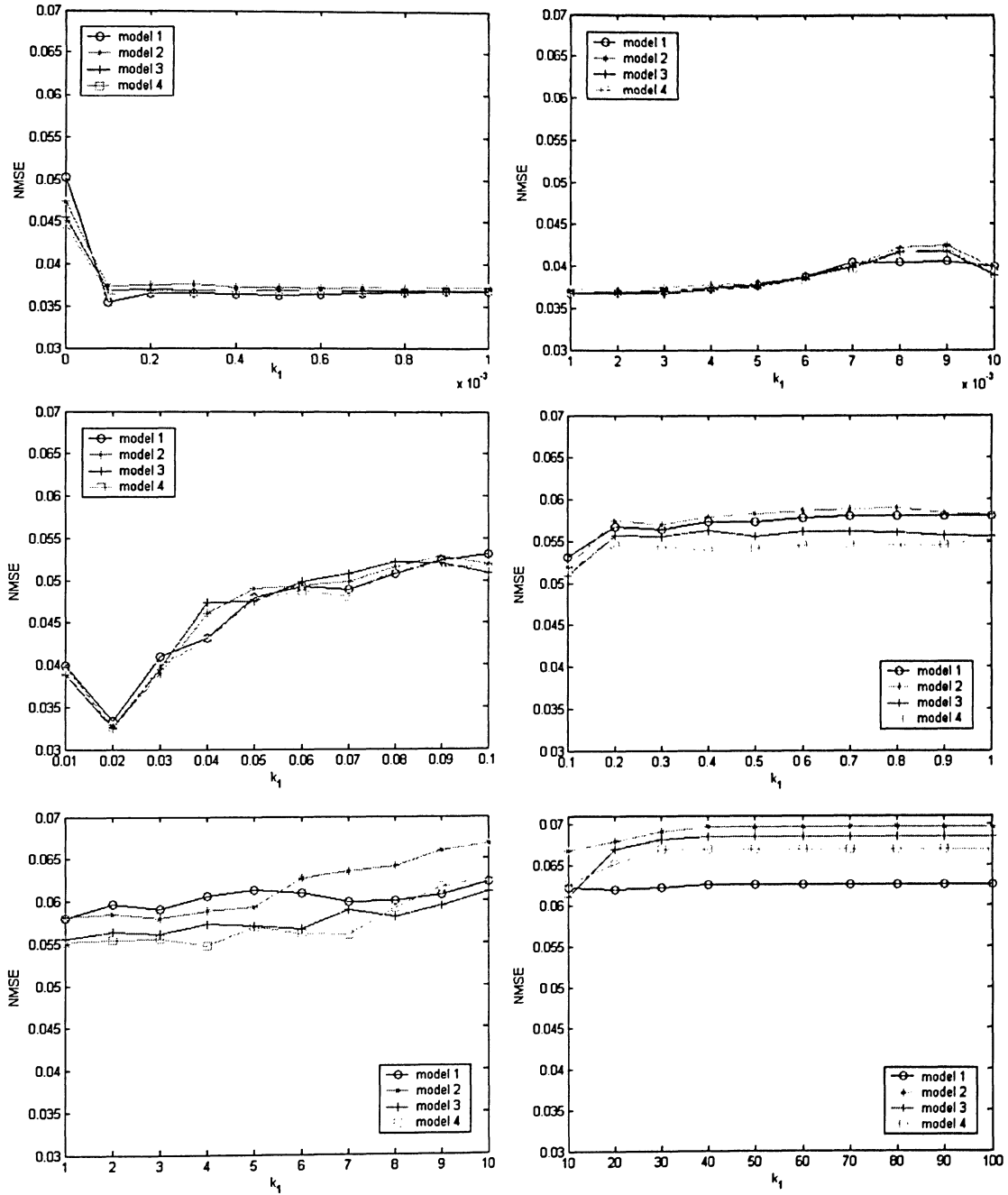


Fig. 6. 3 NMSE of FSF, k_1 from 0 to 100, $k_2 = 0.2$, and $\alpha = 0.9$.

Figures 6.3 and 6.4 illustrate the results of the NMSE and NCD measures. From the simulation experiments it is obvious to conclude that the performance of the FSF is the best for all noise models when k_1 is equal to 0.02. Another obvious observation from the results shown in Figures 6.3 and 6.4 is that the FSF gives the best filtering performance for the impulsive noise (Model 3).

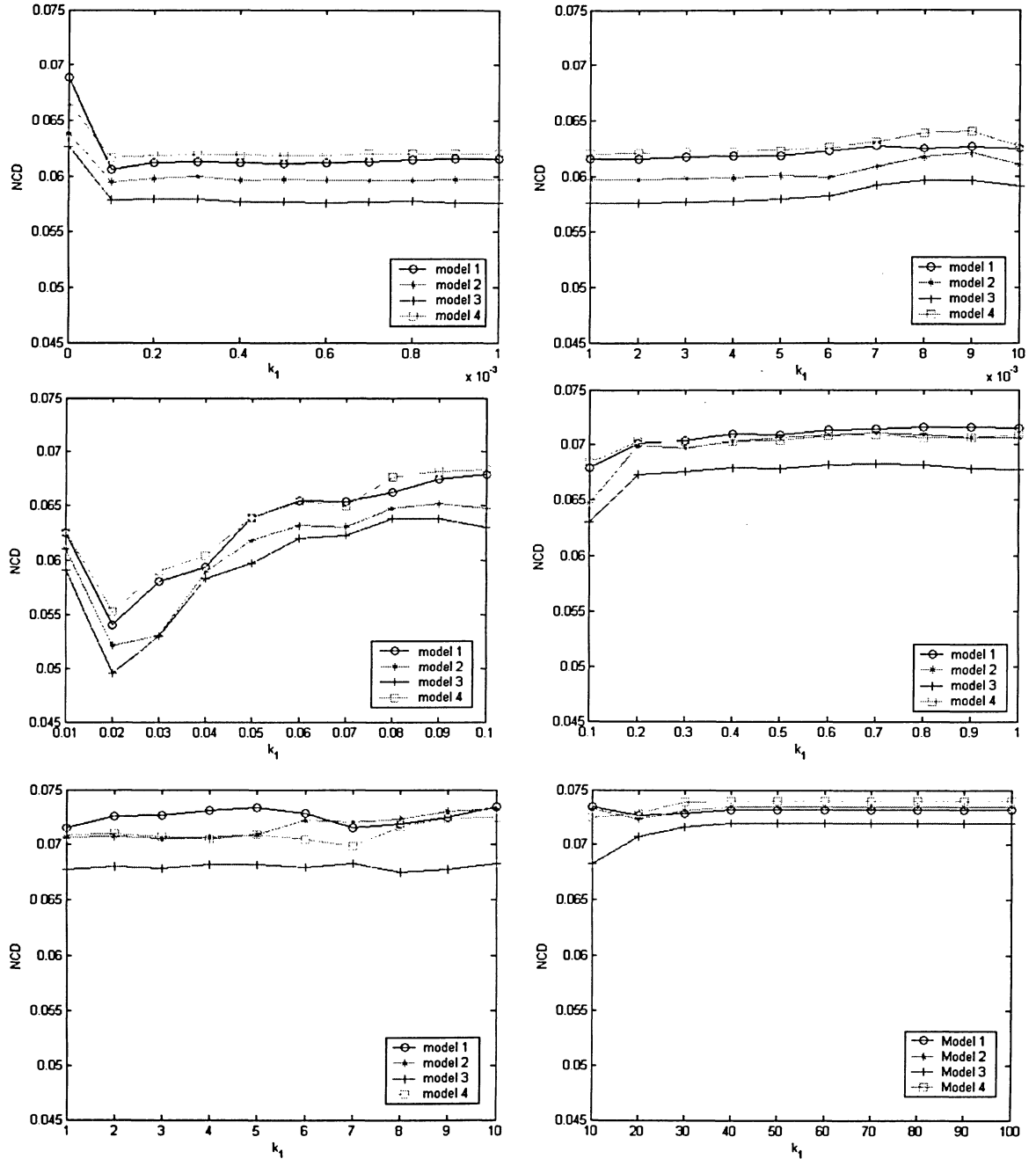


Fig. 6.4 NCD of FSFs, k_1 from 0 to 100, $k_2 = 0.2$, and $\alpha = 0.9$.

When varying k_2 in the interval $[0, 1]$, the filtering results of the FSF are shown in Figure 6.5, where $k_1 = 0.02$ and $\alpha = 0.9$, respectively. From NCD measure results shown in Figure 6.5, it can be seen that there is minimal impact of k_2 on the performance of the FSF for all noise models. From the analysis of the NMSE measures, the impact of k_2 seems to be larger, this phenomena may be caused by the representation of the images in different colour spaces. The results from both measures show that the parameters of the FSF have the same effect on the performances of the FSF for all noise models. For example, for Model 1 and Model 4 noises, their NMSEs and NCDs reduce as k_2 increases. For Model 3 noise, they increase with the decrease of k_2 when k_2 is larger than 0.3. For Model 2 noise, both measures illustrate that k_2 has a trivial effect on the performance of the FSF.

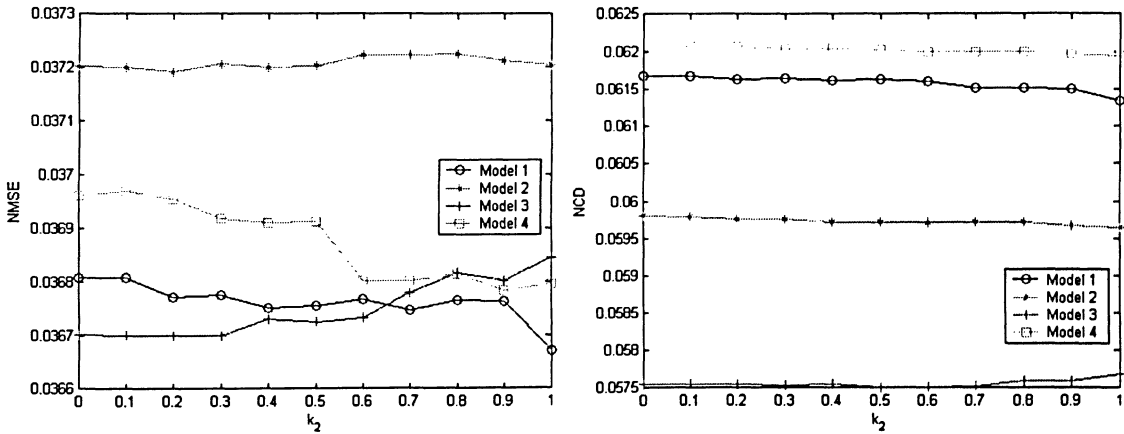


Fig. 6.5 NMSE and NCD of FSF, k_2 from 0 to 1, $k_1 = 0.02$, and $\alpha = 0.9$.

The parameter α is used to adjust the degree of holding a pixel during filtering. The filtering results for FSF under $\alpha = [0, 1]$, $k_1 = 0.02$, and $k_2 = 0.2$ are shown in Figure 6.6. From the results, it can easily be seen that there is no effect on the performance of the

FSF when α is less than 0.7. The results in Figure 6.6 also show that the FSF has the best performance when $\alpha = 0.9$ for all noise models.

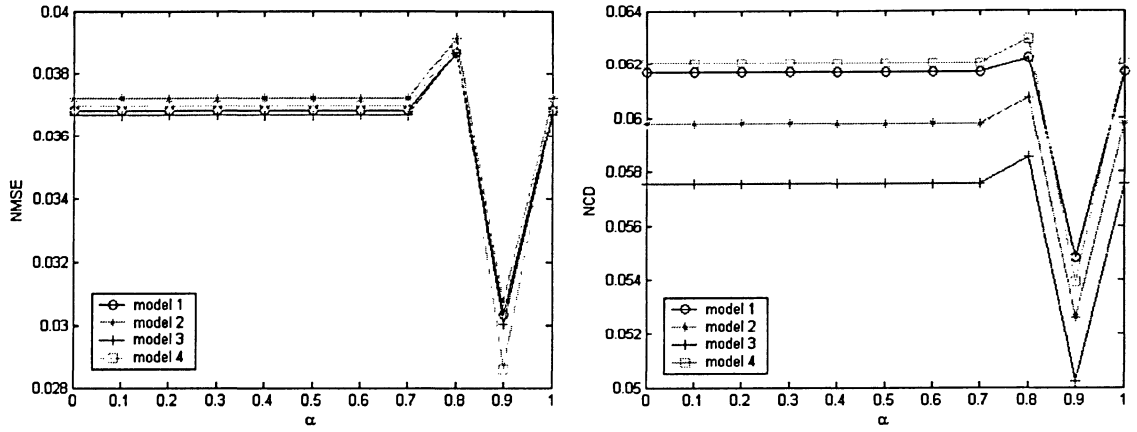


Fig. 6.6 NMSE and NCD of FSF, α from 0 to 1, $k_1 = 0.02$, and $k_2 = 0.2$.

Figure 6.7 shows the filtered images of four types of noise images by the FSF with $k_1 = 0.02$, $k_2 = 0.2$, $\alpha = 0.9$, where Figures 6.7a-d correspond to noise models 1-4. The subjective evaluation gives the impression that the FSF works well under all noise models.

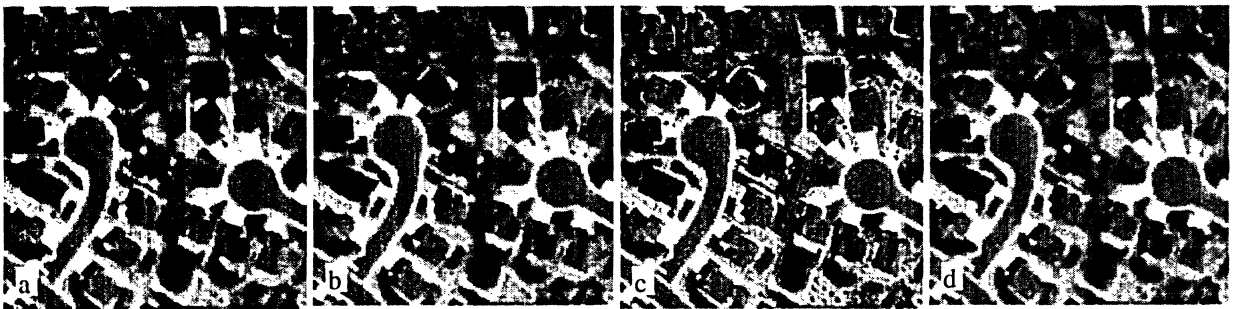


Fig. 6.7 Images after Filtering by the FSF.

During above simulation for evaluating the effects of the parameters, all experiments are conducted with a 3×3 processing window. Figure 6.8 illustrates the effect of window

size on the performance of the FSF, where the window sizes vary from 2×2 to 7×7 , while $k_1 = 0.02$, $k_2 = 0.2$, and $\alpha = 0.9$. From the results of NCD measures for the FSF, it can be observed that the performances of the FSF are improved with the decreasing of the window sizes. The NMSE measures almost give the same results expected for the 2×2 window.

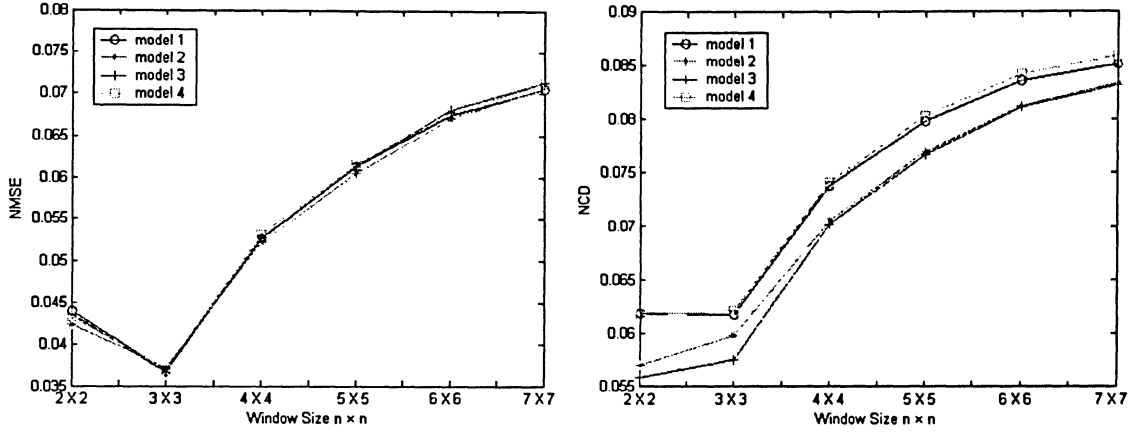


Fig. 6.8 NMSE and NCD of FSF with different window sizes.

6.2.2 Comparison of Performances

In this section, the performance of the proposed FSF and the well-known multivariate filters such as the vector median filter (VMF), the vector directional filter (VDF), and the distance-direction filter (DDF) has been compared. The FSF is designed with $k_1 = 0.02$, $k_2 = 0.2$, and $\alpha = 0.9$. The NMSE and NCD measures are used for this purpose. The results of both measures for all kinds of the filters are shown in Figures 6.9 and 6.10, where (a)-(d) correspond to the noise models 1-4. It follows from Figures 6.9 and 6.10 that the performance of the FSF is better than that of the VMF, VDF, and DDF.

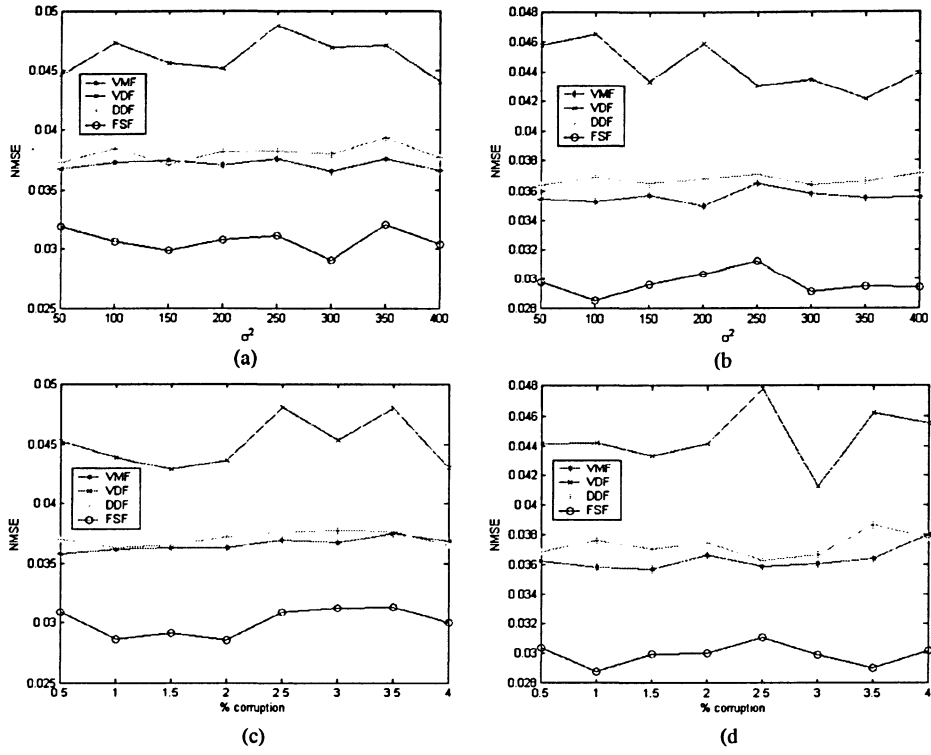


Fig. 6.9 NMSEs of VMF, VDF, DDF, and FSF.

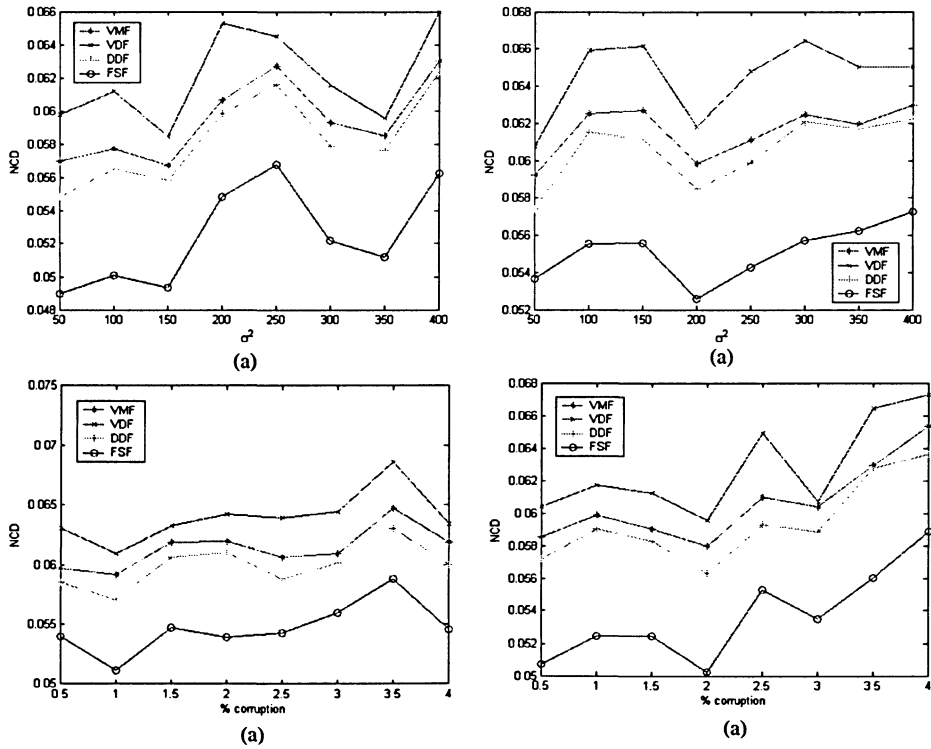


Fig. 6.10 NCDs of VMF, VDF, DDF, and FSF.

The filtered images by VMF, VDF, DDF, and FSF for all noise models are presented in Figures 6.11 to 6.14 for visual and qualitative comparison, since in many cases they are the best measures of performance. All filters operate using a 3×3 window. The FSF preserves edges and smooth noise under different scenarios and outperforms the other filters. A comparison of the filtered images clearly favours the FSF over the VDF, DDF, and VDF. The FSF efficiently removes impulses, smooths out nominal noise and preserves edges, details, and colour uniformity.

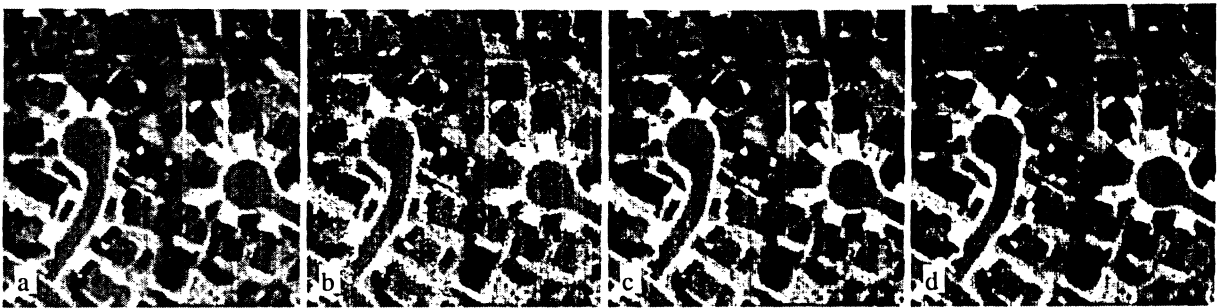


Fig. 6.11 Filtered images of Model 1 noise image by (a) VMF, (b) VDF, (c) DDF, and (d) FSF.

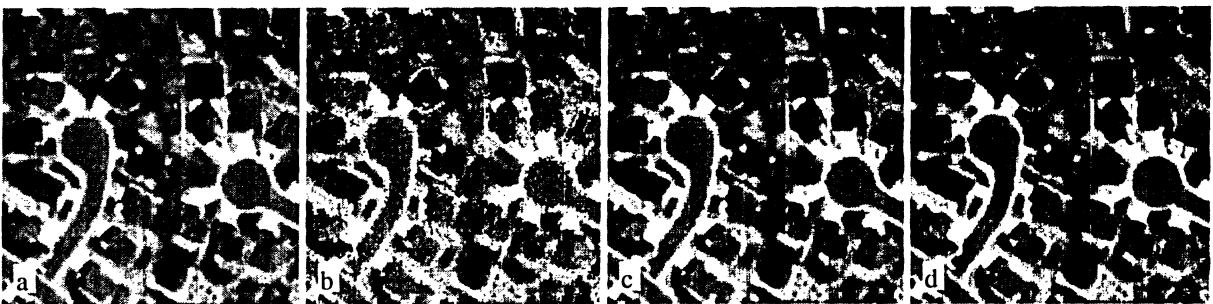


Fig. 6.12 Filtered images of Model 2 noise image by (a) VMF, (b) VDF, (c) DDF, and (d) FSF.

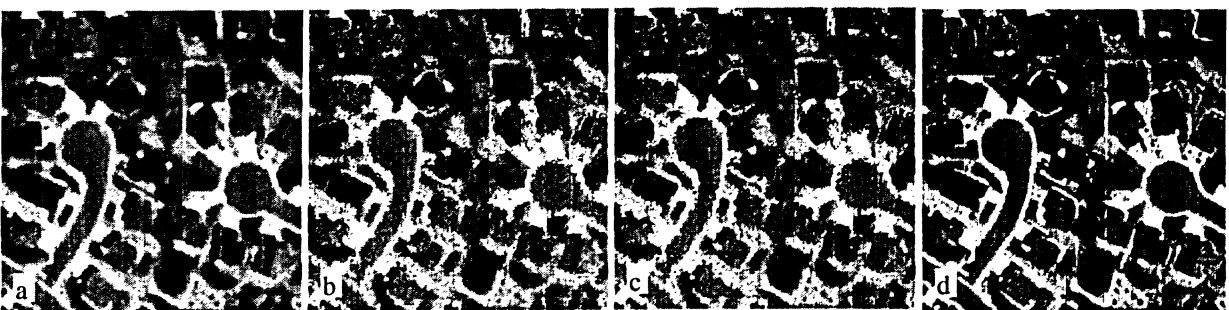


Fig. 6.13 Filtered images of Model 3 noise image by (a) VMF, (b) VDF, (c) DDF, and (d) FSF.

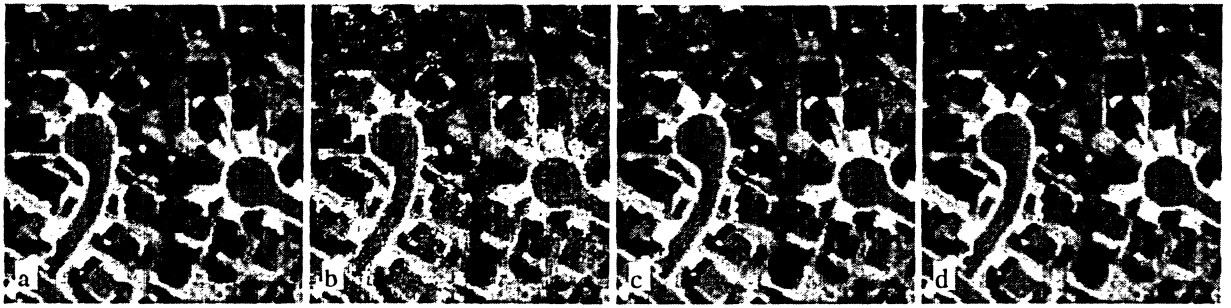


Fig. 6.14 Filtered images of Model 4 noise image by (a) VMF, (b) VDF, (c) DDF, and (d) FSF.

6.3 Chapter Summary

A novel nonlinear multivariate filter, called fuzzy similarity filter (FSF), has been presented in this chapter. This filter is designed based on the FSM defined in Chapter 3. The behaviours of the FSF are analyzed and their performance is compared to that of the most commonly used nonlinear multivariate filters, such as the VMF, VDF, and DDF by using objective measures NMSE and NCD and subjective evaluation.

The FSF not only has the rigid theoretical foundation but a promising performance in a variety of noise characteristics. The simulation results and the subjective evaluation of the filtered colour images indicate that the FSF is comparable with other filters used in the study. As seen from filtered images, the FSF possesses the abilities of noise attenuation and edges or detail preservation but also preserves.

7 CONCLUSIONS AND RECOMMENDATIONS

Motivated by the development of effective multivariate image processing techniques for analyzing, interpreting high-resolution remote sensing images, this study is focus on the definitions and analyses of the fuzzy similarity measure, colour morphology, multivariate clustering, and multivariate filter. In this chapter, the major achievements of the study are summarized in Section 7.1. The conclusions of this study are drawn in Section 7.2. Finally, recommendations for further research are given in Section 7.3.

7.1 Summary

The main contributions of this thesis can be summarized as:

The fuzzy similarity measure(FSM), which can be used to measure the similarity between vectors in a vector space, is introduced. The FSM employs the concepts of the short-range ordering and fuzzification inspired by the same concepts from solid physics and fuzzy mathematics. The results of similarity measures among colours calculated by the FSM shown that it behaves like human perception on colour similarity.

Based on the FSM, three image processing tools, colour morphology, multivariate clustering, and multivariate filtering, have been developed to meet the requirements of high-resolution remote sensing image processing.

Three practical problems arising from engineering applications such as colour edge extraction, road and building extraction, and noise reduction, have been solved by using the developed tools.

7.2 Conclusions

The new finding on the four key issues studied can be summarized as follows.

7.2.1 Fuzzy Similarity Measure

Inspired by the ideas of short-range ordering and fuzzification from solid physics and fuzzy mathematics, the short-range ordering and fuzzification for the relationship among vectors in a vector space are employed as basic assumptions to define the FSM. Based on both distance and angle measures the FSM is presented, which is different from previous methods that use either distance or angle measure only. The exponential function is employed to characterize the contribution of distance between two vectors, and the cosine function is utilized to describe the contribution of their angle. The impact of the distance on the FSM can be controlled by the parameter k_1 . The larger the parameter k_1 is the stronger its impacts on the similarity are. Similarly, another parameter k_2 is used to manage the impact of the angle. The FSM shows the potential for vector-based image processing. It will bring new developments to colour morphology, multivariate clustering, and multivariate filtering.

7.2.2 Colour Morphology

A new framework that extends the concepts of grayscale morphology to colour image processing has been developed, which is based on the FSM. The basic operations of colour morphology such as erosion, dilation, opening, and closing have been defined and their basic properties have been analyzed. The results of the applications of these operations to colour images also have been illustrated. Moreover, it is convenient to apply the new morphology to colour image processing such as colour image edge detection.

7.2.3 Fuzzy Clustering

Remote sensing image segmentation is often accomplished by clustering, in particular, when ground truth is not available to provide samples to train a supervised classifier. The fuzzy clustering is proved to be well suited to deal with the imprecise nature of remote sensing data. According to the fuzzy clustering framework, each cluster is a fuzzy set, and each pixel in the image has a membership value associated to each cluster, which measure how the pixel belongs to that particular cluster. In this thesis, a new fuzzy clustering algorithm, which is based on the FSM, is presented. The new algorithm is obtained by solving a combinational optimum problem. The effectiveness of the proposed clustering algorithm is demonstrated by extracting the road and building from high-resolution remote sensing images such as QuickBird, Ikonos, and aerial images.

7.2.4 Multivariate Filtering

A novel nonlinear multivariate filter, called fuzzy similarity filter (FSF), has been proposed in this thesis. This filter is also based on the FSM which combines both distance and direction criteria. Simulation results and subjective evaluations of the filtered images indicate that the new filter outperform all other filters used in the study (vector median filter (VMF), vector directional filter (VDF), and distance-direction filter (DDF)). Moreover, as seen from images filtered by the FSF, the FSF possesses the capabilities of noise attenuation and edge or detail preservation.

7.3 Recommendations for Future Research

In addition to spectral data, remote sensing data also include spatial and temporal data of the earth's surface, such as maps that show simply topography or more especially geophysical measurements for regions of interest and multitemporal images that provide the spatial distribution of energy coming from the earth during several different periods. Labeling pixels by drawing inferences from several available sources of data, i.e., mixed data types, is an open question. In many cases, the problem is complex, especially when the data are quite different from each other. A feasible scheme is to model each data type in mixed data sources as an attribute and organizes all attributes as an attribute space in which each attribute is multidimensional. For example, for a mixed data consisting of colour image and geographical map, colour and map attributes both are three-

dimensional. The former includes brightness, saturation, and hue and the latter consists of latitude, longitude, and altitude. In order to characterize the relationship between variables with multiattribute, similarity between them is perhaps the most basic approach. Similarity in this case should be complex, should also be sensitive to all attitudes.

Another interesting topic is to study the fuzzy geometry and fuzzy topology and to provide their applications to the geomatics community. The digital geometry plays a key role in calculating geometrical measures of objects such as area, perimeter, diameter, compactness etc. Since the objects in an image have ill-defined or non-crisp boundaries, it would be a good idea to consider them as fuzzy sets. In addition, it is important to represent, store, query, and manipulate spatial information for many non-standard database applications. Specialized systems like geographical information systems (GIS), spatial database systems and image database systems to some extent need model spatial phenomena and their topological relationships through vague or fuzzy concepts due to indeterminate boundaries.

REFERENCES

- Anderberg, M. R., 1973. *Cluster Analysis for Applications*, Academic Press, New York.
- Astola, J., P. Haavisto and Y. Neuovo, 1990. Vector median filters. *Proceedings of the IEEE*, 78 (4), 678-689.
- Aubert, A., D. Jeulin and R. Hashimoto, 2000. Surface texture classification from morphological transformation. In: Goutsias, J. (ed.), *Mathematical Morphology and Its Applications to Image and Signal Processing*, Kluwer Academic Publisher, Boston, USA.
- Bader, M. J, 1995. *Images in Weather Forecasting: A Practical Guide for Interpreting Satellite and Radar Imagery*, Cambridge University Press, Cambridge, England.
- Barnett, V., 1976. The ordering of multivariate data. *Journal of Royal Statistical Society A*, 3: 318-355.
- Beacher, S., 1996. Watershed, hierarchical segmentation and waterfall algorithm. In: Maragos, P. A. (ed.), *Mathematical Morphology and Its Applications to Image and Signal Processing*, Kluwer Academic Publisher, Boston, USA.
- Bezdek, J. C., 1981. *Pattern Recognition with Fuzzy Objective Function Algorithms*, Plenum Press, New York, USA.
- Bieniek, A. and A. Moga, 1998. A connected component approach to the watershed segmentation. In: Heijmans, H. J. (ed.), *Mathematical Morphology and Its Applications to Image and Signal Processing*, Kluwer Academic Publisher, Boston, USA.
- Bloch, I. and H. Maitre, 1995. Fuzzy mathematical morphologies: a comparative study. *Pattern Recognition*, 28(9), 1341-1387.
- Bo, G., S. Dellepiane, P. C. Smits and A. Annoni, 2001. Issues in geographic data quality assessment by remote sensing techniques. *IEEE International Symposium on Geoscience and Remote Sensing*, Sydney, NSW, Australia, Jul. 9-13, vol. 4, pp. 1916-1918.

- Bouchon, M. B., M. Rifqi and S. Bothorel, 1996. General measures of comparison of objects. *Fuzzy Sets and Systems*, 84(2), 143-153.
- Boynton, R., 1979. *Human Color Vision*. Holt, Rinehart and Winston, New York, USA.
- Cain, G. L., 1994. *Introduction to general topology*, Addison-Wesley, Reading, Mass, USA.
- Carleton, A. M., 1991. *Satellite Remote Sensing in Climatology*, Belhaven Press, London, England.
- Comer, M. L. and E. J. Del, 1998. Morphological operations. IN: Sangwine, S. J. and R. E. N. Horne (ed.), *The Color Image Processing Handbook*, Chapman and Hall, London, England.
- Cross, V. V. and T. A. Sudkamp, 2002. *Similarity and Compatibility in Fuzzy Set Theory: Assessment and Applications*. Physica-Verlag, Heidelberg, New York, USA.
- De Baets, B., (1997). Fuzzy morphology: A logical approach. In: *Uncertainty Analysis in Engineering and Science: Fuzzy logic, Statistics, and Neural Network Approach*, Kluwer Academic Publishers, Boston, USA.
- Dell'Acqua, F. and P. Gamba, 2001. Detection of urban structures in SAR images by robust fuzzy clustering algorithms: the example of street tracking. *IEEE Transactions on Geoscience and Remote Sensing*, 39 (10), 2287-2297.
- Demarty, C. H., 1996. Mathematical morphology for image sequence using the knowledge of dynamics. In: Maragos, P. A. (ed) *Mathematical Morphology and its Applications to Image and Signal Processing*, Kluwer Academic Publisher, Boston, USA.
- Dial, G., H. Bowen, F. Gerlach, J. Grodecki and R. Oleszczuk, 2003. IKONOS satellite, imagery, and products. *Remote Sensing of Environment*, 88(1-2), 23-36.
- D'Ornellas, M. C. and R. V. D. Boomgaard, 2000. A morphological multiscale gradient for color images segmentation. In: Goutsias, J. (ed.), *Mathematical Morphology and Its Applications to Image and Signal Processing*, Kluwer Academic Publisher, Boston, USA.
- Dougherty, E. R., 1992. *An Introduction to Morphological Image Processing*, SPIE Optical

- Engineering Press, Bellingham, Wash., USA.
- Dougherty, E. R. 1994. *Digital Image Processing Methods*, Marcel Dekker, New York.
- Dubois, D. and H. Prade, 1980. *Fuzzy Sets and Systems: Theory and Applications*, Academic Press, New York, USA.
- Ehlers, M., M. Gähler and R. Janowsky, 2003. Automated analysis of ultra high resolution remote sensing data for biotope type mapping: new possibilities and challenges. *ISPRS Journal of Photogrammetry and Remote Sensing*, 57(5-6), 315-326.
- Erlich, Z., R. Gelbard and I. Spiegler, 2002. Data mining by means of binary representation: a model for similarity and clustering. *Information System Frontiers*, 4(2), 187-197.
- Eskicioglu, A. M, P. S. Fisher and S. Chen, 1995. Image quality measures and their performance. *IEEE Transactions on Communications*, 43(12), 2959-2965.
- Fairchild, M. D., 1998. *Color Appearance Models*, Addison-Wesley, Readings, Mass, USA.
- Frakes, W. B. and Y. R. Baeza, 1992. *Information retrieval: data structures and algorithms*, Prentice Hall, Englewood Clifs, New Jersey, USA.
- Fu, L.L., and A. Cazenave, 2001. *Satellite Altimetry and Earth Sciences: a Handbook of Techniques and Applications*, Academic Press, San Diego, USA.
- George, J. K. and Y. Bo, 1995. *Fuzzy Sets and Fuzzy Logic: Theory and Applications*, Prentice Hall PTR, Upper Saddle River, New Jersey, USA.
- Georgopoulos, A., A. Loizos and A. Flouda, 1995. Digital image processing as a tool for pavement distress evaluation. *ISPRS Journal of Photogrammetry and Remote Sensing*, 50(1), 23-33.
- Goetcherian, V., 1980. From binary to grey tone image processing using fuzzy logic concepts. *Pattern Recognition*, 12, 7-15.
- Goldberg, D. E., 1989. *Genetic Algorithms in Search, Optimization and Machine Learning*, Addison-Wesley, Reading, Mass, USA.
- Gonzalez, R. and R.E. Woods, 1992. *Digital Image Processing*, Addison-Wesley, Reading.

Mass, USA.

- Goodenough, D. G., A. Dyk, K. O. Niemann, J. S. Pearlman, H. Chen, T. Han, M. Murdoch and C. West, 2003. Processing Hyperion and ALI for forest classification. *IEEE Transactions on Geoscience and Remote Sensing*, 41(6), 1321-1331.
- Gottwald, S., 1979. Set theory for fuzzy sets of higher level. *Fuzzy Sets and Systems*, 2, 125-151.
- Gu, C., 1996. Mathematical morphology and its application in moving object segmentation and tracking. In: Maragos, P. A. (ed.), *Mathematical Morphology and Its Applications to Image and Signal Processing*, Kluwer Academic Publisher, Boston.
- Hall, R., 1999. Comparing spectral color computation methods. *IEEE Computer Graphics and Applications*, 19(4), 36-44.
- Haralick, R. M. and I. G. Shapiro, 1992. *Computer and Robot Vision*, Addison-Wesley, Mass, USA.
- Hartigan, J. A., 1975. *Clustering Algorithms*, Wiley, New York, USA.
- Heijmans, H. J. A. M. and C. Ronse, 1990. The algebraic basis of mathematical morphology, Part I: dilations and erosions. *Computer vision, Graphics and Image processing*, 50, 245-295.
- Heijmans, H. J. A. M., 1996. Self-dual morphological operators and filters. *Journal of Mathematical Imaging and Vision*, 6(1), 15-36.
- Heijmans, H. J. A. M., 1996b. Morphological filters for dummies. In: Maragos, P. A. (ed.), *Mathematical Morphology and Its Applications to Image and Signal Processing*, Kluwer Academic Publisher, Boston, USA.
- Hill, B., T. Roer and F. W. Vorhayen, 1997. Comparative analysis of the quantization of colour spaces on the CIE-Labcolour difference formula. *ACM Transaction on Graphics*, 16(2), 109-154.
- Hinz, S., A. Baumgartner and N. Ebner, 2001. Modeling contextual knowledge for control-ling

- road extraction in urban areas. *Proceedings of IEEE/ISPRS Joint Workshop on Remote Sensing and Data Fusion over Urban Areas*, Rome, Italy, Nov. 2001, pp. 40-44.
- Hoppner, F., F. Klawonn and T. Runkler, 1999. *Fuzzy Cluster Analysis: Methods for Classification, Data analysis, and Image Recognition*, John Wiley, New York, USA.
- Jacobsen, K., 1998. Status and tendency of sensors for mapping. *International Archives of Photogrammetry and Remote Sensing*, Part I, XXXII, 183-190.
- Jain, A. K., 1989. *Fundamentals of Digital Image Processing*, Prentice-Hall, Englewood Cliffs, New Jersey, USA.
- Karakos, D. G. and P. E. Trahanias, 1995. Combining vector median and vector directional filters: the directional-distance filters. *Proceedings of IEEE International Conference on Image Processing*, WDC, USA, Oct., 1995, vol. 1, pp. 171-174.
- Kilston, S., 1998. Capabilities of new remote sensing satellites to support sustainable development. *International Archives of Photogrammetry and Remote Sensing*, Part 1, XXXII, 124-131.
- Klir, G. J. and B. Yuan, 1995. *Fuzzy Sets and Fuzzy Logic: Theory and Applications*, Prentice Hall, Upper Saddle River, New Jersey, USA.
- Langan, D. A., J. W. Modestino and J. Zhang, 1998. Cluster validation for unsupervised stochastic model-based image segmentation. *IEEE Transactions on Image Processing*, 7(2), 180-195.
- Lee, J. S. J., R. M. Haralick and L. G. Shapiro, 1987. Morphologic edge detection. *IEEE Journal of Robotics and Automation*, 3(2), 142-156.
- Lee, H. Y., W. Park, H. K. Lee and T. G. Kim, 2000. Towards knowledge-based extraction of roads from 1-m resolution satellite images. *Proceedings of the 4th IEEE Southwest Symposium on Image Analysis and Interpretation*, Austin, TX, USA, Apr. 2000, pp. 171-176.
- Li, D. and C. Cheng, 2002. New similarity measures of intuitionistic fuzzy sets and application to

- pattern recognitions. *Pattern Recognition Letters*, 23(1-3), 221-225.
- Li, J., Y. Li and H. Dong, 2002. Automated extraction of urban road networks from IKONOS imagery using a fuzzy mathematical morphology approach, *International Archives of Photogrammetry, Remote Sensing and Spatial Information Sciences*, 34(2II): 259-263.
- Liew, A. W. and H. Yan, 2001. Adaptive spatially constrained fuzzy clustering for image segmentation. *The proceedings of 10th IEEE International Conference on Fuzzy Systems*, University of Melbourne, Australia, Dec., 2001, vol. 2, pp. 801-804.
- Lowman, P. D., 2002. *Exploring Space, Exploring Earth: New Understanding of the Earth from Space Research*, Cambridge University Press, New York, USA.
- Maragos, P. and R. D. Ziff, 1990. Threshold superposition in morphological image analysis system. *IEEE Transactions on Pattern Analysis and Machine Intelligence*, 12(5), 498-504.
- Mardia, K. (1976). A comment on the ordering of multivariate data (Barnett, V.). *Journal of Royal Statistical Society A*, 3, 318-355.
- Mardia, K., J. Kent and J. Bibby, 1979. *Multivariate Analysis*, Academic Press, London, England.
- Matheron, G., 1975. *Random Sets and Integral Geometry*, John Wiley and Sons, New York, USA.
- Mehnert, A. J. H. and P. T. Jackway, 2000. Folding induced self-dual filters. In: Goutsias, J. (ed), *Mathematical Morphology and Its Applications to Image and Signal Processing*, Kluwer Academic Publisher, Boston, USA.
- Meyer, F., 1996. Minimum spanning forests for morphological segmentation. In: Maragos, P.A. (ed), *Mathematical Morphology and Its Applications to Image and Signal Processing*, Kluwer Academic Publisher, Boston, USA.
- Nachtegaele, M. and E. Kerre, 2001. Connections between binary, grayscale and fuzzy mathematical morphology. *Fuzzy Sets and Systems*, 124(1), 73-85.
- Neville, R. A. and S. M. Till, 1991. MEIS FM: a multispectral imager for forestry and mapping.

- IEEE Transactions on Geoscience and Remote Sensing*, 29(1), 184-186.
- Ohta, Y., T. Kanade and T. Sakai, (1980). Color information for region segmentation. *Computer Graphics and Image Processing*. 13, 222-241.
- Pesaresi, M. and J. A. Benediktsson, 2000. Image segmentation based on the derivative of the morphological profile In: Goutsias, J. (ed.), *Mathematical Morphology and Its Applications to Image and Signal Processing*, Kluwer Academic Publisher, Boston, USA.
- Pessoa, L. and P. Maragos, 1996. MRL-filters and their adaptive optimal design for image processing. In: Maragos, P. A. (ed.), *Mathematical Morphology and Its Applications to Image and Signal Processing*, Kluwer Academic Publisher, Boston, USA.
- Pitas, I. and A. N. Venetsanopoulos, 1990. *Nonlinear Digital Filters: Principles and Applications*, Kluwer Academic Publishers, Boston, USA.
- Pratt, W. K., 1991. *Digital Image Processing*, Wiley, New York, USA.
- Reeves, C. V., 1999. Geological remote sensing in aerospace and time: introduction. *Geologie en Mijnbouw*. 77, 113–116.
- Richards, J. A., 1993. *Remote Sensing Digital Images Analysis: An Introduction* (2nd), Springer-Verlag, New York, USA.
- Richards, J. A., 1999. *Remote Sensing Digital Images Analysis: An Introduction* (3rd), Springer-Verlag, New York, USA.
- Ronse, C., 1990. Why mathematical morphology needs complete lattices. *Signal Processing*, 21, 129-154.
- Santini, S. and R. Jain, 1999. Similarity measures. *IEEE Transactions on Pattern Analysis and Machine Intelligence*, 21(9), 871-883.
- Sato, M., Y. Sato and L. C. Jain, 1997. *Fuzzy Clustering Models and Applications*, Physica Verlag, Heidelberg, New York, USA.
- Serra, J., 1982. *Image Analysis and Mathematical Morphology*, Academic Press, London, England.

- Schonfeld, D., 1996. Weighted composite order statistics filters: optimal morphological pattern recognition. In: Maragos, P. A. (ed.), *Mathematical Morphology and Its Applications to Image and Signal Processing*, Kluwer Academic Publisher, Boston, USA.
- Sharma, G. and H. J. Trussel, 1997. Digital color processing. *IEEE Transactions on Image Processing*, 6(7), 901–932.
- Short, N. M., 1982. The Landsat tutorial workbook: basics of satellite remote sensing. *National Aeronautics and Space Administration, Scientific and Technical Information Branch*, WDC, USA.
- Sinha, D. and E. R. Dougherty, 1993. Fuzzification of set inclusion: theory and applications. *Fuzzy Sets and Systems*, 55, 15-42.
- Stafford, D. B., 1991. *Civil engineering applications of remote sensing and geographic information systems*. American Society of Civil Engineers.
- Stark, H. and Y. Yang, 1998. *Vector Space Projections: A Numerical Approach to Signal and Image Processing, Neural Nets, and Optics*, Wiley, New York, USA.
- Sternberg, S. R., 1986. Greyscale morphology. *Computer Vision, Graphics, and Image Processing*, 35, 333-355.
- Talbot, H., C. Evans and R. Jones, 1998. Complete ordering and multivariate mathematical morphology. In: Heijmans, H. J. A. M. (ed.), *Mathematical Morphology and Its Applications to Image and Signal Processing*, Kluwer Academic Publisher, Boston, USA.
- Torgerson, W. S., 1965. Multidimensional scaling: I theory and method. *Psychometrika*, 17, 379-393.
- Tou, J. T. and R. C. Gonzalez, 1974. *Pattern Recognition Principles*, Addison-Wesley, Reading, Mass, USA.
- Tourlakis, G. J., 2003. *Lectures in Logic and Set Theory*, Cambridge University Press, Cambridge, New York, USA.
- Trahanias, P. E. and A. N. Venetsanopoulos, 1993. Vector directional filters: a new class of

- multichannel image processing filters. *IEEE Transactions on Image Processing*, 2(4), 528-534.
- Trinder, J. C. and Y. Wang, 1998. Automatic road extraction from aerial images. *Digital Signal Processing*, 8 (4), 215-224.
- Vardavoulia, M. I., I. Andreadis and P. Tsalides, 2002. Vector ordering and morphological operations for color image processing: fundamentals and applications. *Pattern Analysis and Applications*, 5(3), 271-287.
- Verstraete, M. M., 2000. *Observing Land From Space: Science, Customers, And Technology*, Kluwer Academic, Dordrecht, Boston, USA.
- Wechler, W., 1992. *Universal Algebra for Computer Scientists*, Springer-Verlag, Berlin, New York, USA.
- Winston, W. L., 1991. *Introduction to Mathematical Programming: Applications and Algorithms*, Duxbury Press, Belmont, Ca, USA.
- Wyszecki, G. and W. S. Stiles, 1967. *Color Science, Concepts and Methods, Quantitative Data and Formulas*, Wiley, New York, USA.
- Yeung, D. S. and E. C. C. Tsang, 1997. A comparative study on similarity-based fuzzy reasoning methods. *IEEE Transactions on Systems, Man and Cybernetics*, Part B, 27(2), 216-227.
- Young, G., and A. S. Householder, 1959. Discussion of a set of points in terms of their mutual distance. *Psychometrika*, 3, 19-22.
- Zadeh, L. A., 1965. *Fuzzy Sets. Information and Control*, 8(3), 338-353.
- Zeng, Y. and J. Starzyk, 2001. Statistical approach to clustering in pattern recognition. *Proceedings of the 33rd Southeastern Symposium on System Theory*, Athens, OH, USA, Mar., 2001, pp. 177-181.
- Zhang, J. W., 1980. A united treatment of fuzzy set theory and Boolean-valued set theory: fuzzy set structures and normal fuzzy set structures. *Journal of Mathematical Analysis and Applications*, 76, 297-301.

- Zhang, T. Y. and C. Y. Suen, 1984. A fast parallel algorithm for thinning digital patterns. *Communications of the ACM*, 27(3), 236-239.
- Zhao, T., L. H. Tang, H. H. S. Ip and F. Qi, 2003. On relevance feedback and similarity measure for image retrieval with synergetic neural nets. *Neurocomputing*, 51, 105-124.
- Zhong, J. M., C. H. Leung and Y. Y. Tang, 2000. Image compression based on energy clustering and zero-quadtrees representation. *IEEE Proceedings on Vision, Image and Signal Processing*, 147(6), 564-570.

INDEX

A

α -cut 102
Adjunction 19
Aggregation angle 28
Aggregation distance 27
Aggregate ordering 27
Aggregate similarity 101
Angle between two vector 16
Angle measure 16
Attribute space 120

B

Basic vector directional filter 28
Bin 76
Binary closing 17
Binary dilation 17
Binary erosion 17
Binary morphology 16
Binary opening 17
BVDF 28

C

Centre vector 75
Centre vectors set 75
Charateristic function 23
Chessboard distance 14
City block distance 14
Closing 19
Colour closing 51
Colour dilation 51
Colour edge 60
Colour erosion 51
Colour histogram 76
Colour model 8
Colour opening 51
Colour morphology 22 51
Colour similarity 38
Colour space 7
Compatibility class 102
Condition ordering 26
Conjuncter 20
Convex 32
C-ordering 26

Crisp partition matrix 80

D

DDF 29

Dilation 19

Directional-distance filter 28

Domain 21

E

Edging algorithm 93

Erosion 19

Euclidean norm 13

Euclidean distance 14

Euclidean space 16

F

FSEE 62

FSF 102

FSM 32

Fuzzy closing 22

Fuzzy compatibility relation 100

Fuzzy complement 24

Fuzzy c-partition 72

Fuzzy c-partition matrix 73

Fuzzy dilation 21

Fuzzy erosion 21

Fuzzy geometry 121

Fuzzy intersection 24

Fuzzy membership function 33

Fuzzy morphology 19

Fuzzy opening 22

Fuzzy relation 100

Fuzzy set theory 23

Fuzzy similarity edge extractor 62

Fuzzy similarity filter 102

Fuzzy similarity measure 32

Fuzzy subset 23

Fuzzy topology 121

Fuzzy union 24

G

Grayscale morphology 18

I

Identical 32

Implicator 20

Infimum operator 50

Inner product 15

L

L*u*v* colour space 9

M

Marginal ordering 26

Mathematical morphology 16

Maximum aggregate similarity 101

Maximum similar vector 101

Maximum vector 47

Max-min vector pair 47

Median vector 26

Membership degree function 24

Minimum vector 47

M-ordering 26

Most similar vector 48

N

NCD 106

Negator 20

NMSE 106

Norm 12

Normalized colour difference 106

Normalized mean square error 106

O

Objection function 74

Objective measure 106

Opening 19

Order statistics 26

P

Partial ordering 26

Percent partition matrix 80

P-norm 13

P-ordering 26

R

Reduced ordering 27

Reflection operator 17

Reflexivity 100

RGB colour space 8

R-ordering 27

S

Short range ordering 31

Similarity measure 12

Similar vector class 48

Straight line distance 14

Supremum operator 50

Symmetric 32

Symmetry 101

T

Thinning algorithm 90

Translation operator 17

Translation operation 22

U

Uniform colour space 9

V

Vector filters 25

Vector median filter 28

VMF 28

W

Weighted distance 14

Weighting factor 14